UC San Diego

UC San Diego Electronic Theses and Dissertations

Title

The Contribution of p300/CBP and Acetylation Towards Skeletal Muscle Insulin Action

Permalink

https://escholarship.org/uc/item/87p2k3dw

Author

Martins, Vitor Fernandes

Publication Date

2020

Peer reviewed|Thesis/dissertation

eScholarship.org Powered by the California Digital Library
University of California

UNIVERSITY OF CALIFORNIA SAN DIEGO

The Contribution of p300/CBP and Acetylation Towards Skeletal Muscle Insulin Action

A dissertation submitted in partial satisfaction of the
Requirements for the degree Doctor of Philosophy

in

Biomedical Sciences

by

Vitor Fernandes Martins

Committee in charge:

Professor Simon Schenk, Chair
Professor Shelley Halpain
Professor Olivia Osborn
Professor Hemal Patel
Professor Alan Saltiel

2020

Copyright

Vitor Fernandes Martins, 2020

All rights reserved.

The Dissertation of Vitor Fernandes Martins is approved and it is acceptable in quality and form for publication on microfilm and electronically:

_____

_____

_____

_____

_____

Chair

University of California San Diego

2020

DEDICATION

"If I have seen further it is by standing on the shoulders of giants" – Sir Issac Newton letter to Robert Hooke, 1675. I would like to dedicate this thesis to my parents and family, whose hard work and determination have paved the road, giving me the privilege to pursue my passions in higher education; and to my partner who has been alongside me on this road since the beginning.

TABLE OF CONTENTS

LIST OF FIGURES

LIST OF TABLES

ACKNOWLEDGEMENTS

Chapter 2, in full, is a reprint of the material as it appears in the American Journal of Physiology, Cell Physiology 2019 (with edits for style). V. F. Martins, M. Begur, S. Lakkaraju, K. Svensson, J. Park, B. Hetrick, C. E. McCurdy, S. Schenk. The dissertation author was the primary investigator and author of this paper.

Chapter 3, in full, is a reprint of the material as it appears in the American Journal of Physiology, Endocrinology and Metabolism 2019 (with edits for style). V. F. Martins, J. R. Dent, K. Svensson, S. Tahvilian, M. Begur, S. Lakkaraju, E. H. Buckner, S. A. LaBarge, B. Hetrick, C. E. McCurdy, S. Schenk. The dissertation author was the primary investigator and author of this paper.

Chapter 4, in full, is currently being prepared for publication. V. F. Martins, S. Schenk. The dissertation author was the primary investigator and author of this paper.

VITA

2014 Bachelor of Arts, University of Florida

2014 Bachelor of Sciences, University of Florida

2020 Doctor of Philosophy, University of California San Diego

PUBLICATIONS

Svensson K*, Tahvilian S*, **Martins VF**, Dent JR, Lemanek, A, Barooni, N, Greyslak, K, McCurdy CE, Schenk S. Concurrent overexpression of SIRT1 and knockout of GCN5 in adult skeletal muscle does not alter basal or endurance trained exercise capacity in mice. Am J Physiol Metab. 2019. In Press.

Svensson K, LaBarge SA, Sathe A, **Martins VF**, Tahvilian S, Cunliffe JM, Sasik A, Mahata SK, Meyer GA, Philp A, David LL, Ward SR, McCurdy CE, Aslan JE, Schenk S. p300 and CBP are essential for skeletal muscle homeostasis, contractile function and survival. J Cachexia Sarcopenia Muscle. 2019. In Press.

Martins VF, Begur M, Lakkaraju S, Svensson K, Park J, Hetrick B, McCrudy CE, Schenk, S. Acute inhibition of protein deacetylases does not impact skeletal muscle insulin action. Am J Physiol Cell Physiol. 2019. Nov 1;317(5):C964–8.

Martins VF, Dent JR, Svensson K, Tahvilian S, Begur M, Lakkaraju S, Buckner EH, LaBarge SA, Hetrick B, McCurdy CE, Schenk S. Germline or inducible knockout of p300 or CBP in skeletal muscle does not alter insulin sensitivity. Am J Physiol Metab. 2019 Jun 1;316(6):E1024–35.

Svensson K, Dent JR, Tahvilian S, **Martins VF**, Sathe A, Ochala J, Patel MS, Schenk S. Defining the contribution of skeletal muscle pyruvate dehydrogenase α1 to exercise performance and insulin action. Am J Physiol Metab. 2018 Nov 1;315(5):E1034–45.

Martins VF, Tahvilian S, Kang JH, Svensson K, Hetrick B, Chick WS, Schenk S, McCurdy CE. Calorie Restriction-Induced Increase in Skeletal Muscle Insulin Sensitivity Is Not Prevented by Overexpression of the p55α Subunit of Phosphoinositide 3-Kinase. Front Physiol. 2018 Jun 27;9(June):789.

Dent JR, **Martins VF**, Svensson K, LaBarge SA, Schlenk NC, Esparza MC, Buckner EH, Meyer GA, Hamilton DL, Schenk S. Muscle-specific knockout of general control of amino acid synthesis 5 (GCN5) does not enhance basal or endurance exercise-induced mitochondrial adaptation. Mol Metab. 2017 Dec;6(12):1574–84.

Svensson K, LaBarge SA, **Martins VF**, Schenk S. Temporal overexpression of SIRT1 in skeletal muscle of adult mice does not improve insulin sensitivity or markers of mitochondrial biogenesis. Acta Physiol. 2017 Nov;221(3):193–203.

Martins VF, Vaughan MM, Huffaker A, Schmelz EA, Christensen S, Sims J, Benda ND, Swerbilow J, Alborn HT, Teal PEA. Seed Treatment with Live or Dead Fusarium verticillioides Equivalently Reduces the Severity of Subsequent Stalk Rot. J Phytopathol. 2014 Mar;162(3):201–4.

Vaughan MM, Huffaker A, Schmelz EA, Dafoe NJ, Christensen S, Sims J, **Martins VF**, Swerbilow J, Romero M, Alborn HT, Allen LH, Teal PEA. Effects of elevated [CO2] on maize defence against mycotoxigenic Fusarium verticillioides. Plant, Cell Environ. 2014;37(12):2691–706.

ABSTRACT OF THE DISSERTATION

The Contribution of p300/CBP and Acetylation Towards Skeletal Muscle Insulin Action

by

Vitor Fernandes Martins

Doctor of Philosophy in Biomedical Sciences

University of California San Diego, 2020

Professor Simon Schenk, Chair

Impaired insulin-stimulated glucose uptake is a common metabolic disorder in aged and obese skeletal muscle, with this “insulin resistance” being the primary metabolic defect of type 2 diabetes. At a molecular level, skeletal muscle insulin signaling to glucose uptake is regulated by a phosphorylation-based, phosphoinositide 3-kinase (PI3K)/Akt-dependent signaling pathway. However, recent proteomic-based analysis in various tissues, including skeletal muscle, have identified more than 2000 acetylated, non-nuclear, proteins that impact a broad array of cellular processes including insulin signaling. The acetyltransferases p300 (E1A binding protein p300) and

CBP (cAMP response element binding protein binding protein) are phosphorylated and activated by Akt, and p300/CBP can acetylate downstream insulin signaling and GLUT4 trafficking proteins, thus giving rise to a putative Akt-p300/CBP axis. Thus, the objective of this Dissertation was to determine the non-transcriptional importance of p300, CBP, and acetylation to skeletal muscle insulin sensitivity, for which we utilized small molecule inhibitors and muscle-specific knockout models. In Study 1, acute inhibition of deacetylases was sufficient to increase acetylation in L6 myotubes and skeletal muscle, however it did not alter insulin-stimulated glucose uptake or signaling. In Study 2, single knockout of either p300 or CBP in skeletal muscle did not impact glucose tolerance or skeletal muscle insulin action under either control, calorie restriction, or high-fat diet conditions. In Study 3, mice with combined double knockout of p300/CBP in skeletal muscle were severely glucose intolerant and skeletal muscle insulin resistant. Remarkably, this glucose intolerance and inability of skeletal muscle to respond to insulin was reversed in mice with just a single allele of either p300 or CBP. In the p300/CBP double-knockout mice, skeletal muscle insulin resistance was accompanied by significant downregulation of both mRNA and protein networks critical for insulin signaling, GLUT4 trafficking, and glucose metabolism. In summary, acutely increasing acetylation in skeletal muscle does not impact insulin stimulated glucose uptake or signaling. However, p300/CBP together are critical regulators of skeletal muscle insulin sensitivity, at least in part, by transcriptional regulation of the insulin signaling and GLUT4 trafficking pathways.

Chapter 1: Introduction to the Dissertation

Type 2 diabetes (T2D) is a chronic disease which is clinically defined by elevated blood glucose levels and associated with generalized metabolic dysfunction such as obesity and dyslipidemia (23, 32, 39, 58). T2D is a source of substantial morbidity for patients, as it is the primary cause in the United States of non-traumatic toe or foot amputation, adult-onset blindness, and kidney disease/failure (8, 28, 82). Furthermore, T2D increases mortality risk by 50% compared to non-diabetics (28). Importantly, the prevalence of T2D is increasing rapidly, more than doubling between 2000 to 2017, with 9.4% of the US population having T2D currently (9) and projections estimating 33% of the population having diabetes by 2050 (7). Considering the severity of complications, the rapidly increasing prevalence, and the high cost of treatment of ~$245 billion in 2017 (9, 36), understanding the molecular underpinnings of type 2 diabetes could drastically improve human health, quality of life, and aid in preventing an escalating healthcare crisis.

Insulin is an endocrine hormone released from the pancreas which acts on a variety of tissues to lower blood glucose levels and promote energy storage. In the liver, insulin acts to reduce hepatic glucose production and, conversely, in skeletal muscle and adipose tissue insulin stimulates the uptake of glucose. While the direct pathophysiology of T2D is unknown, studies suggest that it is a result of a resistance of peripheral tissues to insulin (23, 32, 39, 58). Importantly, while decreased production of insulin from the pancreas also plays a role in later stages of the disease (23, 32, 39, 58), peripheral insulin resistance is the initial and primary metabolic defect that occurs in T2D (29, 50). In conditions that promote insulin resistance, such as obesity and aging (6, 22, 40, 44, 65), insulin has a decreased ability to act upon peripheral tissues, leading to elevated

blood glucose levels. Considering skeletal muscle accounts for as much as 85% of insulin-stimulated peripheral glucose disposal (17, 18, 49), and this is impaired in skeletal muscle during T2D (17, 27, 62), developing drugs targeted at improving skeletal muscle insulin resistance could be an effective strategy in the management of T2D.

To better design approaches to improve skeletal muscle insulin sensitivity, it is necessary to outline the current model of insulin-stimulated glucose transport. Insulin stimulation to glucose transport is mediated by a phosphorylation-dependent, two-part pathway. First insulin stimulation leads a phosphoinositide 3-kinase (PI3K)/Akt dependent signaling cascade (49, 73). Subsequently, downstream Rab GTPases are activated to traffic glucose transporter 4 (GLUT4) from the peri-nuclear region to the plasma membrane, allowing for facilitated transport of glucose into the cell (49, 73). Notably, glucose transport in adipocytes require both the described PI3K/Akt pathway, as well as the APS (adaptor protein with PH and Src homology 2 (SH2) domain) pathway (49), however, the requirement of the APS pathway in skeletal muscle is unknown (49), and therefore will not be discussed. Importantly, efforts to improve insulin action by targeting phosphorylation-based signaling have generally been unsuccessful (13), in part due to the pleiotropic nature of PI3K/Akt signaling. For example increased PI3K/Akt signaling/activity underlies many cancers (Reviewed in (1, 16, 59)). Indeed, hyperglycemia and hyperinsulinemia are common toxicities of anti-cancer drugs targeting the PI3K/Akt pathway (4, 38, 63), thus, conversely, efforts to improve insulin action via enhancing PI3K/Akt signaling may be carcinogenic. Therefore, identifying novel signals, downstream of the phosphorylation-based PI3K/Akt pathway, has great potential to improve human health and quality of life by uncovering more specific ways to enhance insulin action.

In searching the literature for processes that may play a role in the regulation of insulin

signaling and GLUT4 trafficking, lysine acetylation is revealed as a promising candidate. Acetylation is a highly-abundant post-translational modification (PTM) that regulates protein function (30, 47, 76, 84), much like phosphorylation. Initially, the importance of lysine acetylation to cellular homeostasis was thought to occur strictly via its ability to regulate histone function and gene transcription (74). However, recent proteomic-based analysis in various tissues, including skeletal muscle, have identified more than 2,000 acetylated, non-histone, proteins that impact a broad array of cellular processes (11, 41, 53, 80, 84). In fact, many of these proteins are found in the cytoplasm and are central to numerous metabolic pathways including glucose and amino acid metabolism, membrane trafficking and insulin signaling (11, 41, 47, 80, 84). While recent literature demonstrates that acetylation can act to impact cytosolic protein function, including proteins critical to insulin action (5, 70, 83), which proteins are responsible for the changes in their acetylation status, and how protein acetylation status alters insulin action non-transcriptionally is largely unknown.

While lysine acetylation is a balance of acetyltransferase and deacetylase activity, which add or remove acetyl groups, respectively (12), the deacetylases have been much more heavily studied in relation to insulin sensitivity. There are 18 known deacetylases that are divided into 2 families: the zinc-dependent histone deacetylases (HDACs) and NAD^+-dependent sirtuins (12). Both the HDACs (55, 60, 69, 72, 79) and the sirtuins (2, 24, 48, 68, 71) have been implicated in the regulation of insulin-stimulated glucose uptake in skeletal muscle. The mechanism of action for this regulation appears to primarily occur via deacetylation of transcriptional regulators and/or histones, and subsequent changes in the transcription of insulin signaling proteins (55, 60, 68, 79). Notably, previous studies have demonstrated that pharmacological inhibition of deacetylases enhances insulin action in skeletal muscle (26, 55, 60, 69, 72), but because incubation times were

for over 24h hours, this enhancement could be via changes in transcription of insulin signaling proteins, acetylation of cytosolic insulin signaling proteins, or a combination of the two. Thus, the ability of deacetylases to non-transcriptionally regulate insulin-stimulated glucose uptake, particularly in insulin-responsive tissues such as skeletal muscle, remains to be explored.

Although acetylation is a balance of acetyltransferase and deacetylase activity, the contribution of acetyltransferases towards skeletal muscle insulin sensitivity has been grossly understudied. There are 22 acetyltransferases in human and mouse cells (42), any of which could potentially be important for altering the acetylation status and function of cytosolic insulin signaling proteins. However, for our studies, we chose to focus on acetyltransferases p300 (E1A binding protein p300) and CBP (cAMP response element binding protein [CREB] binding protein) for a number of reasons. Firstly, p300/CBP have a robust cytosolic presence (3, 21, 66). This is essential if they are to acetylate proteins involved in insulin signaling and GLUT4 trafficking, all of which are located in the cytosol. Although p300 and CBP are well known histone (i.e. nuclear-located) acetyltransferases (52, 57, 81), they have well-defined cytosolic substrates (3, 15, 21, 46, 75). Another important example includes platelets, which are anuclear, where over 200 proteins are acetylated by p300, including proteins involved in glucose metabolism (3).

Another reason for focusing on p300/CBP is because they are phosphorylated by both insulin stimulation (35, 77, 85) and Akt (37, 51, 52, 67). Akt is an obligatory protein in the insulin signaling pathway, with activation of Akt alone (without activation of upstream proteins) being sufficient to induce GLUT4 translocation to the plasma membrane (14, 20, 43, 56). Hence, it would be valuable to focus on acetyltransferases that have the potential to be phosphorylated by Akt. To this end, p300/CBP are the only acetyltransferases that are verified Akt substrates in the literature (10, 37, 51, 64, 67, 78). In addition, studies in 293T, HepG2, A549, OSU-2, and hepatic stellate

cells demonstrate that phosphorylation of p300/CBP, by Akt (19, 31, 37, 51, 67, 78), increases their acetyltransferase activity (37, 51, 52, 67), although this is not a universal finding (52).

Lastly, p300/CBP can acetylate insulin signaling and GLUT4 trafficking proteins downstream of Akt (80). A recent study utilizing a combination of inhibitors and genetic knockouts of p300/CBP in mouse embryonic fibroblasts have allowed for the identification of the p300/CBP regulated acetylome (80). Examples of insulin signaling and GLUT4 trafficking proteins downstream of Akt whose acetylation is regulated by p300/CBP include RAB8, RAB10, tether containing UBX domain for GLUT4 (TUG), kinesin family member 5B (KIF5B), and exocyst complex component 3 (EXOC3). This background, taken together, lends critical evidence to the existence of a possible Akt-p300/CBP axis, in which Akt phosphorylates and activates p300/CBP which, in turn, acetylates downstream proteins within the insulin signaling and GLUT4 trafficking pathway (Figure 1.1).

In conclusion, the current phosphorylation-based model of insulin signaling lacks viable, druggable, targets due to the pleiotropic nature of PI3K/Akt signaling (1, 16, 59). Thus, to address this, we propose acetylation, as a complement to phosphorylation, in the regulation of insulin-stimulated glucose uptake. The three studies of this Dissertation were designed to test the hypothesis that p300/CBP mediated acetylation in skeletal muscle is required for insulin action. Specifically, since chronic inhibition of deacetylases enhances skeletal muscle insulin action, in Study 1 we investigated whether acute inhibition of deacetylases would also enhance insulin action. Furthermore, because of the outlined premise that insulin signaling to glucose uptake could be regulated via a putative Akt-p300/CBP axis, in Study 2 and 3 we determined the contribution of p300 and/or CBP to skeletal muscle insulin-stimulated glucose uptake.

References

1. **Altomare DA**, **Testa JR**. Perturbations of the AKT signaling pathway in human cancer. *Oncogene* 24: 7455–7464, 2005.

2. **Arora A**, **Dey CS**. SIRT2 negatively regulates insulin resistance in C2C12 skeletal muscle cells. *Biochim Biophys Acta - Mol Basis Dis* 1842: 1372–1378, 2014.

3. **Aslan JE**, **Rigg RA**, **Nowak MS**, **Loren CP**, **Baker-Groberg SM**, **Pang J**, **David LL**, **McCarty OJT**. Lysine acetyltransfer supports platelet function. *J Thromb Haemost* 13: 1908–17, 2015.

4. **Atkins MB**, **Hidalgo M**, **Stadler WM**, **Logan TF**, **Dutcher JP**, **Hudes GR**, **Park Y**, **Liou SH**, **Marshall B**, **Boni JP**, **Dukart G**, **Sherman ML**. Randomized phase II study of multiple dose levels of CCI-779, a novel mammalian target of rapamycin kinase inhibitor, in patients with advanced refractory renal cell carcinoma. *J Clin Oncol* 22: 909–918, 2004.

5. **Belman JP**, **Bian RR**, **Habtemichael EN**, **Li DT**, **Jurczak MJ**, **Alcázar-Román A**, **McNally LJ**, **Shulman GI**, **Bogan JS**. Acetylation of TUG protein promotes the accumulation of GLUT4 glucose transporters in an insulin-responsive intracellular compartment. *J Biol Chem* 290: 4447–63, 2015.

6. **Bonadonna RC**, **Groop L**, **Kraemer N**, **Ferrannini E**, **Del Prato S**, **DeFronzo RA**. Obesity and insulin resistance in humans: a dose-response study. *Metabolism* 39: 452–9, 1990.

7. **Boyle JP**, **Thompson TJ**, **Gregg EW**, **Barker LE**, **Williamson DF**. Projection of the year 2050 burden of diabetes in the US adult population: dynamic modeling of incidence, mortality, and prediabetes prevalence. *Popul Health Metr* 8: 29, 2010.

8. **Centers for Disease Control and Prevention**. *National Diabetes Statistics Report: Estimates of Diabetes and Its Burden in the United States*. Atlanta, GA: US Department of Health and Human Services: 2014.

9. **Centers for Disease Control and Prevention**. National Diabetes Statistics Report, 2017. *Centers Dis. Control Prev. US Dep. Heal. Hum. Serv.* .

10. **Chen J**, **Halappanavar SS**, **St-Germain JR**, **Tsang BK**, **Li Q**. Role of Akt/protein kinase B in the activity of transcriptional coactivator p300. *Cell Mol Life Sci* 61: 1675–83, 2004.

11. **Choudhary C**, **Kumar C**, **Gnad F**, **Nielsen ML**, **Rehman M**, **Walther TC**, **Olsen J V**, **Mann M**. Lysine acetylation targets protein complexes and co-regulates major cellular functions. *Science* 325: 834–40, 2009.

12. **Choudhary C**, **Weinert BT**, **Nishida Y**, **Verdin E**, **Mann M**. The growing landscape of lysine acetylation links metabolism and cell signalling. *Nat Rev Mol Cell Biol* 15: 536–50, 2014.

13. **Cohen P**. The twentieth century struggle to decipher insulin signalling. *Nat Rev Mol Cell Biol* 7: 867–73, 2006.

14. **Cong LN**, **Chen H**, **Li Y**, **Zhou L**, **McGibbon MA**, **Taylor SI**, **Quon MJ**. Physiological role of AKT in insulin-stimulated translocation of GLUT4 in transfected rat adipose cells. *Mol Endocrinol* 11: 1881–1890, 1997.

15. **Dancy BM**, **Cole PA**. Protein lysine acetylation by p300/CBP. *Chem Rev* 115: 2419–52, 2015.

16. **Daragmeh J**, **Barriah W**, **Saad B**, **Zaid H**. Analysis of PI3K pathway components in human cancers. *Oncol Lett* 11: 2913–2918, 2016.

17. **DeFronzo RA**, **Gunnarsson R**, **Björkman O**, **Olsson M**, **Wahren J**. Effects of insulin on peripheral and splanchnic glucose metabolism in noninsulin-dependent (type II) diabetes mellitus. *J Clin Invest* 76: 149–55, 1985.

18. **DeFronzo RA**, **Jacot E**, **Jequier E**, **Maeder E**, **Wahren J**, **Felber JP**. The effect of insulin on the disposal of intravenous glucose. Results from indirect calorimetry and hepatic and femoral venous catheterization. *Diabetes* 30: 1000–7, 1981.

19. **Dou C**, **Liu Z**, **Tu K**, **Zhang H**, **Chen C**, **Yaqoob U**, **Wang Y**, **Wen J**, **van Deursen J**, **Sicard D**, **Tschumperlin D**, **Zou H**, **Huang WC**, **Urrutia R**, **Shah VH**, **Kang N**. P300 Acetyltransferase Mediates Stiffness-Induced Activation of Hepatic Stellate Cells Into Tumor-Promoting Myofibroblasts. *Gastroenterology* 154: 2209-2221.e14, 2018.

20. **Eyster CA**, **Duggins QS**, **Olson AL**. Expression of Constitutively Active Akt/Protein Kinase B Signals GLUT4 Translocation in the Absence of an Intact Actin Cytoskeleton. *J Biol Chem* 280: 17978–17985, 2005.

21. **Fermento ME**, **Gandini NA**, **Salomón DG**, **Ferronato MJ**, **Vitale CA**, **Arévalo J**, **López Romero A**, **Nuñez M**, **Jung M**, **Facchinetti MM**, **Curino AC**. Inhibition of p300 suppresses growth of breast cancer. Role of p300 subcellular localization. *Exp Mol Pathol* 97: 411–24, 2014.

22. **Fink RI**, **Kolterman OG**, **Griffin J**, **Olefsky JM**. Mechanisms of insulin resistance in aging. *J Clin Invest* 71: 1523–35, 1983.

23. **Fonseca VA**. Defining and characterizing the progression of type 2 diabetes. *Diabetes Care* 32 Suppl 2, 2009.

24. **Fröjdö S**, **Durand C**, **Molin L**, **Carey AL**, **El-Osta A**, **Kingwell BA**, **Febbraio MA**, **Solari F**, **Vidal H**, **Pirola L**. Phosphoinositide 3-kinase as a novel functional target for the regulation of the insulin signaling pathway by SIRT1. *Mol Cell Endocrinol* 335: 166–176, 2011.

25. **Furuyama T**, **Kitayama K**, **Yamashita H**, **Mori N**. Forkhead transcription factor F0X01 (FKHR)-dependent induction of PDK4 gene expression in skeletal muscle during energy

deprivation. *Biochem J* 375: 365–371, 2003.

26. **Gaur V**, **Connor T**, **Venardos K**, **Henstridge DC**, **Martin SD**, **Swinton C**, **Morrison S**, **Aston-Mourney K**, **Gehrig SM**, **van Ewijk R**, **Lynch GS**, **Febbraio MA**, **Steinberg GR**, **Hargreaves M**, **Walder KR**, **McGee SL**. Scriptaid enhances skeletal muscle insulin action and cardiac function in obese mice. *Diabetes, Obes Metab* 19: 936–943, 2017.

27. **Golay A**, **Defronzo RA**, **Thorin D**, **Jequier E**, **Felber JP**. Glucose disposal in obese non-diabetic and diabetic type II patients. A study by indirect calorimetry and euglycemic insulin clamp. *Diabete Metab* 14: 443–51, 1988.

28. **Groeneveld Y**, **Petri H**, **Hermans J**, **Springer MP**. Relationship between blood glucose level and mortality in type 2 diabetes mellitus: a systematic review. *Diabet Med* 16: 2–13, 1999.

29. **Gulli G**, **Ferrannini E**, **Stern M**, **Haffner S**, **Defronzo RA**. The metabolic profile of NIDDM is fully established in glucose-tolerant offspring of two Mexican-American NIDDM parents. *Diabetes* 41: 1575–1586, 1992.

30. **Guo S**. Insulin signaling, resistance, and the metabolic syndrome: insights from mouse models into disease mechanisms. *J Endocrinol* 220: T1–T23, 2014.

31. **Guo S**, **Cichy SB**, **He X**, **Yang Q**, **Ragland M**, **Ghosh AK**, **Johnson PF**, **Unterman TG**. Insulin suppresses transactivation by CAAT/enhancer-binding proteins beta (C/EBPbeta). Signaling to p300/CREB-binding protein by protein kinase B disrupts interaction with the major activation domain of C/EBPbeta. *J Biol Chem* 276: 8516–23, 2001.

32. **Harris MI**. Classification, Diagnostic Criteria, and Screening for Diabetes. *Diabetes Am. 2nd*. .

33. **He L**, **Cao J**, **Meng S**, **Ma A**, **Radovick S**, **Wondisford FE**. Activation of basal gluconeogenesis by coactivator p300 maintains hepatic glycogen storage. *Mol Endocrinol* 27: 1322–32, 2013.

34. **He L**, **Naik K**, **Meng S**, **Cao J**, **Sidhaye AR**, **Ma A**, **Radovick S**, **Wondisford FE**. Transcriptional Co-activator p300 maintains basal hepatic gluconeogenesis. *J Biol Chem* 287: 32069–32077, 2012.

35. **He L**, **Sabet A**, **Djedjos S**, **Miller R**, **Sun X**, **Hussain MA**, **Radovick S**, **Wondisford FE**. Metformin and Insulin Suppress Hepatic Gluconeogenesis through Phosphorylation of CREB Binding Protein. *Cell* 137: 635–646, 2009.

36. **Huang ES**, **Basu A**, **O'Grady M**, **Capretta JC**. Projecting the future diabetes population size and related costs for the U.S. *Diabetes Care* 32: 2225–9, 2009.

37. **Huang W-C**, **Chen C-C**. Akt phosphorylation of p300 at Ser-1834 is essential for its histone acetyltransferase and transcriptional activity. *Mol Cell Biol* 25: 6592–602, 2005.

38. **Ihle NT**, **Paine-murrieta G**, **Berggren MI**, **Baker A**, **Wendy R**, **Wipf P**, **Abraham RT**, **Kirkpatrick DL**, **Powis G**. NIH Public Access. 4: 1349–1357, 2006.

39. **Kahn CR**. Insulin Action, Diabetogenes, and the Cause of Type II Diabetes. *Diabetes* 43: 1066–1085, 1994.

40. **Karakelides H**, **Irving BA**, **Short KR**, **O'Brien P**, **Nair KS**. Age, obesity, and sex effects on insulin sensitivity and skeletal muscle mitochondrial function. *Diabetes* 59: 89–97, 2010.

41. **Kim SC**, **Sprung R**, **Chen Y**, **Xu Y**, **Ball H**, **Pei J**, **Cheng T**, **Kho Y**, **Xiao H**, **Xiao L**, **Grishin N V.**, **White M**, **Yang X-J**, **Zhao Y**. Substrate and functional diversity of lysine acetylation revealed by a proteomics survey. *Mol Cell* 23: 607–18, 2006.

42. **Kimura A**, **Matsubara K**, **Horikoshi M**. A decade of histone acetylation: marking eukaryotic chromosomes with specific codes. *J Biochem* 138: 647–62, 2005.

43. **Kohn AD**, **Summers SA**, **Birnbaum MJ**, **Roth RA**. Expression of a constitutively active Akt Ser/Thr kinase in 3T3-L1 adipocytes stimulates glucose uptake and glucose transporter 4 translocation. *J Biol Chem* 271: 31372–31378, 1996.

44. **Kohrt WM**, **Kirwan JP**, **Staten MA**, **Bourey RE**, **King DS**, **Holloszy JO**. Insulin resistance in aging is related to abdominal obesity. *Diabetes* 42: 273–81, 1993.

45. **Koo SH**, **Flechner L**, **Qi L**, **Zhang X**, **Screaton RA**, **Jeffries S**, **Hedrick S**, **Xu W**, **Boussouar F**, **Brindle P**, **Takemori H**, **Montminy M**. The CREB coactivator TORC2 is a key regulator of fasting glucose metabolism. *Nature* 437: 1109–1114, 2005.

46. **Kuhlmann N**, **Wroblowski S**, **Knyphausen P**, **de Boor S**, **Brenig J**, **Zienert AY**, **Meyer-Teschendorf K**, **Praefcke GJK**, **Nolte H**, **Krüger M**, **Schacherl M**, **Baumann U**, **James LC**, **Chin JW**, **Lammers M**. Structural and Mechanistic Insights into the Regulation of the Fundamental Rho Regulator RhoGDIα by Lysine Acetylation. *J Biol Chem* 291: 5484–99, 2016.

47. **LaBarge S**, **Migdal C**, **Schenk S**. Is acetylation a metabolic rheostat that regulates skeletal muscle insulin action? *Mol Cells* 38: 297–303, 2015.

48. **Lantier L**, **Williams AS**, **Williams IM**, **Yang KK**, **Bracy DP**, **Goelzer M**, **James FD**, **Gius D**, **Wasserman DH**. SIRT3 Is Crucial for Maintaining Skeletal Muscle Insulin Action and Protects Against Severe Insulin Resistance in High-Fat–Fed Mice. *Diabetes* 64: 3081–3092, 2015.

49. **Leto D**, **Saltiel AR**. Regulation of glucose transport by insulin: traffic control of GLUT4. *Nat Rev Mol Cell Biol* 13: 383–96, 2012.

50. **Lillioja S**, **Mott DM**, **Spraul M**, **Ferraro R**, **Foley JE**, **Ravussin E**, **Knowler WC**, **Bennett PH**, **Bogardus C**. Insulin Resistance and Insulin Secretory Dysfunction as Precursors of Non-Insulin-Dependent Diabetes Mellitus: Prospective Studies of Pima Indians. *N Engl J Med* 329: 1988–1992, 1993.

51. **Liu Y**, **Denlinger CE**, **Rundall BK**, **Smith PW**, **Jones DR**. Suberoylanilide hydroxamic acid induces Akt-mediated phosphorylation of p300, which promotes acetylation and transcriptional activation of RelA/p65. *J Biol Chem* 281: 31359–31368, 2006.

52. **Liu Y**, **Xing Z**, **Zhang J**, **Fang Y**. Akt kinase targets the association of CBP with histone H3 to regulate the acetylation of lysine K18. *FEBS Lett* 587: 847–853, 2013.

53. **Lundby A**, **Lage K**, **Weinert BT**, **Bekker-Jensen DB**, **Secher A**, **Skovgaard T**, **Kelstrup CD**, **Dmytriyev A**, **Choudhary C**, **Lundby C**, **Olsen J V**. Proteomic analysis of lysine acetylation sites in rat tissues reveals organ specificity and subcellular patterns. *Cell Rep* 2: 419–31, 2012.

54. **Lundell LS**, **Massart J**, **Altıntaş A**, **Krook A**, **Zierath JR**. Regulation of glucose uptake and inflammation markers by FOXO1 and FOXO3 in skeletal muscle. *Mol Metab* 20: 79–88, 2019.

55. **McGee SL**, **Van Denderen BJW**, **Howlett KF**, **Mollica J**, **Schertzer JD**, **Kemp BE**, **Hargreaves M**. AMP-activated protein kinase regulates GLUT4 transcription by phosphorylating histone deacetylase 5. *Diabetes* 57: 860–867, 2008.

56. **Ng Y**, **Ramm G**, **Lopez JA**, **James DE**. Rapid activation of Akt2 is sufficient to stimulate GLUT4 translocation in 3T3-L1 adipocytes. *Cell Metab* 7: 348–56, 2008.

57. **Ogryzko V V**, **Schiltz RL**, **Russanova V**, **Howard BH**, **Nakatani Y**. The Transcriptional Coactivators p300 and CBP Are Histone Acetyltransferases. *Cell* 87: 953–959, 1996.

58. **Olokoba AB**, **Obateru OA**, **Olokoba LB**. Type 2 diabetes mellitus: A review of current trends. *Oman Med J* 27: 269–273, 2012.

59. **Porta C**, **Paglino C**, **Mosca A**. Targeting PI3K/Akt/mTOR Signaling in Cancer. *Front Oncol* 4: 1–11, 2014.

60. **Raichur S**, **Teh SH**, **Ohwaki K**, **Gaur V**, **Long YC**, **Hargreaves M**, **McGee SL**, **Kusunoki J**. Histone deacetylase 5 regulates glucose uptake and insulin action in muscle cells. *J Mol Endocrinol* 49: 203–211, 2012.

61. **Ravnskjaer K**, **Kester H**, **Liu Y**, **Zhang X**, **Lee D**, **Yates JR**, **Montminy M**. Cooperative interactions between CBP and TORC2 confer selectivity to CREB target gene expression. *EMBO J* 26: 2880–2889, 2007.

62. **Ravussin E**, **Bogardus C**, **Schwartz RS**, **Robbins DC**, **Wolfe RR**, **Horton ES**, **Danforth E**. Thermic effect of infused glucose and insulin in man. Decreased response with increased insulin resistance in obesity and noninsulin-dependent diabetes mellitus. *J Clin Invest* 72: 893–902, 1983.

63. **Rhodes N**, **Heerding DA**, **Duckett DR**, **Eberwein DJ**, **Knick VB**, **Lansing TJ**, **McConnell RT**, **Gilmer TM**, **Zhang SY**, **Robell K**, **Kahana JA**, **Geske RS**, **Kleymenova E V.**, **Choudhry AE**, **Lai Z**, **Leber JD**, **Minthorn EA**, **Strum SL**, **Wood ER**, **Huang PS**,

Copeland RA, **Kumar R**. Characterization of an Akt kinase inhibitor with potent pharmacodynamic and antitumor activity. *Cancer Res* 68: 2366–2374, 2008.

64. **Roth U**, **Curth K**, **Unterman TG**, **Kietzmann T**. The transcription factors HIF-1 and HNF-4 and the coactivator p300 are involved in insulin-regulated glucokinase gene expression via the phosphatidylinositol 3-kinase/protein kinase B pathway. *J Biol Chem* 279: 2623–31, 2004.

65. **Rowe JW**, **Minaker KL**, **Pallotta JA**, **Flier JS**. Characterization of the insulin resistance of aging. *J Clin Invest* 71: 1581–7, 1983.

66. **Ruiz L**, **Gurlo T**, **Ravier MA**, **Wojtusciszyn A**, **Mathieu J**, **Brown MR**, **Broca C**, **Bertrand G**, **Butler PC**, **Matveyenko A V**, **Dalle S**, **Costes S**. Proteasomal degradation of the histone acetyl transferase p300 contributes to beta-cell injury in a diabetes environment. *Cell Death Dis* 9: 600, 2018.

67. **Sanchez M**, **Sauvé K**, **Picard N**, **Tremblay A**. The hormonal response of estrogen receptor beta is decreased by the phosphatidylinositol 3-kinase/Akt pathway via a phosphorylation-dependent release of CREB-binding protein. *J Biol Chem* 282: 4830–40, 2007.

68. **Schenk S**, **McCurdy CE**, **Philp A**, **Chen MZ**, **Holliday MJ**, **Bandyopadhyay GK**, **Osborn O**, **Baar K**, **Olefsky JM**. Sirt1 enhances skeletal muscle insulin sensitivity in mice during caloric restriction. *J Clin Invest* 121: 4281–8, 2011.

69. **Sun C**, **Zhou J**. Trichostatin A improves insulin stimulated glucose utilization and insulin signaling transduction through the repression of HDAC2. *Biochem Pharmacol* 76: 120–127, 2008.

70. **Sundaresan NR**, **Pillai VB**, **Wolfgeher D**, **Samant S**, **Vasudevan P**, **Parekh V**, **Raghuraman H**, **Cunningham JM**, **Gupta M**, **Gupta MP**. The deacetylase SIRT1 promotes membrane localization and activation of Akt and PDK1 during tumorigenesis and cardiac hypertrophy. *Sci Signal* 4: ra46, 2011.

71. **Svensson K**, **LaBarge SA**, **Martins VF**, **Schenk S**. Temporal overexpression of SIRT1 in skeletal muscle of adult mice does not improve insulin sensitivity or markers of mitochondrial biogenesis. *Acta Physiol* 221: 193–203, 2017.

72. **TAKIGAWA-IMAMURA H**, **SEKINE T**, **MURATA M**, **TAKAYAMA K**, **NAKAZAWA K**, **NAKAGAWA J**. Stimulation of Glucose Uptake in Muscle Cells by Prolonged Treatment with Scriptide, a Histone Deacetylase Inhibitor. *Biosci Biotechnol Biochem* 67: 1499–1506, 2003.

73. **Taniguchi CM**, **Emanuelli B**, **Kahn CR**. Critical nodes in signalling pathways: insights into insulin action. *Nat Rev Mol Cell Biol* 7: 85–96, 2006.

74. **Turner BM**. Histone acetylation and control of gene expression. *J Cell Sci* 99 (Pt 1): 13–20, 1991.

75. **Ventura M**, **Mateo F**, **Serratosa J**, **Salaet I**, **Carujo S**, **Bachs O**, **Pujol MJ**. Nuclear translocation of glyceraldehyde-3-phosphate dehydrogenase is regulated by acetylation. *Int J Biochem Cell Biol* 42: 1672–80, 2010.

76. **Verdin E**, **Ott M**. 50 years of protein acetylation: from gene regulation to epigenetics, metabolism and beyond. *Nat Rev Mol Cell Biol* 16: 258–64, 2015.

77. **Wan W**, **You Z**, **Xu Y**, **Zhou L**, **Guan Z**, **Peng C**, **Wong CCL**, **Su H**, **Zhou T**, **Xia H**, **Liu W**. mTORC1 Phosphorylates Acetyltransferase p300 to Regulate Autophagy and Lipogenesis. *Mol Cell* 68: 323-335.e6, 2017.

78. **Wang QE**, **Han C**, **Zhao R**, **Wani G**, **Zhu Q**, **Gong L**, **Battu A**, **Racoma I**, **Sharma N**, **Wani AA**. P38 MAPK- and Akt-mediated p300 phosphorylation regulates its degradation to facilitate nucleotide excision repair. *Nucleic Acids Res* 41: 1722–1733, 2013.

79. **Weems J**, **Olson AL**. Class II histone deacetylases limit GLUT4 gene expression during adipocyte differentiation. *J Biol Chem* 286: 460–468, 2011.

80. **Weinert BT**, **Narita T**, **Satpathy S**, **Srinivasan B**, **Hansen BK**, **Schölz C**, **Hamilton WB**, **Zucconi BE**, **Wang WW**, **Liu WR**, **Brickman JM**, **Kesicki EA**, **Lai A**, **Bromberg KD**, **Cole PA**, **Choudhary C**. Time-Resolved Analysis Reveals Rapid Dynamics and Broad Scope of the CBP/p300 Acetylome. *Cell* 174: 231-244.e12, 2018.

81. **Wondisford AR**, **Xiong L**, **Chang E**, **Meng S**, **Meyers DJ**, **Li M**, **Cole PA**, **He L**. Control of Foxo1 Gene Expression by Co-activator p300. *J Biol Chem* 289: 4326–4333, 2014.

82. **Yau JWY**, **Rogers SL**, **Kawasaki R**, **Lamoureux EL**, **Kowalski JW**, **Bek T**, **Chen S-J**, **Dekker JM**, **Fletcher A**, **Grauslund J**, **Haffner S**, **Hamman RF**, **Ikram MK**, **Kayama T**, **Klein BEK**, **Klein R**, **Krishnaiah S**, **Mayurasakorn K**, **O'Hare JP**, **Orchard TJ**, **Porta M**, **Rema M**, **Roy MS**, **Sharma T**, **Shaw J**, **Taylor H**, **Tielsch JM**, **Varma R**, **Wang JJ**, **Wang N**, **West S**, **Xu L**, **Yasuda M**, **Zhang X**, **Mitchell P**, **Wong TY**, **Meta-Analysis for Eye Disease (META-EYE) Study Group**. Global prevalence and major risk factors of diabetic retinopathy. *Diabetes Care* 35: 556–64, 2012.

83. **Zhang J**. The direct involvement of SirT1 in insulin-induced insulin receptor substrate-2 tyrosine phosphorylation. *J Biol Chem* 282: 34356–34364, 2007.

84. **Zhao S**, **Xu W**, **Jiang W**, **Yu W**, **Lin Y**, **Zhang T**, **Yao J**, **Zhou L**, **Zeng Y**, **Li H**, **Li Y**, **Shi J**, **An W**, **Hancock SM**, **He F**, **Qin L**, **Chin J**, **Yang P**, **Chen X**, **Lei Q**, **Xiong Y**, **Guan K-L**. Regulation of cellular metabolism by protein lysine acetylation. *Science* 327: 1000–4, 2010.

85. **Zhou XY**, **Shibusawa N**, **Naik K**, **Porras D**, **Temple K**, **Ou H**, **Kaihara K**, **Roe MW**, **Brady MJ**, **Wondisford FE**. Insulin regulation of hepatic gluconeogenesis through phosphorylation of CREB-binding protein. *Nat Med* 10: 633–637, 2004.

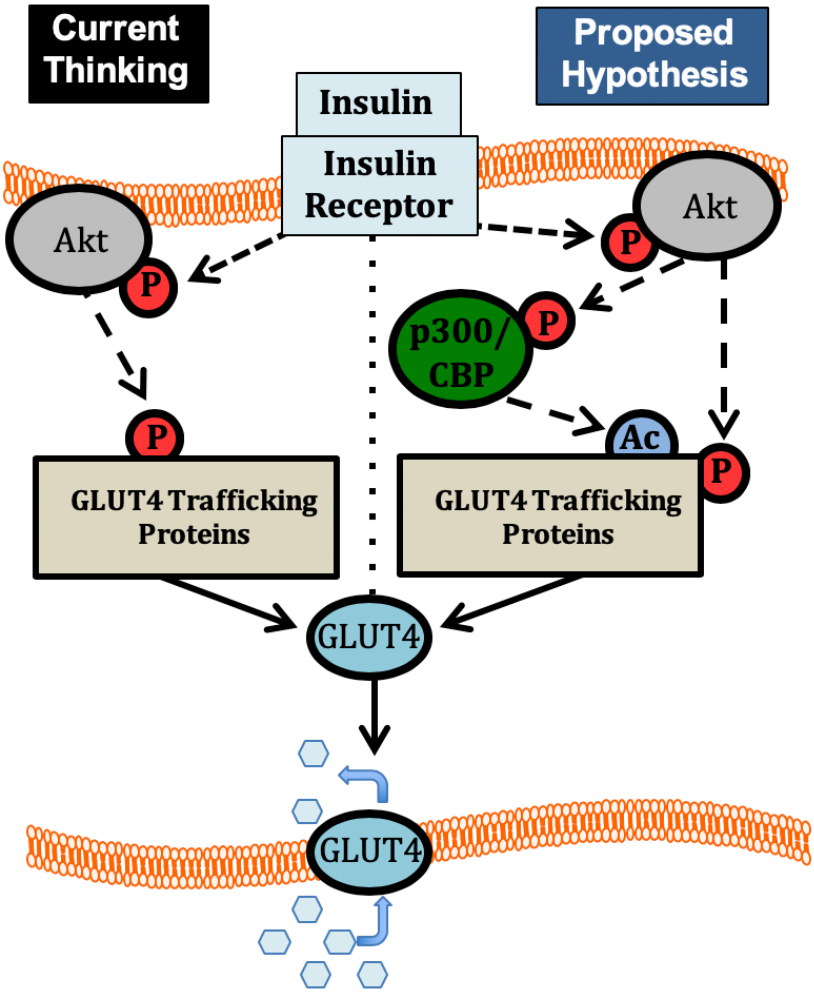

Figure 1.1. Regulation of insulin-stimulated glucose uptake. Canonical insulin signaling (left) is mediated by a phosphorylation-dependent (P), Akt-mediated signaling pathway leading to the translocation of GLUT4 to the plasma membrane, allowing for facilitated transport of glucose (blue hexagons). This Dissertation (right) proposes an additional, but necessary level of regulation by acetylation (Ac), in which Akt phosphorylates p300/CBP, leading to acetylation of downstream GLUT4 trafficking proteins, inducing GLUT4 trafficking and glucose uptake.

CHAPTER 2

Acute inhibition of protein deacetylases does not impact skeletal muscle insulin action

Abstract

Introduction: Whether the histone deacetylase (HDAC) and sirtuin families of protein deacetylases regulate insulin-stimulated glucose uptake, independent of their transcriptional effects, has not been studied. Our objective herein was to determine the non-transcriptional role of HDACs and sirtuins in regulating skeletal muscle insulin action.

Methods: Basal and insulin-stimulated glucose uptake and signaling, and acetylation were assessed in L6 myotubes and skeletal muscle from C57BL/6J mice that were treated acutely (1 hour) with HDAC (trichostatin A, panobinostat, TMP195) and sirtuin inhibitors (nicotinamide).

Results: Treatment of L6 myotubes with HDAC inhibitors, or skeletal muscle with a combination of HDAC and sirtuin inhibitors increased tubulin and pan-protein acetylation, demonstrating effective impairment of HDAC and sirtuin deacetylase activities. Despite this, neither basal or insulin-stimulated glucose uptake or insulin signaling were impacted.

Conclusions: Acutely reducing the deacetylase activity of HDACs and/or sirtuins does not impact insulin action in skeletal muscle.

Introduction

Insulin-mediated glucose uptake by skeletal muscle is posited to occur through phosphorylation-based signaling (9). Interestingly, various proteins within the insulin signaling and GLUT4 trafficking pathway are reversibly acetylated on lysine residues (3, 11, 27), with direct changes in their acetylation altering their activity (3, 23, 27). Lysine acetylation is a balance between the activity of protein acetyltransferases and deacetylases, which add and remove acetyl groups, respectively (5). There are 18 known deacetylases that are divided into 2 families: the zinc-dependent histone deacetylases (HDACs) and NAD^+-dependent sirtuins (5). Indeed, both the HDACs (17, 20, 22, 25, 26) and the sirtuins (1, 7, 13, 21, 24) have been implicated in the regulation of insulin-stimulated glucose uptake in skeletal muscle. Importantly, however, this regulation appears to primarily occur via acetylation of transcriptional regulators and/or histones, and subsequent changes in the transcription of insulin signaling proteins (17, 20, 21, 26). To our knowledge, the ability of these deacetylases to non-transcriptionally (i.e. "directly") regulate insulin-stimulated glucose uptake, particularly in insulin-responsive tissues such as skeletal muscle, has not been thoroughly studied. Notably, while previous studies have demonstrated that pharmacological inhibition of deacetylases enhances insulin action in skeletal muscle (8, 17, 20, 22, 25), because incubation times were for multiple days, this enhancement could be via changes in transcription of insulin signaling proteins, acetylation of cytosolic insulin signaling proteins, or a combination of the two.

Thus, the primary goal of this study was to investigate the non-transcriptional contribution of HDACs and sirtuins to insulin-mediated glucose uptake in skeletal muscle. For this, we assessed basal- and insulin-stimulated glucose uptake in L6 myotubes and mouse skeletal muscle after brief

(i.e. 1 hour) pharmacological inhibition of HDACs and/or sirtuins. We hypothesized that, similar to chronic inhibition, acute inhibition of deacetylases would augment insulin-stimulated glucose uptake in skeletal muscle.

Methods

Cell culture conditions. L6 myoblasts were maintained in Minimum Essential Media *a* (MEM*a*) with 10% fetal bovine serum (FBS) at 5% CO_2 and 37°C. Myoblasts were differentiated into myotubes in MEM*a* with 2% FBS for 4 days.

Inhibitors. Trichostatin A (9950S) was from Cell Signaling, nicotinamide (98092-0) was from Sigma-Aldrich, panobinostat (A8178) was from Apexbio Technology, and TMP195 was from Selleck Chemical (NC1452975). The IC_{50} for inhibitors is shown in Table 1.1 (2, 4, 14).

Flow cytometry. L6 myoblasts were serum-starved, in suspension, for 3 hours in 0.5% fatty-acid free BSA in MEM*a*, followed by 1.5 hours in HEPES-buffered Krebs-Ringer bicarbonate buffer (HKRB; 10mM HEPES, 4.8mM KCL, 1mM $CaCl_2$, 1mM $MgCl_2$, 0.5% fatty-acid free BSA in Dulbecco's Phospho-buffered saline [DPBS]) with DMSO or inhibitors, *at 37℃*. Myoblasts were fixed in 2% paraformaldehyde at room temperature (RT) for 30 minutes, washed 2x with DPBS, permeabilized with 0.5% saponin at RT for 30 minutes, and incubated with Alexa Fluor-647-labeled acetylated-lysine (Ac-Lys; 1:20 dilution; Biolegend 623405) at RT for 30 minutes. Cells were then washed 1x with DPBS and resuspended in 500µL DPBS. Flow cytometric acquisitions were performed using a ZE5 Cell Analyzer (Bio-Rad) and analyzed using FloJo (Treestar, Ashland, OR). In all cases at least 5,000 cells were counted.

L6 myotube 2-deoxy-D-glucose uptake. L6 myotubes were treated, as above, but adherent to 24-well plates. For the last 30 minutes in HKRB, 100nM insulin was present, followed by a 10 minute incubation with 1mM 2-[^{3}H]-deoxy-D-glucose (2DOG; 6 mCi/mmol, PerkinElmer). Cells were washed twice with ice-cold DPBS, lysed with 1M NaOH, neutralized with 1M HCl, and radioactivity of cell lysates were measured using a liquid scintillation counter.

Radioactivity was normalized to the protein concentration of each sample, using the Pierce BCA protein assay kit. Data was normalized to cells treated with DMSO and no insulin, within each experiment.

Immunoprecipitation. Protein A and G magnetic beads (25/25 μL; Bio-Rad Laboratories, Hercules, CA, USA) were washed three times with PBS with 0.1% Tween 20 (PBS-T). Anti-acetyl-lysine (AAC01; Cytoskeleton, Denver, CO, USA) was then added to the bead mixture and rotated end over end for 1 hour (4ºC). Subsequently, beads were washed three more times with PBS-T and then 180 μg of whole cell lysate, from the tibialis anterior, were added and the samples were rotated overnight (4ºC). The following morning, beads were washed three times with PBS-T, and antigens were eluted with 1X Laemmli sample buffer (40 μL). Samples were boiled for 6 min, and lysate was removed from protein A/G magnetic beads via a magnetic rack (Bio-Rad) prior to SDS-PAGE.

Immunoblotting. Equivalent amounts of protein (15 μg) were separated on XT Criterion Precast gels (Bio-Rad) under reducing conditions, and transferred to Amersham Protran nitrocellulose membranes (MilliporeSigma, Burlington, MA, USA). Membranes were reversibly stained with a ponceau S solution (0.1% (w/v) ponceau S in 5% acetic acid), blocked in 5% milk/TBST and incubated overnight in primary antibodies. Subsequently, membranes were incubated for 1 h at room temperature in relevant secondary antibodies and developed using chemiluminescence horseradish peroxidase. For immunoblotting, all antibodies were used at a dilution of 1:1000. Akt (CS 9272B), phosphorylated (p)Akt^{T308} (CS 9275), pAkt^{S473} (CS 4058), glycogen synthase kinase 3 α/β (GSK3α/β; CS 5676), pGSK3α/β$^{S21/9}$ (CS 9331), eukaryotic elongation factor 2 (eEF2; CS 2332), acetylated-tubulin (Ac-tubulin; CS 5335) and tubulin (CS 2148) were from Cell Signaling. Densitometric analysis of immunoblots was performed using

Image Lab (Bio-Rad, Hercules, CA, USA). Phosphorylated and acetylated protein abundance was normalized to respective total protein abundance. Gels used for silver staining were assayed according to manufacturer's instructions (Pierce Silver Stain Kit 24612; Thermo Scientific, Waltham, MA, USA). All bands on the silver stain were quantified together (excluding the IgG bands) and normalized to the IgG band at 25 kDa.

Mice. Studies were conducted in female C57BL/6J mice housed in a conventional facility with a 12-h light/12-h dark cycle. Procedures were carried out with the approval of, and in accordance with, the Animal Care Program and Institutional Animal Care and Use Committee at the University of California, San Diego.

Muscle 2DOG uptake. Ex vivo muscle insulin sensitivity was measured by the 2DOGU technique as previously described (16, 21), with some modifications. Fasted (4 hours) mice were anesthetized and paired soleus and extensor digitorum longus (EDL) muscles were incubated at 35°C for 60 minutes in oxygenated (95% O2, 5% CO2) flasks of Krebs-Henseleit buffer (KHB) containing 0.1% BSA, 2 mM Na-pyruvate, and 6 mM mannitol plus DMSO or inhibitors. After 60 minutes, muscles were transferred to a second flask and incubated at 35°C for 20 minutes in KHB plus 0.1% BSA, 9 mM [14C]-mannitol (0.053 mCi/mmol; PerkinElmer), and 1 mM [3H]-2DG (6 mCi/mmol; PerkinElmer), with muscles from one side being exposed to insulin (60 μU/ml [0.36 nM]; Humulin R, Eli Lilly and Company) and the contralateral side to no insulin. During this incubation, muscles continued to be incubated with DMSO or inhibitors. After the second incubation phase, muscles were blotted on ice cold filter paper, trimmed, freeze-clamped, and then stored (−80°C).

Statistical analysis. Statistical analyses were performed using Prism 8 (GraphPad Software Incorporated, La Jolla, CA). L6 myotube 2DOG uptake, muscle 2DOG uptake, and

phosphorylated-proteins (Insulin x inhibitor) were analyzed by 2-way ANOVA. Acetylated-tubulin in L6 myotubes, and Ac-Lys flow cytometry were analyzed by 1-way ANOVA with Tukey's multiple comparison test. Muscle insulin-stimulated 2DOG uptake, and acetylated-tubulin and Akt were analyzed by Student's *t*-test. All data are expressed as mean ± SEM.

Results

Acute inhibition of HDACs does not affect insulin-stimulated glucose uptake in L6 myotubes. Treating L6 myoblasts for 1.5h with the pan-HDAC inhibitor trichostatin A led to a dose-dependent increase in lysine-acetylated proteins, as assessed by flow cytometry (Figure 2.1A-C). Validating this flow-based approach, the difference in signal between unstained L6 myoblasts and stained but unpermeabilized (i.e. no saponin) L6 myoblasts was not statistically significant (Figure 2.1C). In addition to increasing pan-protein lysine acetylation, trichostatin A dose-dependently increased the acetylation of a cytosolic target of HDACs, tubulin, in L6 myotubes (Figure 2.1D). Insulin increased glucose uptake ~2.5-fold in DMSO-treated L6 myotubes, as compared to basal (Figure 2.1E). One-hour pre-treatment with increasing doses of trichostatin A did not impact basal or insulin-stimulated 2DOG uptake in L6 myotubes (Figure 2.1E). Furthermore, basal and insulin-stimulated phosphorylation of Akt^{T308}, Akt^{S473}, and $GSK3\beta^{S9}$ were comparable between DMSO- and trichostatin A-treated L6 myotubes, regardless of the trichostatin A concentration (Figure 2.1F-G). Similarly, while one-hour pre-treatment of L6 myotubes with an alternate HDAC inhibitor, panobinostat, dose-dependently increased tubulin-acetylation, basal and insulin-stimulated glucose uptake were comparable to DMSO-treated myotubes (Figure 2.1H). Since we were interested in the non-nuclear effects of inhibiting HDACs, we utilized TMP195 which is a potent inhibitor of the class IIa HDACs (14), which are, at least partly, found in the cytosol (10). Nevertheless, one-hour pre-treatment with TMP195 had no effect on basal or insulin-stimulated glucose uptake (Figure 2.1I). Lastly, we utilized a combination of trichostatin A (4μM) and nicotinamide (1mM, 10mM, 20mM) in order to inhibit both the HDAC and sirtuin families in L6 myotubes. Joint pre-incubation of L6 myotubes with trichostatin A and nicotinamide for 1 hour

did not affect basal or insulin-stimulated 2DOG uptake, as compared to DMSO (Figure 2.1J).

Concurrent inhibition of HDACs and sirtuins does not affect insulin-stimulated glucose uptake in skeletal muscle ex vivo. To validate these *in vitro* findings, we studied mature mouse skeletal muscle. Pre-treatment of mouse soleus with trichostatin A (4μM) and nicotinamide (20mM) for 1-hour resulted in a ~20% increase in total protein acetylation, as measured in immunoprecipitates using a pan acetyl-lysine antibody (Figure 2.2A), and an ~8-fold increase in acetylated-tubulin (Figure 2.2B); however, there were no changes in acetylated-Akt (Figure 2.2B). Pre-treatment of either the soleus or EDL with trichostatin A and nicotinamide did not affect basal, insulin, or insulin-stimulated (i.e. insulin 2DOG uptake minus basal 2DOG uptake) 2DOG uptake, as compared to DMSO treatment (Figure 2.2C-D). Likewise, basal and insulin-stimulated phosphorylation of Akt^{T308}, Akt^{S473}, and $GSK3\beta^{S9}$ were comparable between DMSO- and trichostatin A and nicotinamide-treated EDL muscles (Figure 2.2E).

Discussion

Both the HDAC (17, 20, 22, 25, 26) and sirtuin (1, 7, 13, 21, 24) deacetylase families have been extensively studied for their role in the transcriptional modulation of skeletal muscle insulin action. However, as insulin signaling and GLUT4 trafficking proteins can be reversibly acetylated (3, 11, 23), which alters their function (3, 23, 27), it is possible that HDACs and sirtuins could also impact skeletal muscle insulin action through non-transcriptional mechanisms. To address this, we acutely inhibited the HDAC and/or sirtuin deacetylase families for one hour and assessed insulin-stimulated glucose uptake in L6 myotubes and mature mouse skeletal muscle. Our results demonstrate that brief inhibition of the HDAC and/or sirtuin families does not impact insulin-stimulated glucose uptake or signaling in skeletal muscle.

Using both knockdown and overexpression models, several of the eleven HDACs have been implicated in the transcriptional regulation of insulin signaling proteins (17, 20, 22, 25, 26). For example, HDACs 4 and 9 work in conjunction with HDAC5, to transcriptionally repress the GLUT4 gene via the deacetylation of GLUT4 enhancer factor and myocyte enhancer factor 2 (17, 20, 26). When considering inhibitor-based studies, 24-hour treatment with trichostatin A, a commonly used HDAC inhibitor, increases insulin-stimulated glucose uptake, and phosphorylation of Akt^{S473} and $GSK3\beta^{S9}$ in C2C12 myotubes (22). This increase, however, is not manifested with 6 or 12 hours of treatment (22). Likewise, at least 24 hour treatment with another HDAC inhibitor, scriptaid, increased GLUT4 mRNA expression in human primary muscle cells (17, 20)**,** basal and insulin-stimulated glucose uptake in L6 myotubes (20, 25)**,** and insulin-stimulated glucose uptake in isolated EDL muscles of obese mice (8). Importantly, however, treatment with scriptaid or trichostatin A for less than 24 hours does not increase insulin-stimulated

glucose uptake in L6 myotubes (25). In accordance with previous studies, we demonstrate that brief (1 hour) pre-treatment with HDAC inhibitors (trichostatin A, panobinostat, or TMP195) did not improve basal or insulin-stimulated glucose uptake in L6 myotubes. Furthermore, while acute treatment with trichostatin A was sufficient to increase both pan acetylation and acetylation of a cytosolic HDAC target (tubulin), it did not alter insulin-stimulated phosphorylation of Akt^{T308}, Akt^{S473}, or $GSK3\beta^{S9}$ in L6 myotubes. Hence, our results, together with the previous literature, demonstrate that HDAC inhibitors likely improve insulin action through transcriptional mechanisms.

The contribution of the sirtuins to skeletal muscle insulin action has been heavily studied (1, 7, 13, 21, 24). In L6 myotubes, SIRT1 overexpression increases, while SIRT1 knockdown reduces, insulin-stimulated phosphorylation of Akt (7). Furthermore, prolonged incubation (6 hours) of H4IIE rat hepatoma liver cells with nicotinamide reduces insulin-stimulated phosphorylation of Akt (27). Conversely, however, SIRT2 knockdown improves insulin-stimulated glucose uptake and phosphorylation of Akt and GSK3β in C2C12 myotubes grown in insulin-resistant conditions (1). In *in vivo* mouse models, knockout or overexpression of SIRT1 in skeletal muscle does not impact insulin sensitivity (21, 24), although SIRT1 does mediate calorie restriction-induced enhancement of skeletal muscle insulin sensitivity via a transcriptional mechanism (21). Furthermore, mice with whole-body knockout of SIRT2 have impaired skeletal muscle insulin sensitivity, while mice with a knockout of SIRT2 (12) or SIRT3 (13) have exacerbated skeletal muscle insulin resistance while on a high-fat diet; however, due to the whole-body nature of these models it is not possible to determine the role of SIRT2 or SIRT3 in skeletal muscle, per se. Regardless, these studies do not discern whether sirtuins regulate insulin action via transcriptional or non-transcriptional mechanisms. Addressing this, we found that insulin-stimulated glucose

uptake in L6 myotubes is not affected by acute incubation with trichostatin A and nicotinamide. Similarly, in mature mouse muscle, while acute treatment with trichostatin A and nicotinamide was sufficient to increase overall protein acetylation, including increased acetylated-tubulin, there was no effect on insulin-stimulated glucose uptake, regardless of muscle fiber type. Furthermore, acute trichostatin A and nicotinamide treatment did not alter acetylated-Akt levels or insulin-stimulated phosphorylation of Akt^{T308}, Akt^{S473}, or $GSK3\beta^{S9}$. Hence, while there is evidence for both sirtuins and HDACs altering insulin action in skeletal muscle via transcriptional mechanisms, our data demonstrate that short-term, pan-inhibition of deacetylases does not alter skeletal muscle insulin sensitivity.

While the purpose of the study was to determine the effects of acute deacetylase inhibition, a possible limitation was our choice of incubation time. Importantly, in both L6 myotubes and mature mouse muscle, pan-acetylated proteins as well as acetylated tubulin, which is a cytosolic target of deacetylases (6), was significantly increased by only 1 hour treatment with deacetylase inhibitors. Furthermore, time-course studies in C2C12 myotubes and SH-SY5Y neuroblastoma cells have established that 3-4 hours incubation with trichostatin A is the earliest time point at which there are significant changes in mRNA expression of HDAC target genes, with no significant changes at 1-2 hours of treatment (15, 18, 19). Together with this, previous studies only demonstrate changes to insulin signaling and/or glucose uptake with at least 24 hours of treatment with inhibitors of deacetylases (8, 22, 25). Therefore, we believe that the one-hour preincubation period used was sufficient to impair HDAC and/or sirtuin function and sufficiently short to investigate insulin action independent of effects on gene expression.

In summary, we studied the non-transcriptional role of HDACs and sirtuins in the regulation of insulin action in skeletal muscle. In contrast to our hypothesis, we found that acute, pan-

inhibition of HDACs and/or sirtuins in L6 myotubes or mature mouse muscle does not enhance insulin-stimulated signaling or glucose uptake. Taken together, our results suggest that deacetylases do not "directly" modulate skeletal muscle insulin action, but rather do so "indirectly" via transcriptional mechanisms.

Acknowledgments

This work was supported, in part, by U.S. National Institutes of Health grants R01 AG043120 (to S.S.), T32 AR060712 and F30 DK115035 (to V.F.M.), a UC San Diego Frontiers of Innovation Scholars Program grant (to S.S.), Graduate Student Research Support from the UC San Diego Institute of Engineering in Medicine (to V.F.M), post-doctoral fellowships from the Swiss National Science Foundation P2BSP3-165311 and the American Federation of Aging Research PD18120 (to K.S.), and a Medical Student Training in Aging Research Grant T35 AG26757 (to M.B.).

SS and VFM were responsible for the conception and design of the study, and the analysis and interpretation of the data. VFM was responsible for the design and drafting of the manuscript and SS revised the manuscript critically. MB, SL, KS, JP, BH, and CM contributed to analysis, interpretation of data, and critical revision of the manuscript. All authors gave final approval.

Chapter 2, in full, is a reprint of the material as it appears in the American Journal of Physiology, Cell Physiology 2019 (with edits for style). V. F. Martins, M. Begur, S. Lakkaraju, K. Svensson, J. Park, B. Hetrick, C. E. McCurdy, S. Schenk. The dissertation author was the primary investigator and author of this paper.

References

1. **Arora A**, **Dey CS**. SIRT2 negatively regulates insulin resistance in C2C12 skeletal muscle cells. *Biochim Biophys Acta - Mol Basis Dis* 1842: 1372–1378, 2014.

2. **Atadja P**. Development of the pan-DAC inhibitor panobinostat (LBH589): Successes and challenges. *Cancer Lett* 280: 233–241, 2009.

3. **Belman JP**, **Bian RR**, **Habtemichael EN**, **Li DT**, **Jurczak MJ**, **Alcázar-Román A**, **McNally LJ**, **Shulman GI**, **Bogan JS**. Acetylation of TUG protein promotes the accumulation of GLUT4 glucose transporters in an insulin-responsive intracellular compartment. *J Biol Chem* 290: 4447–63, 2015.

4. **Chiang YL**, **Lin H**. An improved fluorogenic assay for SIRT1, SIRT2, and SIRT3. *Org Biomol Chem* 14: 2186–2190, 2016.

5. **Choudhary C**, **Weinert BT**, **Nishida Y**, **Verdin E**, **Mann M**. The growing landscape of lysine acetylation links metabolism and cell signalling. *Nat Rev Mol Cell Biol* 15: 536–50, 2014.

6. **Denu JM**. The Sir2 family of protein deacetylases. *Curr Opin Chem Biol* 9: 431–440, 2005.

7. **Fröjdö S**, **Durand C**, **Molin L**, **Carey AL**, **El-Osta A**, **Kingwell BA**, **Febbraio MA**, **Solari F**, **Vidal H**, **Pirola L**. Phosphoinositide 3-kinase as a novel functional target for the regulation of the insulin signaling pathway by SIRT1. *Mol Cell Endocrinol* 335: 166–176, 2011.

8. **Gaur V**, **Connor T**, **Venardos K**, **Henstridge DC**, **Martin SD**, **Swinton C**, **Morrison S**, **Aston-Mourney K**, **Gehrig SM**, **van Ewijk R**, **Lynch GS**, **Febbraio MA**, **Steinberg GR**, **Hargreaves M**, **Walder KR**, **McGee SL**. Scriptaid enhances skeletal muscle insulin action and cardiac function in obese mice. *Diabetes, Obes Metab* 19: 936–943, 2017.

9. **Klip A**, **Sun Y**, **Chiu TT**, **Foley KP**. Signal transduction meets vesicle traffic: the software and hardware of GLUT4 translocation. *Am J Physiol Physiol* 306: C879–C886, 2014.

10. **Kuilenburg ABP van**, **Ruijter AJM de**, **Gennip AH van**, **Caron HN**, **Kemp S**. Histone deacetylases (HDACs): characterization of the classical HDAC family. *Biochem J* 370: 737–749, 2003.

11. **LaBarge S**, **Migdal C**, **Schenk S**. Is acetylation a metabolic rheostat that regulates skeletal muscle insulin action? *Mol Cells* 38: 297–303, 2015.

12. **Lantier L**, **Williams AS**, **Hughey CC**, **Bracy DP**, **James FD**, **Ansari MA**, **Gius D**, **Wasserman DH**. SIRT2 knockout exacerbates insulin resistance in high fat-fed mice. *PLoS One* 13: 1–20, 2018.

13. **Lantier L**, **Williams AS**, **Williams IM**, **Yang KK**, **Bracy DP**, **Goelzer M**, **James FD**, **Gius D**, **Wasserman DH**. SIRT3 Is Crucial for Maintaining Skeletal Muscle Insulin Action and Protects Against Severe Insulin Resistance in High-Fat–Fed Mice. *Diabetes* 64: 3081–3092, 2015.

14. **Lobera M**, **Madauss KP**, **Pohlhaus DT**, **Wright QG**, **Trocha M**, **Schmidt DR**, **Baloglu E**, **Trump RP**, **Head MS**, **Hofmann GA**, **Murray-Thompson M**, **Schwartz B**, **Chakravorty S**, **Wu Z**, **Mander PK**, **Kruidenier L**, **Reid RA**, **Burkhart W**, **Turunen BJ**, **Rong JX**, **Wagner C**, **Moyer MB**, **Wells C**, **Hong X**, **Moore JT**, **Williams JD**, **Soler D**, **Ghosh S**, **Nolan MA**. Selective class IIa histone deacetylase inhibition via a nonchelating zinc-binding group. *Nat Chem Biol* 9: 319–325, 2013.

15. **Maehara K**, **Uekawa N**, **Isobe KI**. Effects of histone acetylation on transcriptional regulation of manganese superoxide dismutase gene. *Biochem Biophys Res Commun* 295: 187–192, 2002.

16. **Martins VF**, **Tahvilian S**, **Kang JH**, **Svensson K**, **Hetrick B**, **Chick WS**, **Schenk S**, **McCurdy CE**. Calorie Restriction-Induced Increase in Skeletal Muscle Insulin Sensitivity Is Not Prevented by Overexpression of the p55α Subunit of Phosphoinositide 3-Kinase. *Front Physiol* 9: 789, 2018.

17. **McGee SL**, **Van Denderen BJW**, **Howlett KF**, **Mollica J**, **Schertzer JD**, **Kemp BE**, **Hargreaves M**. AMP-activated protein kinase regulates GLUT4 transcription by phosphorylating histone deacetylase 5. *Diabetes* 57: 860–867, 2008.

18. **Nunes MJ**, **Milagre I**, **Schnekenburger M**, **Gama MJ**, **Diederich M**, **Rodrigues E**. Sp proteins play a critical role in histone deacetylase inhibitor-mediated derepression of CYP46A1 gene transcription. *J Neurochem* 113: 418–431, 2010.

19. **Nunes MJ**, **Moutinho M**, **Milagre I**, **Gama MJ**, **Rodrigues E**. Okadaic acid inhibits the trichostatin A-mediated increase of human CYP46A1 neuronal expression in a ERK1/2-Sp3-dependent pathway. *J Lipid Res* 53: 1910–1919, 2012.

20. **Raichur S**, **Teh SH**, **Ohwaki K**, **Gaur V**, **Long YC**, **Hargreaves M**, **McGee SL**, **Kusunoki J**. Histone deacetylase 5 regulates glucose uptake and insulin action in muscle cells. *J Mol Endocrinol* 49: 203–211, 2012.

21. **Schenk S**, **McCurdy CE**, **Philp A**, **Chen MZ**, **Holliday MJ**, **Bandyopadhyay GK**, **Osborn O**, **Baar K**, **Olefsky JM**. Sirt1 enhances skeletal muscle insulin sensitivity in mice during caloric restriction. *J Clin Invest* 121: 4281–8, 2011.

22. **Sun C**, **Zhou J**. Trichostatin A improves insulin stimulated glucose utilization and insulin signaling transduction through the repression of HDAC2. *Biochem Pharmacol* 76: 120–127, 2008.

23. **Sundaresan NR**, **Pillai VB**, **Wolfgeher D**, **Samant S**, **Vasudevan P**, **Parekh V**, **Raghuraman H**, **Cunningham JM**, **Gupta M**, **Gupta MP**. The deacetylase SIRT1 promotes membrane localization and activation of Akt and PDK1 during tumorigenesis and

cardiac hypertrophy. *Sci Signal* 4: ra46, 2011.

24. **Svensson K**, **LaBarge SA**, **Martins VF**, **Schenk S**. Temporal overexpression of SIRT1 in skeletal muscle of adult mice does not improve insulin sensitivity or markers of mitochondrial biogenesis. *Acta Physiol* 221: 193–203, 2017.

25. **Takigawa-Imamura H**, **Sekine T**, **Murata M**, **Takayama K**, **Nakazawa K**, **Nakagawa J**. Stimulation of Glucose Uptake in Muscle Cells by Prolonged Treatment with Scriptide, a Histone Deacetylase Inhibitor. *Biosci Biotechnol Biochem* 67: 1499–1506, 2003.

26. **Weems J**, **Olson AL**. Class II histone deacetylases limit GLUT4 gene expression during adipocyte differentiation. *J Biol Chem* 286: 460–468, 2011.

27. **Zhang J**. The direct involvement of SirT1 in insulin-induced insulin receptor substrate-2 tyrosine phosphorylation. *J Biol Chem* 282: 34356–34364, 2007.

Table 2.1. IC_{50}'s for inhibitors used

	Deacetylase Class		
	I (HDACs)	II (HDACs)	III (Sirtuins)
Trichostatin A	~10 nM	~1 μM	
Panobinostat	~100 nM	~100 nM	
TMP195	>100 nM	~100 nM	
Nicotinamide			~100 μM

HDAC, histone deacetylase.

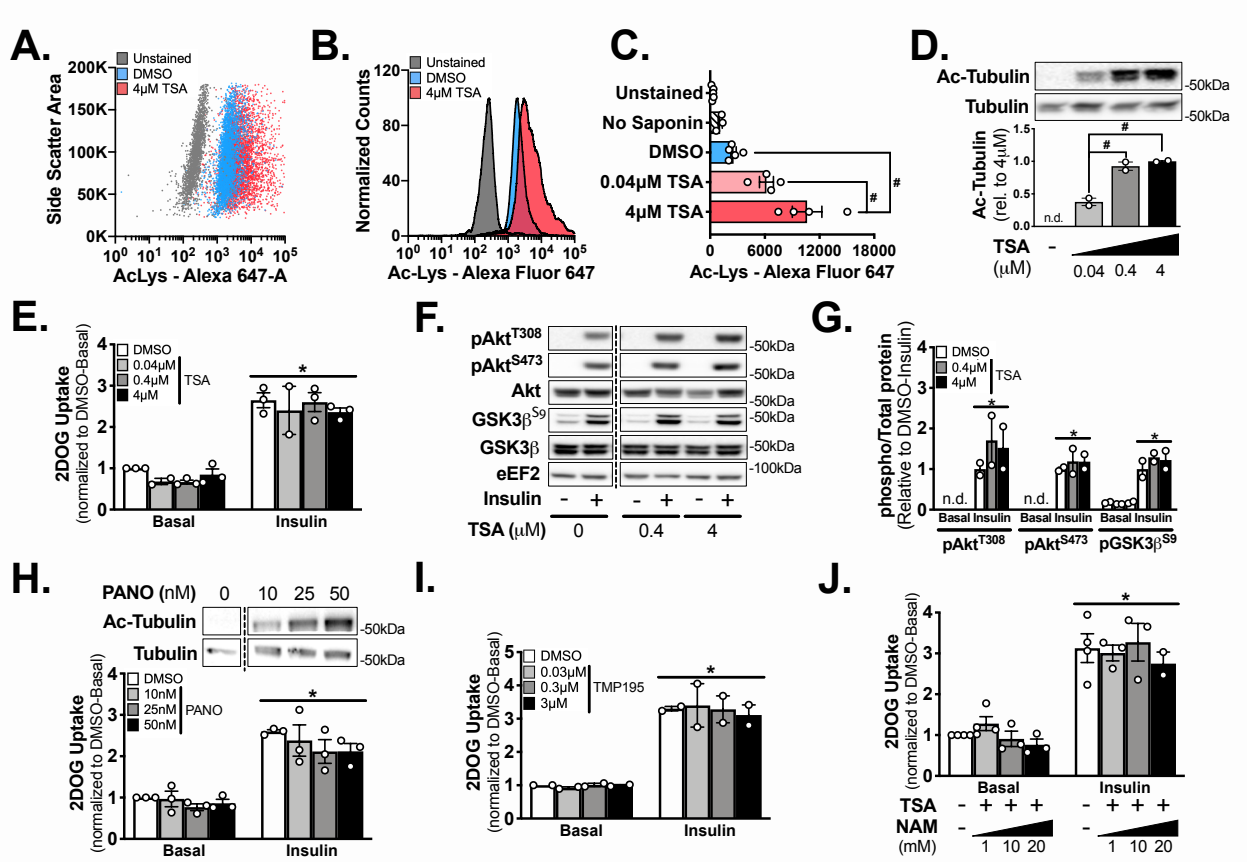

Figure 2.1. Acute inhibition of HDACs increases acetylation but does not alter insulin-stimulated glucose uptake in L6 myotubes. A-B) Representative experiment and C) mean fluorescence intensity for total acetylated-proteins in unstained, stained without saponin, DMSO, and trichostatin A (TSA) treated L6 myoblasts, as analyzed by flow cytometry. Representative of 4 independent experiments. D) Representative image and quantification for acetylated-tubulin (Ac-Tubulin) and total tubulin in L6 myotubes pre-treated for 1 hour with DMSO or TSA. Normalized basal and insulin (100nM) 2-deoxy-glucose (2DOG) uptake in L6 myotubes pre-treated for 1 hour with DMSO or E) TSA, H) Panobinostat (PANO), I) TMP195, or J) TSA (4μM) and nicotinamide (NAM). F) Representative image and G) quantification of Phospho-Akt^{T308} (pAkt^{T308}), pAkt^{TS473}, total Akt, pGSK3β^{S9}, and total GSK3β in basal and insulin-stimulated (- and +, respectively) L6 myotubes pre-treated with or without TSA for 1 hour. #, $p<0.05$ 1-way ANOVA with Tukey multiple comparison test. *, $p<0.05$ 2-way ANOVA main effect of insulin. Trichostatin A treatment western blots are representative of 2 independent experiments and 2DOG uptake assays are representative of 3 independent experiments. Data reported as mean ± SEM.

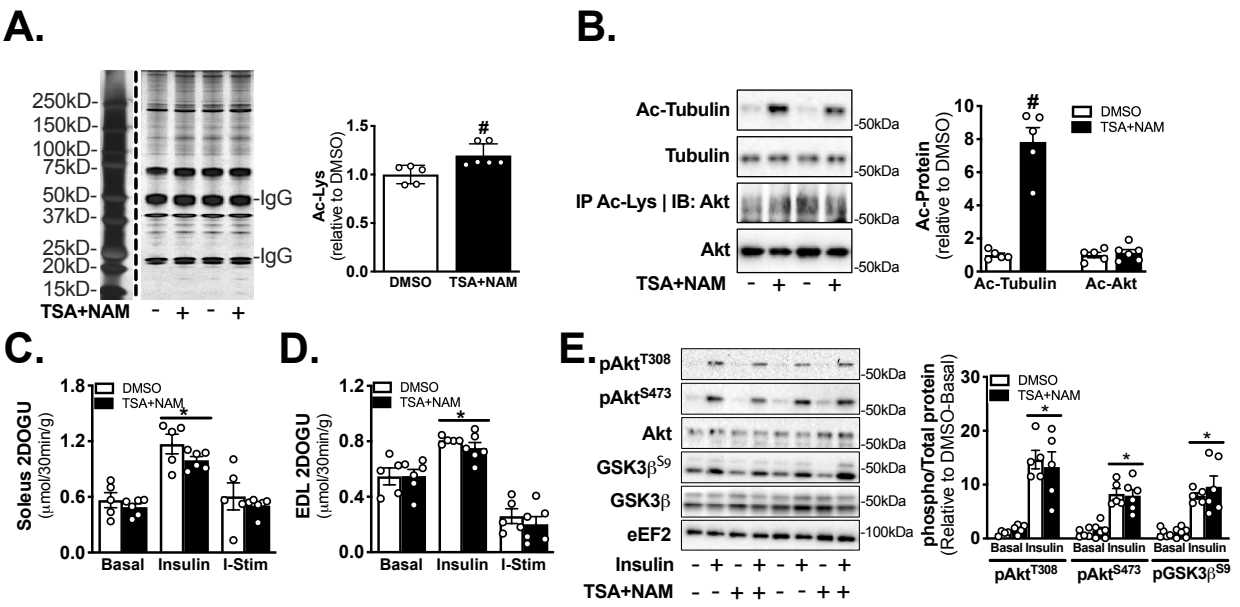

Figure 2.2. Concurrent inhibition of HDACs and sirtuins does not affect insulin-stimulated glucose uptake in skeletal muscle *ex vivo*. A) Silver stain of acetyl-lysine immunoprecipitates from DMSO or trichostatin A and nicotinamide treated soleus muscles (TSA+NAM; 4 µM TSA and 20mM NAM). B) Quantitation and representative images of acetylated-tubulin (Ac-Tubulin), tubulin, acetylated-Akt (Ac-Akt), and Akt from DMSO or TSA+NAM treated soleus muscles. Ac-Akt was determined by immunoprecipitation (IP) with an acetyl-lysine antibody and subsequent immunoblotting (IB) with an Akt antibody. C-D) Basal 2DOG uptake (2DOGU), insulin (0.36 nM) 2DOGU, and insulin-stimulated 2DOGU (I-Stim; calculated as insulin 2DOGU – basal 2DOGU) in isolated C) soleus and D) extensor digitorum longus (EDL) muscles, from female C57BL/6J mice, pre-treated for 1 hour with DMSO or TSA+NAM. E) Representative image and quantification of Phospho-Akt^{T308} (pAkt^{T308}), pAkt^{TS473}, total Akt, pGSK3β^{S9}, and total GSK3β in basal and insulin-stimulated (- and +, respectively) EDL muscles pre-treated with DMSO or TSA+NAM for 1 hour. DMSO (n=5), TSA+NAM (n=6). #, $p<0.05$ unpaired Student's *t*-test. *, $p<0.05$ 2-way ANOVA, main effect of insulin. Data reported as mean ± SEM.

CHAPTER 3

Germline or inducible knockout of p300 or CBP in skeletal muscle does not alter insulin sensitivity

Abstract

Introduction: Akt is a critical mediator of insulin-stimulated glucose uptake in skeletal muscle. The acetyltransferases, E1A binding protein p300 (p300) and cAMP response element-binding protein binding protein (CBP) are phosphorylated and activated by Akt, and p300/CBP can acetylate and inactivate Akt, thus giving rise to a possible Akt-p300/CBP axis. Our objective was to determine the importance of p300 and CBP to skeletal muscle insulin sensitivity.

Methods: We used Cre-LoxP methodology to generate mice with germline (muscle creatine kinase promoter [P-MCK and C-MCK]) or inducible (tamoxifen-activated, human skeletal actin promoter [P-iHSA and C-iHSA]) knockout of p300 or CBP. A subset of P-MCK and C-MCK mice were switched to a calorie restriction diet (60% of *ad libitum* intake) or high-fat diet at 10 weeks of age. For P-iHSA and C-iHSA mice, knockout was induced at 10 weeks of age. At 13-15 weeks of age, we measured whole-body energy expenditure, oral glucose tolerance and/or *ex vivo* skeletal muscle insulin sensitivity.

Results: While p300 and CBP protein abundance and mRNA expression was reduced 55-90% in p300 and CBP knockout mice, there were no genotype differences in energy expenditure or fasting glucose and insulin concentrations. Moreover, neither loss of p300 or CBP impacted

oral glucose tolerance or skeletal muscle insulin sensitivity, nor did their loss impact alterations in these parameters in response to a calorie restriction or high-fat diet.

Conclusions: Muscle-specific loss of either p300 or CBP, be it germline or in adulthood, does not impact energy expenditure, glucose tolerance or skeletal muscle insulin action.

Introduction

Protein lysine acetylation alters the function of thousands of proteins, and by extension, impacts the biological processes that they comprise (1, 9, 34, 71, 75, 82). Initially, the importance of lysine acetylation to cellular homeostasis was thought to occur via its ability to regulate histone function and gene transcription (70). However, recent proteomic-based analysis in various tissues, including skeletal muscle, have identified more than 2000 acetylated, non-histone, proteins that impact a broad array of cellular processes (9, 34, 44, 75, 82). In fact, many of these proteins are not only found in the cytoplasm, but they are central to numerous metabolic pathways, including glucose and amino acid metabolism, membrane trafficking and insulin signaling (9, 34, 37, 75, 82).

The acetylation status of lysine residues within a protein is primarily regulated by the activity of acetyltransferases and deacetylases, which add or remove acetyl groups, respectively (10). Considering acetyl-CoA is both the substrate used by acetyltransferases to acetylate lysine residues and a hub metabolite within carbohydrate, lipid and protein metabolism, it is logical to think that acetyltransferases, and by extension, acetylation, could play a key role in the regulation of pathways central to cellular metabolic homeostasis, such as insulin action. Nevertheless, while the contribution of deacetylases, particularly the sirtuins (SIRT1) 1 and SIRT3, to skeletal muscle insulin sensitivity has been heavily studied (30, 40, 62, 68, 77, 78), no studies to date have investigated the contribution of acetyltransferases.

Akt isoform 2 (Akt2) is required for insulin-stimulated glucose uptake in skeletal muscle (8, 39, 49), with its regulation traditionally thought to occur through phosphorylation (5). Interestingly, however, in HeLa cells the Akt isoform 1 (Akt1) was found to be acetylated on lysine

(Lys) 14 and Lys20 by the acetyltransferase E1A binding protein p300 (p300), with acetylation on these residues decreasing Akt activity (66). In addition, studies in 293T, HepG2, A549, OSU-2, and hepatic stellate cells demonstrate that phosphorylation of p300 and its functional homolog, cAMP response element-binding protein binding protein (CBP), by Akt (13, 18, 27, 42, 61, 74), including Akt1 (27, 42, 43, 61), increases their acetyltransferase activity (27, 42, 43, 61), although this is not a universal finding (43). Taken together, these studies provide evidence for reciprocal regulation between Akt and p300/CBP, and by extension, it is possible that p300 and CBP could be important to the regulation of insulin signaling to glucose uptake. Supporting this, p300 and CBP have a strong cytosolic presence (3, 17, 60), which is important if they are to directly regulate Akt and/or other insulin signaling proteins. Also, p300 and CBP acetylate numerous cytosolic proteins (12, 36, 64, 75), including proteins that are fundamental to insulin signaling and GLUT4 trafficking (36, 64, 75), and in the liver insulin stimulation leads to phosphorylation of CBP (21, 83). Nevertheless, whether p300 or CBP, or for that matter acetyltransferases in general, mediate insulin action in skeletal muscle is unknown.

p300 and CBP share 61% sequence homology across the entire protein and ~80-90% sequence homology in the acetyltransferase domain (2, 12), and as such, are widely considered to be functional homologues (10, 12, 72). Moreover, p300 and CBP share many common substrates (12, 79), although they also have distinct targets (16, 24, 28, 31). Thus, to study the separate contributions of p300 and CBP to whole-body glucose metabolism and skeletal muscle insulin sensitivity *in vivo*, we used CreLoxP methodology to generate mice with germline-mediated or adulthood-mediated, muscle-specific knockout of p300 or CBP; germline knockout was driven by the muscle creatine kinase (MCK) promoter (7), whilst temporal knockout in adult mice was driven in a tamoxifen (TMX)-inducible manner via the human α-skeletal actin (iHSA) promoter (48).

Our rationale for employing these two Cre approaches was to allow us to determine the impact of embryonic versus temporal knockout of p300 or CBP in skeletal muscle, which was particularly important as knockout of p300 or CBP can impact skeletal muscle development both *in vitro* (15, 16, 57, 58) and *in vivo* (59, 81). Considering the regulatory cross-talk between p300/CBP and Akt, we hypothesized that knockout of either p300 or CBP in skeletal muscle would impair whole-body glucose tolerance and insulin-stimulated glucose uptake and Akt signaling in skeletal muscle. Furthermore, a subset of mice were placed on a calorie-restriction (CR) or high-fat diet (HFD) in order to determine if p300/CBP mediated their effects on skeletal muscle insulin sensitivity.

Methods

Mouse models. Studies were conducted in male mice on a C57BL/6J background and housed in a conventional facility with a 12-h light/12-h dark cycle. Germline, muscle-specific, p300 and CBP knockout mice were generated by crossing *p300* floxed mice (33) or *cbp* floxed mice (32) with mice expressing Cre recombinase (Cre) under the control of the MCK promoter; these mice are referred to as P-MCK and C-MCK, respectively. Generation of the P-MCK mouse has been described, previously (38). To generate mice with inducible, skeletal muscle-specific knockout of p300 or CBP, aforementioned floxed mice were crossed with mice expressing Cre, in a tamoxifen (TMX)-inducible manner, under the iHSA promoter (48); these mice are referred to as P-iHSA and C-iHSA, respectively. Respective floxed, but Cre negative, littermates were used as experimental controls for all four mouse lines; these mice are referred to as wildtype (WT). For P-iHSA and C-iHSA mice, at 10 weeks of age, all mice were orally gavaged with TMX (2mg) for five consecutive days to activate Cre. This study was carried out with the approval of, and in accordance with, the Animal Care Program and Institutional Animal Care and Use Committee at the University of California, San Diego.

Experimental design. For studies in P-MCK and C-MCK mice, oral glucose tolerance tests (OGTT) and *ex vivo* 2-deoxyglucose (2DOG) uptake assays were performed at 12-14 weeks of age. For studies in P-iHSA and C-iHSA mice, OGTT, whole-body energy expenditure, and 2DOG uptake assays were conducted 3-5 weeks after starting TMX (i.e. 13-15 weeks of age). The HFD studies were performed in P-MCK mice, as previously described (76). Briefly, at 10 weeks of age, mice were randomly assigned to continue on the control diet (10% calories from fat) or they were switched to a HFD (60% calories from fat. Cat#D12492, Research Diets, New

Brunswick, NJ) for 20 days. The CR studies were performed as previously described (62). Briefly, at 9 weeks of age mice were individually housed and *ad libitum* food intake was assessed for 7 consecutive days at 1200 h. At 10 weeks of age, mice were randomly assigned to continue ad libitum feeding or they were switched to a CR diet (60% of ad libitum intake) for 20 days. Food for CR mice was provided daily between 1100 and 1200 h. For the diet studies in P-MCK and C-MCK mice, the OGTT was conducted 15-17 days after starting diet, and 2DOG uptake was assessed 20-22 days after starting diet.

Tissue and blood collection. Tissues were excised from fasted (4 h), anesthetized mice. Skeletal muscles (gastrocnemius and tibialis anterior), heart, liver and epididymal white adipose tissue (WAT) were rinsed in sterile saline, blotted dry, weighed and immediately frozen in liquid nitrogen. Whole blood was collected with EDTA from the inferior vena cava, centrifuged at 5,000 g at 4°C for 5 min and the plasma isolated. Tissue and plasma were stored at -80°C for subsequent analysis.

Plasma insulin concentration. Plasma insulin was analyzed using an ELISA kit, per the manufacturer's instructions (80-INSMS-E01; ALPCO Diagnostics, Salem, NH, USA).

Immunoprecipitation. Protein A and G magnetic beads (25/25 μL; Bio-Rad Laboratories, Hercules, CA, USA) were washed three times with PBS with 0.1% Tween 20 (PBS-T). Anti-acetyl-lysine (AAC01; Cytoskeleton, Denver, CO, USA) was then added to the bead mixture and rotated end over end for 1 hour (4^{o}C). Subsequently, beads were washed three more times with PBS-T and then 180 μg of whole cell lysate, from the tibialis anterior, were added and the samples were rotated overnight (4^{o}C). The following morning, beads were washed three times with PBS-T, and antigens were eluted with 1X Laemmli sample buffer (40 μL). Samples were boiled for 6 min, and lysate was removed from protein A/G magnetic beads via a magnetic rack (Bio-Rad)

prior to SDS-PAGE.

Immunoblotting. Immunoblotting was conducted as described in Study 1. The following antibodies were used at a concentration of 1:1000 dilution unless otherwise stated: CBP (CS 7389S, 1:500), Akt (CS 9272B), phosphorylated (p)Akt^{S473} (CS 4058, 1:500), pAkt^{T308} (CS 9275), GSK3α/β (CS 5676), pGSK3α/β$^{S21/9}$ (CS 9331) and eukaryotic elongation factor 2 (eEF2; CS 2332) were from Cell Signaling; p300 (sc-585, 1:200) was from Santa Cruz; glyceraldehyde-3-phosphate (GAPDH; 10R-G109a, 1:100,000) was from Fitzgerald Industries. Akt, GSK3β and their respective phosphorylated protein abundance were all normalized against actual protein load (ponceau stain) before being expressed as a ratio (phosphorylated protein to total protein) and are presented relative to average WT basal (i.e. non-insulin stimulated) values. p300 and CBP protein abundance was normalized against eEF2 or GAPDH and are presented relative to average WT values. Antibodies used in this study have been used in previous published studies by our lab: p300 and CBP (38); Akt, pAkt^{T308} , Akt^{S473}, GSK3α/β, pGSK3α/β$^{S21/9}$, eEF2, and GAPDH (47, 67); and were validated by determining if bands were at the correct molecular weight by using recombinant proteins and/or assessing changes in band intensity according to appropriate interventions (e.g. knockout, insulin stimulation). Gels used for silver staining were assayed according to manufacturer's instructions (Pierce Silver Stain Kit 24612; Thermo Scientific, Waltham, MA, USA). All bands on the silver stain were quantified together (excluding the IgG bands) and normalized to the IgG band at 25 kDa.

qPCR. Total RNA was isolated from snap-frozen quadriceps muscle using TRIzol Reagent (Thermo Fisher Scientific). RNA concentration was adjusted, and 1 lg of total RNA was used for cDNA synthesis. Semi- quantitative real-time PCR analysis was performed using iTaqTM SYBR Green master mix (Bio-Rad) on a CFX384 TouchTM real-time PCR system (Bio-Rad). Relative

expression levels were calculated by the $\Delta\Delta C_t$ method, using TATA-box binding protein (*tbp*) as the normalization control. The *ep300* (p300) and *crebbp* (CBP) primers were designed so that one of the primers would anneal onto exon 9 (i.e. the exon that is floxed in the p300 and CBP floxed mouse) and the other to exon 10. Primer sequences used were – *ep300*: 5'-ATG CTC GTA AAG TGG AAG GGG-3', 5'-ATC TTC TCG GCT AGG AGG TGA-3'; *crebbp*: 5'-GCA CTG GTG TTC GAA AAG GC-3', 5'-CAG GGT CTG GAG TTG GGA AG-3'; *tbp*: 5'-GGG ATT CAG GAA GAC CAC ATA G-3', 5'-CCT CAC CAA CTG TAC CAT CAG-3'.

Energy expenditure and body composition. Whole-body energy expenditure was assessed via indirect calorimetry, using the Comprehensive Lab Animals Monitoring System (CLAMS; Columbus Instruments, Columbus, OH, USA). Oxygen consumption (VO_2), respiratory exchange ratio (RER), and total activity were continuously measured for 3 consecutive days and values were averaged from the light and dark phases recorded on days 2 and 3. Body composition was assessed by magnetic resonance imaging (MRI; EchoMRI-100TM, Houston, TX, USA).

Oral glucose tolerance test (OGTT). Fasted (4h) mice were orally gavaged with dextrose (2 g/kg) and blood glucose concentration was measured via the tail vein at 0 (before gavage), 20, 30, 45, 60, 90, and 120 min after gavage using a handheld glucose meter (Ascensia Contour, Bayer HealthCare, Mishawaka, IL, USA). Area under the curve (AUC) was calculated using Prism 7 (GraphPad Software Incorporated, La Jolla, CA, USA) with 0 mg/dL used as the baseline.

2DOG uptake. Basal and insulin-stimulated 2DOG uptake was measured in isolated and paired soleus and extensor digitorum longus (EDL) muscles, as described in Study 1, with some modifications. Fasted (4 hours) mice were anesthetized and paired soleus and extensor digitorum longus (EDL) muscles were incubated at 35°C for 30 minutes in oxygenated (95% O2, 5% CO2) flasks of Krebs-Henseleit buffer (KHB) containing 0.1% BSA, 2 mM Na-pyruvate, and 6 mM

mannitol. One muscle per pair was incubated in KHB without insulin, and the contralateral muscle was incubated in KHB with insulin (60 μU/ml [0.36 nM]; Humulin R, Eli Lilly and Company). After 30 minutes, muscles were transferred to a second flask and incubated at 35°C for 20 minutes in KHB plus 0.1% BSA, 9 mM [14C]-mannitol (0.053 mCi/mmol; PerkinElmer), and 1 mM [3H]-2DG (6 mCi/mmol; PerkinElmer), with the same insulin concentration as in the first incubation. After the second incubation phase, muscles were blotted on ice cold filter paper, trimmed, freeze-clamped, and then stored (−80°C).

Statistics. Statistical analyses were performed using Prism 8 (GraphPad Software Incorporated, La Jolla, CA, USA). Data were analyzed using an unpaired Student's *t*-test or 2-way analysis of variance (ANOVA), with Sidak's multiple comparisons test where appropriate, with significant differences at $p<0.05$. Specifically, p300 and CBP protein abundance and mRNA expression, acetyl-lysine silver stain, acetyl-Akt, body composition, tissue weights, fasting glucose, fasting insulin, OGTT AUC, and insulin-stimulated 2DOG uptake were analyzed by an unpaired Student's *t*-test. CLAMS (light x genotype), OGTT AUC and insulin stimulated 2DOG uptake for HFD and CR (diet x genotype), 2DOG uptake for P-iHSA and C-iHSA, and Akt, GSK3β, $pAkt^{T308/S473}$/Akt, $pGSK3\beta^{S9}$/GSK3β for all models (insulin x genotype) were analyzed using a 2-way ANOVA. For the OGTT, a 2-way ANOVA (time x genotype) with repeated measures or a 2-way ANOVA within each time point (genotype x diet) was used. For 2DOG uptake diet studies, a 2-way ANOVA was used within ad libitum and within CR samples first (insulin x genotype) to determine a main effect of insulin, subsequently, a 2-way ANOVA was used within basal and within insulin samples to determine a main effect of calorie restriction (genotype x diet). All data are expressed as mean ± SEM.

Results

Validation of mouse models. In C-MCK mice, skeletal muscle CBP protein abundance was reduced ~65% as compared to WT littermates (Figure 3.1A). Functional loss of CBP was confirmed by a ~30% reduction in total protein acetylation in C-MCK compared to WT skeletal muscle, as measured in immunoprecipitates using a pan acetyl-lysine antibody (Figure 3.1B; WT: 1.00 ± 0.11, C-MCK: 0.73 ± 0.03, $p = 0.054$). We have previously validated a that pan-lysine acetylation of skeletal muscle proteins is reduced in the P-MCK mouse (38). In C-iHSA mice, CBP protein abundance in skeletal muscle was reduced ~60%, as compared to WT littermates, (Figure 3.1C). In P-iHSA mice, p300 protein abundance in skeletal muscle was reduced ~50%, as compared to WT littermates, and there was no compensatory increase in CBP protein abundance (data not shown). To further validate these knockout models, we used primers that align to exon 9 (i.e. the exon that is excised after Cre-mediated recombination) and exon 10 of p300 or CBP. In C-iHSA mice, skeletal muscle CBP mRNA expression was reduced 77%, while p300 mRNA was modestly higher, as compared to WT mice (Figure 3.1E). In P-iHSA mice, skeletal muscle p300 mRNA expression was reduced 87%, and CBP mRNA was reduced 25% as compared to WT mice (Figure 3.1F).

Akt acetylation. Because Akt has been found to be acetylated by p300 (66), we assessed Akt acetylation in skeletal muscle of P-iHSA and C-iHSA mice, by immunoprecipitating with a pan acetyl-lysine antibody and immunoblotting for Akt. We found no difference in acetylated-Akt between C-iHSA (Figure 3.1G) or P-iHSA (Figure 3.1I) mice and their respective wildtypes. The abundance of Akt in the whole-cell lysate used for immunoprecipitation was not different between genotypes (Figure 3.1H and J).

Energy expenditure and activity are unaffected in P-iHSA and C-iHSA mice. Whole-body oxygen consumption (VO_2), RER, and total activity (i.e., total z + x-axis beam breaks) were similar between C-iHSA (Figures 3.2A-C) and P-iHSA (Figures 3.2D-F) mice and their respective WT littermates during both light and dark phases.

Body mass, body composition, tissue weights, and fasting glucose and insulin are unaffected by germline (Table 3.1 and Table 3.2) or inducible (Table 3.3) knockout of p300 or CBP. As compared to their WT littermates, body weight was not different between P-MCK, P-iHSA, and C-iHSA mice that were fed a control diet, while C-MCK mice were lighter compared to WT littermates. In these same mice, there were no differences in % body fat, % lean muscle mass, normalized tissue weights (as a % of body weight) fasting glucose or insulin concentrations, as compared to their WT littermates. For Table 2.1, P-MCK ad libitum and control diet mice were combined as no differences were noted between the groups. As expected, calorie restriction significantly reduced body weight, % body fat, normalized epididymal WAT weight, and fasting glucose in P-MCK (Table 2.1) and C-MCK (Table 2.2) mice, with no differences noted between genotypes. Furthermore, as expected, high-fat diet significantly increased body weight, % body fat, normalized epididymal WAT weight, and fasting glucose in P-MCK mice (Table 2.1), with no differences between P-MCK and WT mice.

Germline knockout of p300 in skeletal muscle does not affect insulin sensitivity. In the control diet mice for the HFD and CR studies (i.e. mice fed a control diet or ad libitum), blood glucose concentrations and the AUC during an OGTT were comparable between P-MCK and WT littermates (Figure 3.3A-D). As expected, HFD significantly impaired glucose tolerance (Figure 3.3 A-B), and CR diet significantly enhanced glucose tolerance (Figure 3.3C-D), as compared to their respective dietary controls, but there were no genotype differences in the response to these

diets. In the CR diet study mice, we also assessed *ex vivo* skeletal muscle insulin sensitivity in the soleus and EDL muscles. Insulin significantly increased 2DOG uptake in soleus and EDL of AL-fed mice, with the "insulin-stimulated" 2DOG uptake (i.e. Insulin 2DOG uptake minus Basal 2DOG uptake) being comparable between genotypes (Figures 3.3E-H). Moreover, in line with the OGTT data, CR significantly and comparably enhanced insulin-stimulated 2DOG uptake ~3-4-fold in the EDL and soleus of WT and P-MCK mice (Figures 3.3F, H). Notably, there were no genotype differences in basal 2DOG uptake in soleus or EDL muscles, although there was a main effect of CR to increase basal 2DOG uptake in the EDL and soleus (Figure 3.3E, G). To complement the 2DOG uptake data we also assessed insulin signaling in control diet-fed mice. Insulin significantly increased the phosphorylation of $Akt^{S473/T308}$ and $GSK3ß^{S9}$ in the soleus of P-MCK (Figure 3.3I-J) mice, however, there was no effect of genotype. Total Akt and GSK3β abundance were not different by genotype or insulin treatment ($p>0.05$).

Germline knockout of CBP in skeletal muscle does not affect insulin sensitivity. In the ad libitum diet mice, blood glucose concentrations and the AUC during an OGTT were comparable between C-MCK and WT littermates (Figure 3.4A-B). As expected, CR significantly enhanced glucose tolerance (Figure 3.4A-B), however there were no genotype differences. Insulin significantly increased 2DOG uptake in soleus and EDL of ad libitum-fed mice, with the "insulin-stimulated" 2DOG uptake being comparable between genotypes (Figures 3.4C-F). Moreover, in line with the OGTT data, CR significantly and comparably enhanced insulin-stimulated 2DOG uptake ~3-4-fold in the EDL and soleus of WT and C-MCK mice (Figures 3.4D, F). Notably, while there were no genotype differences in basal 2DOG uptake in soleus or EDL muscles, CR increased basal 2DOG uptake only in the soleus of C-MCK mice (Figure 3.4E), and not the EDL (Figure 3.4C). To complement the 2DOG uptake data we also assessed insulin signaling in ad libitum-fed

mice. Insulin significantly increased the phosphorylation of $Akt^{S473/T308}$ and $GSK3ß^{S9}$ in the soleus of P-MCK (Figure 3.4G-H) mice, however, there was no effect of genotype. There was no effect of genotype or insulin stimulation on total Akt or GSK3β protein abundance ($p>0.05$).

Inducible knockout of p300 in adult skeletal muscle does not affect insulin sensitivity. Blood glucose concentrations and the AUC during an OGTT were comparable between P-iHSA (Figure 3.5A-B) mice and their respective WT littermates. Similarly, basal 2DOG uptake, 2DOG uptake in the presence of insulin, and insulin-stimulated 2DOG uptake were comparable in the EDL and soleus of P-iHSA (Figure 3.5C-D) mice, as compared to WT mice. Complementing the 2DOG uptake data, insulin significantly increased phosphorylation of $Akt^{S473/T308}$ and $GSK3ß^{S9}$ in the soleus of P-iHSA (Figure 3.5E-F) and their WT littermates. Notably, insulin-mediated stimulation of Akt phosphorylation was significantly lower in P-iHSA mice as compared to their WT littermates (Figure 3.5E-F). However, there were no genotype effects for the insulin-mediated stimulation of $GSK3ß^{S9}$ phosphorylation in P-iHSA (Figure 3.5E-F) mice. Also, there was no effect of genotype or insulin stimulation on total Akt or GSK3β protein abundance ($p>0.05$).

Inducible knockout of CBP in adult skeletal muscle does not affect insulin sensitivity. Blood glucose concentrations and the AUC during an OGTT were comparable between C-iHSA (Figure 3.6A-B) mice and their respective WT littermates. Similarly, basal 2DOG uptake, 2DOG uptake in the presence of insulin, and insulin-stimulated 2DOG uptake were comparable in the EDL and soleus of C-iHSA mice (Figure 3.6C-D), as compared to WT mice. Complementing the 2DOG uptake data, insulin significantly increased phosphorylation of $Akt^{S473/T308}$ and $GSK3ß^{S9}$ in the soleus of C-iHSA mice (Figure 3.6E-F) and their WT littermates, with no genotype differences (Figure 3.6E-F). Also, there was no effect of genotype or insulin stimulation on total Akt or GSK3β protein abundance ($p>0.05$).

Discussion

Recent proteomic studies have demonstrated numerous insulin signaling and GLUT4 trafficking proteins are acetylated on lysine residues (6, 37, 53, 55, 82), including in skeletal muscle (44). Although the contribution of deacetylases to insulin sensitivity has been heavily studied, particularly in regards to SIRT1 (62, 68, 77, 78) and SIRT3 (30, 40), the contribution of acetyltransferases have been understudied. In fact, to our knowledge, this is the first study to investigate the contribution of acetyltransferases to skeletal muscle insulin sensitivity. Accordingly, herein we investigated the separate contributions of skeletal muscle p300 and CBP to whole-body energy expenditure, glucose tolerance and skeletal muscle insulin sensitivity. Our rationale for studying p300 and CBP relates to the fact that they can cross-signal with Akt (13, 18, 27, 42, 43, 61, 74), which is a fundamental signaling node in insulin-stimulated glucose uptake in skeletal muscle (39, 49). Furthermore, not only do p300/CBP have a strong cytosolic presence (3, 17, 60), but various proteins within the insulin signaling and GLUT4 trafficking pathway are acetylated by p300/CBP (75). Overall, using two different Cre approaches to knockout p300 or CBP in skeletal muscle either during development (i.e. germline) or in adulthood (i.e. inducible), our results demonstrate that loss of p300 or CBP does not impact glucose tolerance or skeletal muscle insulin sensitivity, including in response to a calorie restriction or high-fat diet.

p300 and CBP have been implicated, in a variety of mouse models, in the regulation of whole-body metabolism and glucose handling (4, 51, 79, 80). CBP heterozygous mice demonstrate improved glucose and insulin tolerance, in both control diet and high-fat diet conditions, as compared to WT mice (80). Furthermore, mice with a mutation in the CH1 domain of either p300 or CBP demonstrate improved glucose and insulin tolerance (4). In contrast, mice with conditional

knockout of CBP in the hypothalamus develop fasting hyperglycemia and glucose and insulin intolerance as compared to control mice (51). Similarly, mice with knockout of p300 or CBP in pancreatic islets are more glucose intolerant during an intraperitoneal GTT, and have lower fasting insulin levels (79). In the present study, however, we observed no differences in fasting insulin, fasting glucose, or oral glucose tolerance in any of our transgenic mice. Therefore, while loss of p300 or CBP, be it in the hypothalamus or pancreas, or at the whole-body level, can impact glucose tolerance, these results demonstrate that loss of p300 or CBP in skeletal muscle is not required for maintenance of whole-body glucose metabolism.

Various *in vitro* studies have demonstrated that Akt can physically interact with p300 (26, 74) and CBP (43). In fact, p300 (13, 18, 27, 42, 74) and CBP (43, 61) can be phosphorylated by Akt, including Akt1 (27, 42, 43, 61), with phosphorylation at the Akt regulatable site increasing p300/CBP acetyltransferase activity (27, 42, 61). Conversely, various proteins within the insulin signaling and GLUT4 trafficking pathway are acetylated by p300/CBP (75), including Akt1 (66). Importantly, while Akt1 is present in skeletal muscle, it is the isoform Akt2 that is present in highest abundance (41) and known to regulate glucose uptake (8, 39, 49); however, whether Akt2 specifically is also lysine acetylated by p300/CBP, or if Akt2 can phosphorylate p300/CBP, is unknown. Taken together, however, these studies provide the premise that insulin signaling to glucose uptake could be regulated via an Akt-p300/CBP axis. Until now, however, a possible Akt-p300/CBP axis and its relevance to insulin-stimulated glucose uptake in skeletal muscle has not been studied. In the present study, we observed no effect on insulin-stimulated 2DOG uptake in soleus or EDL in any of the p300 or CBP knockout models, as compared to their respective WT mice. Furthermore, the insulin-stimulated 2DOG uptake data were complimented by comparable insulin-mediated phosphorylation of Akt and GSK3β, although notably, insulin-stimulated Akt

phosphorylation was lower in P-iHSA mice. While it is not immediately clear why insulin-stimulated $pAkt^{S473}$ and $pAkt^{T308}$ was lower in P-iHSA versus WT mice, downstream phosphorylation of the direct Akt target, GSK3β, was comparable between P-iHSA and WT mice. This not only suggests that Akt function was comparable between genotypes, but that the insulin-stimulated Akt phosphorylation in P-iHSA mice was sufficient to bring about the physiological effects of insulin on glucose uptake. Lastly, in contrast to our hypothesis, loss of either p300 or CBP in skeletal muscle did not alter acetylated-Akt levels in P-iHSA or C-iHSA mice, despite a reduction in pan acetylation of muscle proteins in both p300 (38) and CBP knockout models. The likely reason for this lack of effect on Akt acetylation and insulin sensitivity is the well-described compensatory actions of p300 and CBP when one of them is not present (12, 23, 51, 79).

The substrate used by p300 and CBP, and acetyltransferases in general, when acetylating lysine residues is acetyl CoA (12). Intracellular acetyl CoA concentration is sensitive to changes in nutrient intake, with reduced calorie intake lowering muscle acetyl CoA concentration (46) and high-fat diet feeding increasing muscle acetyl CoA concentration (22, 52). Accompanying these changes in acetyl CoA, calorie restriction robustly enhances the sensitivity of skeletal muscle to insulin (49, 50, 62, 65), whereas high-fat diet feeding reduces skeletal muscle insulin-sensitivity (67, 76, 78). With this in mind, we investigated whether p300 or CBP mediated these effects of calorie restriction or high-fat diet on glucose tolerance and/or skeletal muscle insulin sensitivity. Overall, while high-fat diet worsened glucose tolerance and calorie restriction enhanced glucose tolerance and skeletal muscle insulin sensitivity in WT mice, these dietary effects were not affected by the loss of p300 or CBP. Taken together with the insulin signaling and insulin sensitivity findings in control diet-fed mice, these results clearly demonstrate that loss of p300 or CBP does not impact insulin-mediated glucose uptake in skeletal muscle.

Many substrates of p300 and CBP, such as PPARα (14), PGC1α (56, 73), FoxO1 (11), and GAPDH (64) are important regulators of cellular metabolism, mitochondrial biogenesis and oxidative capacity, particularly in skeletal muscle (20, 54), which could impact body weight and composition or energy expenditure. Indeed, mice with hypothalamus-specific knockout of CBP have large increases in body weight, food intake, and fat pad mass when fed a chow diet, despite no change in activity (51). In contrast, mice with a mutation in the CH1 domain of either p300 or CBP exhibit reduced WAT as percentage of body weight and reduced body weight compared to WT mice (4). However, mice with a whole-body heterozygous knockout of CBP exhibit no changes in body weight (80), while mice with pancreatic islet knockout of p300 demonstrate similar body weight, activity, and energy expenditure to WT mice (79). Similarly, we have previously described that germline knockout of p300 in skeletal muscle (i.e. P-MCK mice) does not alter body weight, body composition, or energy expenditure (38). Complimenting this lack of effect of germline loss of p300, here we find that neither germline loss of CBP, or knockout of p300 or CBP in adulthood impacts body composition, relative tissue mass, energy expenditure, nor activity. Thus, while there is evidence that loss of p300 or CBP in some tissues can alter the regulation of body weight and/or energy expenditure (4, 51), our data demonstrate that skeletal muscle p300 or CBP is not required to maintain normal whole-body energy expenditure or body composition.

Whole body knockout of p300 (81) or CBP (69) is embryonically lethal, and many studies, although not all (59), demonstrate that p300 (15, 57–59) and CBP (15) are required for terminal differentiation of C2C12 myotubes and human primary myotubes (16). As such, normal development of skeletal muscle is thought to require p300, and potentially CBP. In contrast, we have previously demonstrated that germline deletion of p300 in skeletal muscle, via the MCK

promoter, is not embryonically lethal and does not affect muscle structure, fiber-type expression, or development (38). We extend these findings by demonstrating that germline loss of CBP is also not embryonically lethal, and does not impact muscle development or growth, as evidenced by comparable muscle weights in C-MCK versus WT mice. Hence, our P-MCK and C-MCK mouse models clearly establish that loss of p300 or CBP during embryogenesis does not impair muscle development.

A limitation of this study is that we did not see complete loss of CBP or p300 at the protein level in the respective mouse models, with the knockout being ~50-60%. The primary reason for this likely relates to the fact that only ~45% of nuclei within skeletal muscle tissue are within muscle fibers (63). Supporting this, we (67, 76) and others (19, 25, 29, 45) have previously demonstrated that a lack of complete knockout in whole skeletal muscle tissue is due to the presence of a variety of cell types within skeletal muscle (e.g. endothelial cells, fibroblasts, adipocytes, immune cells). As such, given the ubiquitous presence of p300 and/or CBP across all cell types (72), it is not unexpected that we see ~50% knockout of p300 or CBP in whole muscle lysates from the P-iHSA/C-MCK/C-iHSA models. Indeed, when immunoprecipitating p300 from nuclear fractions from skeletal muscle of P-MCK mice, we find essentially complete (~95%) knockout of p300 in skeletal muscle (38). Moreover, when using primers targeted to include exon 9 of p300 or CBP, which is the exon that is excised after Cre-mediated recombination, we find an 87% reduction in p300 mRNA expression in P-iHSA and an 77% reduction in CBP mRNA expression in C-iHSA mouse muscle. Thus, overall, we believe that our mouse models appropriately allow us to study the impact of loss of p300 or CBP on energy expenditure and skeletal muscle insulin signaling and action.

In summary, to our knowledge, this is the first study to describe the contribution of acetyltransferases to skeletal muscle insulin sensitivity. In contrast to our hypothesis, our results demonstrate that loss of either p300 or CBP in skeletal muscle, be it during embryogenesis or in adulthood, does not impair glucose tolerance or skeletal muscle insulin sensitivity. A lack of an effect on insulin action is likely due to the large redundancy of function between p300 and CBP and their ability to compensate for one another (12, 23, 51, 79). Thus, it will be interesting in future studies to investigate the impact of combined loss of p300 and CBP, as has been done in other tissues (23, 79), on skeletal muscle insulin action and physiology as a whole. Finally, considering thus far that 22 acetyltransferases have been identified in human and mouse cells (10), it is conceivable that acetyltransferases other than CBP and p300 are more important regulators of skeletal muscle insulin action and metabolism. Overall, while it is clear that acetylation is a common post-translational modification that is present in skeletal muscle (35, 44), much work remains to be done to identify those acetyltransferases (and deacetylases) that mediate skeletal muscle protein acetylation, and also to define their broader significance to skeletal muscle physiology and biology.

Acknowledgments

We are grateful to the UC San Diego Animal Care Program Phenotyping Core for CLAMS and MRI measurements.

This work was supported, in part, by U.S. National Institutes of Health grants R01 AG043120 (to S.S.), T32 AR060712 and F30 DK115035 (to V.F.M.), R01 DK095926 (to C.E.M.), a UC San Diego Frontiers of Innovation Scholars Program grant (to S.S.), Graduate Student Research Support from the UC San Diego Institute of Engineering in Medicine and the Office of Graduate Studies (to V.F.M), post-doctoral fellowships from the Swiss National Science Foundation and the American Federation of Aging Research (to K.S.), a Medical Student Training in Aging Research Grant (to M.B.), and a UC San Diego URS Eureka! Research Scholarship (to S.L.).

SS, VFM, and JRD were responsible for the conception and design of the study, and the analysis and interpretation of the data. VFM and JRD were responsible for the design and drafting of the manuscript and SS revised the manuscript critically. KS, ST, MB, SL, EHB, SAL, BH and CEM contributed to analysis, interpretation of data, and critical revision of the manuscript. All authors gave final approval.

Chapter 3, in full, is a reprint of the material as it appears in the American Journal of Physiology, Endocrinology and Metabolism 2019 (with edits for style). V. F. Martins, J. R. Dent, K. Svensson, S. Tahvilian, M. Begur, S. Lakkaraju, E. H. Buckner, S. A. LaBarge, B. Hetrick, C. E. McCurdy, S. Schenk. The dissertation author was the primary investigator and author of this paper.

References

1. **Allfrey VG**, **Faulkner R**, **Mirsky AE**. Acetylation and methylation of histones and their possible role in the regulation of RNA synthesis. *Proc Natl Acad Sci* 51: 786–794, 1964.

2. **Arany Z**, **Sellers WR**, **Livingston DM**, **Eckner R**. E1A-associated p300 and CREB-associated CBP belong to a conserved family of coactivators. *Cell* 77: 799–800, 1994.

3. **Aslan JE**, **Rigg RA**, **Nowak MS**, **Loren CP**, **Baker-Groberg SM**, **Pang J**, **David LL**, **McCarty OJT**. Lysine acetyltransfer supports platelet function. *J Thromb Haemost* 13: 1908–17, 2015.

4. **Bedford DC**, **Kasper LH**, **Wang R**, **Chang Y**, **Green DR**, **Brindle PK**. Disrupting the CH1 domain structure in the acetyltransferases CBP and p300 results in lean mice with increased metabolic control. *Cell Metab* 14: 219–30, 2011.

5. **Beg M**, **Abdullah N**, **Thowfeik FS**, **Altorki NK**, **McGraw TE**. Distinct Akt phosphorylation states are required for insulin regulated Glut4 and Glut1-mediated glucose uptake. *Elife* 6: 1–22, 2017.

6. **Belman JP**, **Bian RR**, **Habtemichael EN**, **Li DT**, **Jurczak MJ**, **Alcázar-Román A**, **McNally LJ**, **Shulman GI**, **Bogan JS**. Acetylation of TUG protein promotes the accumulation of GLUT4 glucose transporters in an insulin-responsive intracellular compartment. *J Biol Chem* 290: 4447–63, 2015.

7. **Brüning JC**, **Michael MD**, **Winnay JN**, **Hayashi T**, **Hörsch D**, **Accili D**, **Goodyear LJ**, **Kahn CR**. A muscle-specific insulin receptor knockout exhibits features of the metabolic syndrome of NIDDM without altering glucose tolerance. *Mol Cell* 2: 559–69, 1998.

8. **Cho H**, **Mu J**, **Kim JK**, **Thorvaldsen JL**, **Chu Q**, **Crenshaw EB**, **Kaestner KH**, **Bartolomei MS**, **Shulman GI**, **Birnbaum MJ**. Insulin resistance and a diabetes mellitus-like syndrome in mice lacking the protein kinase Akt2 (PKB beta). *Science* 292: 1728–31, 2001.

9. **Choudhary C**, **Kumar C**, **Gnad F**, **Nielsen ML**, **Rehman M**, **Walther TC**, **Olsen J V**, **Mann M**. Lysine acetylation targets protein complexes and co-regulates major cellular functions. *Science* 325: 834–40, 2009.

10. **Choudhary C**, **Weinert BT**, **Nishida Y**, **Verdin E**, **Mann M**. The growing landscape of lysine acetylation links metabolism and cell signalling. *Nat Rev Mol Cell Biol* 15: 536–50, 2014.

11. **Daitoku H**, **Hatta M**, **Matsuzaki H**, **Aratani S**, **Ohshima T**, **Miyagishi M**, **Nakajima T**, **Fukamizu A**. Silent information regulator 2 potentiates Foxo1-mediated transcription through its deacetylase activity. *Proc Natl Acad Sci* 101: 10042–10047, 2004.

12. **Dancy BM**, **Cole PA**. Protein lysine acetylation by p300/CBP. *Chem Rev* 115: 2419–52, 2015.

13. **Dou C**, **Liu Z**, **Tu K**, **Zhang H**, **Chen C**, **Yaqoob U**, **Wang Y**, **Wen J**, **van Deursen J**, **Sicard D**, **Tschumperlin D**, **Zou H**, **Huang WC**, **Urrutia R**, **Shah VH**, **Kang N**. P300 Acetyltransferase Mediates Stiffness-Induced Activation of Hepatic Stellate Cells Into Tumor-Promoting Myofibroblasts. *Gastroenterology* 154: 2209-2221.e14, 2018.

14. **Dowell P**, **Ishmael JE**, **Avram D**, **Peterson VJ**, **Nevrivy DJ**, **Leid M**. P300 Functions As a Coactivator for the Peroxisome Proliferator- Activated Receptor α. *J Biol Chem* 272: 33435–33443, 1997.

15. **Eckner R**, **Yao TP**, **Oldread E**, **Livingston DM**. Interaction and functional collaboration of p300/CBP and bHLH proteins in muscle and B-cell differentiation. *Genes Dev* 10: 2478–2490, 1996.

16. **Fauquier L**, **Azzag K**, **Parra MAM**, **Quillien A**, **Boulet M**, **Diouf S**, **Carnac G**, **Waltzer L**, **Gronemeyer H**, **Vandel L**. CBP and P300 regulate distinct gene networks required for human primary myoblast differentiation and muscle integrity. *Sci Rep* 8: 12629, 2018.

17. **Fermento ME**, **Gandini NA**, **Salomón DG**, **Ferronato MJ**, **Vitale CA**, **Arévalo J**, **López Romero A**, **Nuñez M**, **Jung M**, **Facchinetti MM**, **Curino AC**. Inhibition of p300 suppresses growth of breast cancer. Role of p300 subcellular localization. *Exp Mol Pathol* 97: 411–24, 2014.

18. **Guo S**, **Cichy SB**, **He X**, **Yang Q**, **Ragland M**, **Ghosh AK**, **Johnson PF**, **Unterman TG**. Insulin suppresses transactivation by CAAT/enhancer-binding proteins beta (C/EBPbeta). Signaling to p300/CREB-binding protein by protein kinase B disrupts interaction with the major activation domain of C/EBPbeta. *J Biol Chem* 276: 8516–23, 2001.

19. **Hamilton DL**, **Philp A**, **MacKenzie MG**, **Baar K**. A limited role for PI(3,4,5)P3regulation in controlling skeletal muscle mass in response to resistance exercise. *PLoS One* 5: 1–9, 2010.

20. **Handschin C**. Regulation of skeletal muscle cell plasticity by the peroxisome proliferator-activated receptor γ coactivator 1α. *J Recept Signal Transduct* 30: 376–384, 2010.

21. **He L**, **Sabet A**, **Djedjos S**, **Miller R**, **Sun X**, **Hussain MA**, **Radovick S**, **Wondisford FE**. Metformin and Insulin Suppress Hepatic Gluconeogenesis through Phosphorylation of CREB Binding Protein. *Cell* 137: 635–646, 2009.

22. **Heigenhauser GJ**, **Spriet LL**, **Putman CT**, **Jones NL**, **Lands LC**, **Cederblad G**, **Hultman E**, **Lindinger MI**, **McKelvie RS**. Pyruvate dehydrogenase activity and acetyl group accumulation during exercise after different diets. *Am J Physiol Metab* 265: E752–E760, 2017.

23. **Hennig AK**, **Peng GH**, **Chen S**. Transcription Coactivators p300 and CBP Are Necessary for Photoreceptor-Specific Chromatin Organization and Gene Expression. *PLoS One* 8,

2013.

24. **Henry RA**, **Kuo Y**, **Andrews AJ**. Differences in Specificity and Selectivity Between CBP and p300 Acetylation of Histone H3 and H3/H4. *Biochemistry* 52: 5746–5759, 2013.

25. **Holt LJ**, **Brandon AE**, **Small L**, **Suryana E**, **Preston E**, **Wilks D**, **Mokbel N**, **Coles CA**, **White JD**, **Turner N**, **Daly RJ**, **Cooney GJ**. Ablation of Grb10 Specifically in Muscle Impacts Muscle Size and Glucose Metabolism in Mice. *Endocrinology* 159: 1339–1351, 2018.

26. **Howie HL**, **Koop JI**, **Weese J**, **Robinson K**, **Wipf G**, **Kim L**, **Galloway DA**. Beta-hpv 5 and 8 E6 promote p300 degradation by blocking AKT/p300 association. *PLoS Pathog* 7, 2011.

27. **Huang W-C**, **Chen C-C**. Akt phosphorylation of p300 at Ser-1834 is essential for its histone acetyltransferase and transcriptional activity. *Mol Cell Biol* 25: 6592–602, 2005.

28. **Ianculescu I**, **Wu DY**, **Siegmund KD**, **Stallcup MR**. Selective roles for cAMP response element-binding protein binding protein and p300 protein as coregulators for androgen-regulated gene expression in advanced prostate cancer cells. *J Biol Chem* 287: 4000–4013, 2012.

29. **Jackson KC**, **Tarpey MD**, **Valencia AP**, **Iñigo MR**, **Pratt SJ**, **Patteson DJ**, **McClung JM**, **Lovering RM**, **Thomson DM**, **Spangenburg EE**. Induced Cre-mediated knockdown of Brca1 in skeletal muscle reduces mitochondrial respiration and prevents glucose intolerance in adult mice on a high-fat diet. *FASEB J* 32: 3070–3084, 2018.

30. **Jing E**, **O'Neill BT**, **Rardin MJ**, **Kleinridders A**, **Ilkeyeva OR**, **Ussar S**, **Bain JR**, **Lee KY**, **Verdin EM**, **Newgard CB**, **Gibson BW**, **Kahn CR**. Sirt3 regulates metabolic flexibility of skeletal muscle through reversible enzymatic deacetylation. *Diabetes* 62: 3404–17, 2013.

31. **Kaida A**, **Ariumi Y**, **Baba K**, **Matsubae M**, **Takao T**, **Shimotohno K**. Identification of a novel p300-specific-associating protein, PRS1 (phosphoribosylpyrophosphate synthetase subunit 1). *Biochem J* 391: 239–247, 2005.

32. **Kang-Decker N**, **Tong C**, **Boussouar F**, **Baker DJ**, **Xu W**, **Leontovich AA**, **Taylor WR**, **Brindle PK**, **van Deursen JMA**. Loss of CBP causes T cell lymphomagenesis in synergy with p27Kip1 insufficiency. *Cancer Cell* 5: 177–89, 2004.

33. **Kasper LH**, **Fukuyama T**, **Biesen MA**, **Boussouar F**, **Tong C**, **de Pauw A**, **Murray PJ**, **van Deursen JMA**, **Brindle PK**. Conditional Knockout Mice Reveal Distinct Functions for the Global Transcriptional Coactivators CBP and p300 in T-Cell Development. *Mol Cell Biol* 26: 789–809, 2006.

34. **Kim SC**, **Sprung R**, **Chen Y**, **Xu Y**, **Ball H**, **Pei J**, **Cheng T**, **Kho Y**, **Xiao H**, **Xiao L**, **Grishin N V.**, **White M**, **Yang X-J**, **Zhao Y**. Substrate and functional diversity of lysine acetylation revealed by a proteomics survey. *Mol Cell* 23: 607–18, 2006.

35. **Koltai E**, **Szabo Z**, **Atalay M**, **Boldogh I**, **Naito H**, **Goto S**, **Nyakas C**, **Radak Z**. Exercise alters SIRT1, SIRT6, NAD and NAMPT levels in skeletal muscle of aged rats. *Mech Ageing Dev* 131: 21–8, 2010.

36. **Kuhlmann N**, **Wroblowski S**, **Knyphausen P**, **de Boor S**, **Brenig J**, **Zienert AY**, **Meyer-Teschendorf K**, **Praefcke GJK**, **Nolte H**, **Krüger M**, **Schacherl M**, **Baumann U**, **James LC**, **Chin JW**, **Lammers M**. Structural and Mechanistic Insights into the Regulation of the Fundamental Rho Regulator RhoGDIα by Lysine Acetylation. *J Biol Chem* 291: 5484–99, 2016.

37. **LaBarge S**, **Migdal C**, **Schenk S**. Is acetylation a metabolic rheostat that regulates skeletal muscle insulin action? *Mol Cells* 38: 297–303, 2015.

38. **LaBarge SA**, **Migdal CW**, **Buckner EH**, **Okuno H**, **Gertsman I**, **Stocks B**, **Barshop BA**, **Nalbandian SR**, **Philp A**, **McCurdy CE**, **Schenk S**. p300 is not required for metabolic adaptation to endurance exercise training. *FASEB J* 30: 1623–33, 2016.

39. **Lai Y-C**, **Liu Y**, **Jacobs R**, **Rider MH**. A novel PKB/Akt inhibitor, MK-2206, effectively inhibits insulin-stimulated glucose metabolism and protein synthesis in isolated rat skeletal muscle. *Biochem J* 447: 137–147, 2012.

40. **Lantier L**, **Williams AS**, **Williams IM**, **Yang KK**, **Bracy DP**, **Goelzer M**, **James FD**, **Gius D**, **Wasserman DH**. SIRT3 Is Crucial for Maintaining Skeletal Muscle Insulin Action and Protects Against Severe Insulin Resistance in High-Fat–Fed Mice. *Diabetes* 64: 3081–3092, 2015.

41. **Leandry LA**, **Abdalla MN**, **Matheny RW**, **Pasiakos SM**, **McClung HL**, **Ford M**, **Geddis A V.** AKT2 is the predominant AKT isoform expressed in human skeletal muscle. *Physiol Rep* 6: e13652, 2018.

42. **Liu Y**, **Denlinger CE**, **Rundall BK**, **Smith PW**, **Jones DR**. Suberoylanilide hydroxamic acid induces Akt-mediated phosphorylation of p300, which promotes acetylation and transcriptional activation of RelA/p65. *J Biol Chem* 281: 31359–31368, 2006.

43. **Liu Y**, **Xing Z**, **Zhang J**, **Fang Y**. Akt kinase targets the association of CBP with histone H3 to regulate the acetylation of lysine K18. *FEBS Lett* 587: 847–853, 2013.

44. **Lundby A**, **Lage K**, **Weinert BT**, **Bekker-Jensen DB**, **Secher A**, **Skovgaard T**, **Kelstrup CD**, **Dmytriyev A**, **Choudhary C**, **Lundby C**, **Olsen J V**. Proteomic analysis of lysine acetylation sites in rat tissues reveals organ specificity and subcellular patterns. *Cell Rep* 2: 419–31, 2012.

45. **Madsen AB**, **Knudsen JR**, **Henriquez-Olguin C**, **Angin Y**, **Zaal KJ**, **Sylow L**, **Schjerling P**, **Ralston E**, **Jensen TE**. β-Actin shows limited mobility and is required only for supraphysiological insulin-stimulated glucose transport in young adult soleus muscle. *Am J Physiol Metab* 315: E110–E125, 2018.

46. **Mariño G**, **Pietrocola F**, **Eisenberg T**, **Kong Y**, **Malik SA**, **Andryushkova A**, **Schroeder**

S, **Pendl T**, **Harger A**, **Niso-Santano M**, **Zamzami N**, **Scoazec M**, **Durand S**, **Enot DP**, **Fernández ÁF**, **Martins I**, **Kepp O**, **Senovilla L**, **Bauvy C**, **Morselli E**, **Vacchelli E**, **Bennetzen M**, **Magnes C**, **Sinner F**, **Pieber T**, **López-Otín C**, **Maiuri MC**, **Codogno P**, **Andersen JS**, **Hill JA**, **Madeo F**, **Kroemer G**. Regulation of autophagy by cytosolic acetyl-coenzyme A. *Mol Cell* 53: 710–25, 2014.

47. **Martins VF**, **Tahvilian S**, **Kang JH**, **Svensson K**, **Hetrick B**, **Chick WS**, **Schenk S**, **McCurdy CE**. Calorie Restriction-Induced Increase in Skeletal Muscle Insulin Sensitivity Is Not Prevented by Overexpression of the p55α Subunit of Phosphoinositide 3-Kinase. *Front Physiol* 9: 789, 2018.

48. **McCarthy JJ**, **Srikuea R**, **Kirby TJ**, **Peterson CA**, **Esser KA**. Inducible Cre transgenic mouse strain for skeletal muscle-specific gene targeting. *Skelet Muscle* 2: 8, 2012.

49. **McCurdy CE**, **Cartee GD**. Akt2 is essential for the full effect of calorie restriction on insulin-stimulated glucose uptake in skeletal muscle. *Diabetes* 54: 1349–56, 2005.

50. **McCurdy CE**, **Davidson RT**, **Cartee GD**. Calorie restriction increases the ratio of phosphatidylinositol 3-kinase catalytic to regulatory subunits in rat skeletal muscle. *Am J Physiol Endocrinol Metab* 288: E996–E1001, 2005.

51. **Moreno CL**, **Yang L**, **Dacks PA**, **Isoda F**, **Van Deursen JMA**, **Mobbs C V.** Role of hypothalamic Creb-binding protein in obesity and molecular reprogramming of metabolic substrates. *PLoS One* 11: 1–15, 2016.

52. **Park MJ**, **Aja S**, **Li Q**, **Degano AL**, **Penati J**, **Zhuo J**, **Roe CR**, **Ronnett G V.** Anaplerotic triheptanoin diet enhances mitochondrial substrate use to remodel the metabolome and improve lifespan, motor function, and sociability in MeCP2-null mice. *PLoS One* 9, 2014.

53. **Parker BL**, **Yang G**, **Humphrey SJ**, **Chaudhuri R**, **Ma X**, **Peterman S**, **James DE**. Targeted phosphoproteomics of insulin signaling using data-independent acquisition mass spectrometry. *Sci Signal* 8, 2015.

54. **Pérez-Schindler J**, **Svensson K**, **Vargas-Fernández E**, **Santos G**, **Wahli W**, **Handschin C**. The coactivator PGC-1α regulates skeletal muscle oxidative metabolism independently of the nuclear receptor PPARβ/δ in sedentary mice fed a regular chow diet. *Diabetologia* 57: 2405–2412, 2014.

55. **Pirola L**, **Zerzaihi O**, **Vidal H**, **Solari F**. Protein acetylation mechanisms in the regulation of insulin and insulin-like growth factor 1 signalling. *Mol Cell Endocrinol* 362: 1–10, 2012.

56. **Puigserver P**, **Adelmant G**, **Wu Z**, **Fan M**, **Xu J**, **O'Malley B**, **Spiegelman BM**. Activation of PPARgamma coactivator-1 through transcription factor docking. *Science* 286: 1368–71, 1999.

57. **Puri PL**, **Avantaggiati ML**, **Balsano C**, **Sang N**, **Graessmann A**, **Giordano A**, **Levrero M**. p300 is required for MyoD-dependent cell cycle arrest and muscle-specic gene transcription. *EMBO J* 16: 369–383, 1997.

58. **Puri PL**, **Sartorelli V**, **Yang XJ**, **Hamamori Y**, **Ogryzko V V.**, **Howard BH**, **Kedes L**, **Wang JYJ**, **Graessmann A**, **Nakatani Y**, **Levrero M**. Differential roles of p300 and PCAF acetyltransferases in muscle differentiation. *Mol Cell* 1: 35–45, 1997.

59. **Roth JF**, **Shikama N**, **Henzen C**, **Desbaillets I**, **Lutz W**, **Marino S**, **Wittwer J**, **Schorle H**, **Gassmann M**, **Eckner R**. Differential role of p300 and CBP acetyltransferase during myogenesis: p300 acts upstream of MyoD and Myf5. *EMBO J* 22: 5186–5196, 2003.

60. **Ruiz L**, **Gurlo T**, **Ravier MA**, **Wojtusciszyn A**, **Mathieu J**, **Brown MR**, **Broca C**, **Bertrand G**, **Butler PC**, **Matveyenko A V**, **Dalle S**, **Costes S**. Proteasomal degradation of the histone acetyl transferase p300 contributes to beta-cell injury in a diabetes environment. *Cell Death Dis* 9: 600, 2018.

61. **Sanchez M**, **Sauvé K**, **Picard N**, **Tremblay A**. The hormonal response of estrogen receptor beta is decreased by the phosphatidylinositol 3-kinase/Akt pathway via a phosphorylation-dependent release of CREB-binding protein. *J Biol Chem* 282: 4830–40, 2007.

62. **Schenk S**, **McCurdy CE**, **Philp A**, **Chen MZ**, **Holliday MJ**, **Bandyopadhyay GK**, **Osborn O**, **Baar K**, **Olefsky JM**. Sirt1 enhances skeletal muscle insulin sensitivity in mice during caloric restriction. *J Clin Invest* 121: 4281–8, 2011.

63. **Schmalbruch H**, **Hellhammer U**. The number of nuclei in adult rat muscles with special reference to satellite cells. *Anat Rec* 189: 169–175, 1977.

64. **Sen N**, **Hara MR**, **Kornberg MD**, **Cascio MB**, **Bae B-I**, **Shahani N**, **Thomas B**, **Dawson TM**, **Dawson VL**, **Snyder SH**, **Sawa A**. Nitric oxide-induced nuclear GAPDH activates p300/CBP and mediates apoptosis. *Nat Cell Biol* 10: 866–73, 2008.

65. **Sharma N**, **Arias EB**, **Bhat AD**, **Sequea D a**, **Ho S**, **Croff KK**, **Sajan MP**, **Farese R V**, **Cartee GD**. Mechanisms for increased insulin-stimulated Akt phosphorylation and glucose uptake in fast- and slow-twitch skeletal muscles of calorie-restricted rats. *Am J Physiol Endocrinol Metab* 300: E966–E978, 2011.

66. **Sundaresan NR**, **Pillai VB**, **Wolfgeher D**, **Samant S**, **Vasudevan P**, **Parekh V**, **Raghuraman H**, **Cunningham JM**, **Gupta M**, **Gupta MP**. The deacetylase SIRT1 promotes membrane localization and activation of Akt and PDK1 during tumorigenesis and cardiac hypertrophy. *Sci Signal* 4: ra46, 2011.

67. **Svensson K**, **Dent JR**, **Tahvilian S**, **Martins VF**, **Sathe A**, **Ochala J**, **Patel MS**, **Schenk S**. Defining the contribution of skeletal muscle pyruvate dehydrogenase α1 to exercise performance and insulin action. *Am J Physiol Metab* 315: E1034–E1045, 2018.

68. **Svensson K**, **LaBarge SA**, **Martins VF**, **Schenk S**. Temporal overexpression of SIRT1 in skeletal muscle of adult mice does not improve insulin sensitivity or markers of mitochondrial biogenesis. *Acta Physiol* 221: 193–203, 2017.

69. **Tanaka Y**, **Naruse I**, **Maekawa T**, **Masuya H**, **Shiroishi T**, **Ishii S**. Abnormal skeletal patterning in embryos lacking a single Cbp allele: A partial similarity with Rubinstein-Taybi

syndrome. *Proc Natl Acad Sci* 94: 10215–10220, 1997.

70. **Turner BM**. Histone acetylation and control of gene expression. *J Cell Sci* 99 (Pt 1): 13–20, 1991.

71. **Verdin E**, **Ott M**. 50 years of protein acetylation: from gene regulation to epigenetics, metabolism and beyond. *Nat Rev Mol Cell Biol* 16: 258–64, 2015.

72. **Vo N**, **Goodman RH**. CREB-binding protein and p300 in transcriptional regulation. *J Biol Chem* 276: 13505–8, 2001.

73. **Wallberg AE**, **Yamamura S**, **Malik S**, **Spiegelman BM**, **Roeder RG**. Coordination of p300-mediated chromatin remodeling and TRAP/mediator function through coactivator PGC-1α. *Mol Cell* 12: 1137–1149, 2003.

74. **Wang QE**, **Han C**, **Zhao R**, **Wani G**, **Zhu Q**, **Gong L**, **Battu A**, **Racoma I**, **Sharma N**, **Wani AA**. P38 MAPK- and Akt-mediated p300 phosphorylation regulates its degradation to facilitate nucleotide excision repair. *Nucleic Acids Res* 41: 1722–1733, 2013.

75. **Weinert BT**, **Narita T**, **Satpathy S**, **Srinivasan B**, **Hansen BK**, **Schölz C**, **Hamilton WB**, **Zucconi BE**, **Wang WW**, **Liu WR**, **Brickman JM**, **Kesicki EA**, **Lai A**, **Bromberg KD**, **Cole PA**, **Choudhary C**. Time-Resolved Analysis Reveals Rapid Dynamics and Broad Scope of the CBP/p300 Acetylome. *Cell* 174: 231-244.e12, 2018.

76. **White AT**, **LaBarge SA**, **McCurdy CE**, **Schenk S**. Knockout of STAT3 in skeletal muscle does not prevent high-fat diet-induced insulin resistance. *Mol Metab* 4: 569–75, 2015.

77. **White AT**, **McCurdy CE**, **Philp A**, **Hamilton DL**, **Johnson CD**, **Schenk S**. Skeletal muscle-specific overexpression of SIRT1 does not enhance whole-body energy expenditure or insulin sensitivity in young mice. *Diabetologia* 56: 1629–37, 2013.

78. **White AT**, **Philp A**, **Fridolfsson HN**, **Schilling JM**, **Murphy AN**, **Hamilton DL**, **McCurdy CE**, **Patel HH**, **Schenk S**. High-fat diet-induced impairment of skeletal muscle insulin sensitivity is not prevented by SIRT1 overexpression. *Am J Physiol Endocrinol Metab* 307: E764-72, 2014.

79. **Wong CK**, **Wade-Vallance AK**, **Luciani DS**, **Brindle PK**, **Lynn FC**, **Gibson WT**. The p300 and CBP Transcriptional Coactivators are Required for Beta Cell and Alpha Cell Proliferation. *Diabetes* : db170237, 2017.

80. **Yamauchi T**, **Oike Y**, **Kamon J**, **Waki H**, **Komeda K**, **Tsuchida A**, **Date Y**, **Li M-X**, **Miki H**, **Akanuma Y**, **Nagai R**, **Kimura S**, **Saheki T**, **Nakazato M**, **Naitoh T**, **Yamamura K**, **Kadowaki T**. Increased insulin sensitivity despite lipodystrophy in Crebbp heterozygous mice. *Nat Genet* 30: 221–6, 2002.

81. **Yao TP**, **Oh SP**, **Fuchs M**, **Zhou ND**, **Ch'ng LE**, **Newsome D**, **Bronson RT**, **Li E**, **Livingston DM**, **Eckner R**. Gene dosage-dependent embryonic development and proliferation defects in mice lacking the transcriptional integrator p300. *Cell* 93: 361–372,

1998.

82. **Zhao S**, **Xu W**, **Jiang W**, **Yu W**, **Lin Y**, **Zhang T**, **Yao J**, **Zhou L**, **Zeng Y**, **Li H**, **Li Y**, **Shi J**, **An W**, **Hancock SM**, **He F**, **Qin L**, **Chin J**, **Yang P**, **Chen X**, **Lei Q**, **Xiong Y**, **Guan K-L**. Regulation of cellular metabolism by protein lysine acetylation. *Science* 327: 1000–4, 2010.

83. **Zhou XY**, **Shibusawa N**, **Naik K**, **Porras D**, **Temple K**, **Ou H**, **Kaihara K**, **Roe MW**, **Brady MJ**, **Wondisford FE**. Insulin regulation of hepatic gluconeogenesis through phosphorylation of CREB-binding protein. *Nat Med* 10: 633–637, 2004.

Table 3.1. Body composition, tissue weights, and fasting glucose and insulin for P-MCK mice on high-fat and calorie restriction diets

	Control/Ad Libitum		High-Fat Diet		Calorie Restriction	
	WT	P-MCK	WT	P-MCK	WT	P-MCK
Body weight, g	23.7 ± 0.5	23.2 ± 0.5	26.7 ± 0.8*	27.9 ± 0.6*	18.3 ± 0.6*	18.5 ± 0.6*
% Body fat	10.5 ± 0.9	9.9 ± 1.8	23.1 ± 2.3*	20.2 ± 2.4*	5.7 ± 1.0*	7.3 ± 0.9*
% Lean muscle mass	87.2 ± 0.9	86.7 ± 0.9	74.1 ± 2.2*	77.3 ± 2.5*	91.0 ± 1.39*	90.1* ± 1.4*
Epididymal WAT, %BW	1.23 ± 0.14	1.29 ± 0.11	3.78 ± 0.36*	3.36 ± 0.45*	0.56 ± 0.13*	0.63 ± 0.11*
Tibialis anterior, %BW	0.173 ± 0.003	0.171 ± 0.005	0.148 ± 0.006*	0.159 ± 0.007*	0.185 ± 0.005	0.179 ± 0.006
Gastrocnemius, %BW	0.48 ± 0.01	0.48 ± 0.01	0.43 ± 0.01*	0.39 ± 0.02*	0.48 ± 0.01	0.51 ± 0.01
Heart, %BW	0.46 ± 0.01	0.44 ± 0.01	0.41 ± 0.02*	0.39 ± 0.02*	0.47 ± 0.01	0.45 ± 0.01
Liver, %BW	4.46 ± 0.11	4.71 ± 0.29	4.11 ± 0.40	4.46 ± 0.53	4.20 ± 0.08*	4.14 ± 0.09*
Fasting glucose, mg/dl	107 ± 5	105 ± 3	130 ± 5*	136 ± 8*	88 ± 6*	86 ± 4*
Fasting insulin, ng/ml	0.39 ± 0.03	0.38 ± 0.03	n.d.	n.d.	n.d.	n.d.

Data reported as mean ± SE; for body weight, % body fat, % lean muscle mass, and tissue weights: $n = 6–10$/group; for fasting glucose and insulin: $n = 5–9$/group. Control diet and ad libitum diet groups have been pulled together. BW, body weight; n.d., not determined; WAT, white adipose tissue; WT, wild type. Two-way ANOVA: *$P < 0.05$ main effect of diet vs. control/ad libitum.

Table 3.2. Body composition, tissue weights, and fasting glucose and insulin for C-MCK mice

	Ad Libitum		Calorie Restriction	
	WT	C-MCK	WT	C-MCK
Body weight, g	26.3 ± 0.5	23.0 ± 0.6#	19.1 ± 0.7*	18.1 ± 0.4*#
% Body fat	17.0 ± 1.1	15.3 ± 0.7	n.d.	n.d.
% Lean muscle mass	78.2 ± 1.2	80.4 ± 0.5	n.d.	n.d.
Epididymal WAT, %BW	2.47 ± 0.23	2.07 ± 0.27	0.64 ± 0.10*	0.77 ± 0.11*
Tibialis anterior, %BW	0.141 ± 0.004	0.145 ± 0.004	0.158 ± 0.007*	0.171 ± 0.005*
Gastrocnemius, %BW	0.42 ± 0.01	0.42 ± 0.01	0.42 ± 0.02	0.44 ± 0.02
Heart, %BW	0.39 ± 0.01	0.39 ± 0.01	0.42 ± 0.02	0.41 ± 0.01
Liver, %BW	4.87 ± 0.13	4.66 ± 0.26	4.32 ± 0.16*	4.42 ± 0.13*
Fasting glucose, mg/dl	124 ± 4	118 ± 8	92 ± 2*	98 ± 10*
Fasting insulin, ng/ml	0.48 ± 0.04	0.49 ± 0.08	n.d.	n.d.

Data reported as mean ± SE; for body weight, % body fat, % lean muscle mass, and tissue weights: n = 5–10/group; for fasting glucose and insulin: n = 5–9/group. BW, body weight; n.d., not determined; WAT, white adipose tissue; WT, wild type. Two-way ANOVA: *$P < 0.05$ main effect of diet, #$P < 0.05$ main effect of genotype.

Table 3.3. Body composition, tissue weights, and fasting glucose and insulin for iHSA mice

	WT	P-iHSA	WT	C-iHSA
Body weight, g	31.0 ± 1.5	32.2 ± 1.2	27.9 ± 0.7	27.8 ± 0.4
% Body fat	11.2 ± 1.0	12.9 ± 1.5	11.5 ± 1.2	9.7 ± 1.5
% Lean muscle mass	84.6 ± 1.7	82.9 ± 1.3	85.8 ± 1.3	84.1 ± 1.3
Epididymal WAT, %BW	1.59 ± 0.08	1.73 ± 0.18	1.44 ± 0.10	1.30 ± 0.12
Tibialis anterior, %BW	0.169 ± 0.004	0.161 ± 0.004	0.150 ± 0.004	0.157 ± 0.003
Gastrocnemius, %BW	0.48 ± 0.01	0.47 ± 0.01	0.43 ± 0.01	0.46 ± 0.01
Heart, %BW	0.45 ± 0.01	0.43 ± 0.01	0.43 ± 0.00	0.45 ± 0.02
Liver, %BW	5.01 ± 0.11	5.11 ± 0.09	5.34 ± 0.10	5.69 ± 0.15
Fasting glucose, mg/dl	132 ± 4	130 ± 5	147 ± 4	149 ± 4
Fasting insulin, ng/ml	0.43 ± 0.05	0.51 ± 0.09	0.57 ± 0.08	0.51 ± 0.05

Data reported as mean ± SE; for body weight, % body fat, % lean muscle mass, and tissue weights: $n = 5–8$/group; for fasting glucose: $n = 6–9$/group; for fasting insulin: $n = 4–7$/group. BW, body weight; WAT, white adipose tissue; WT, wild type.

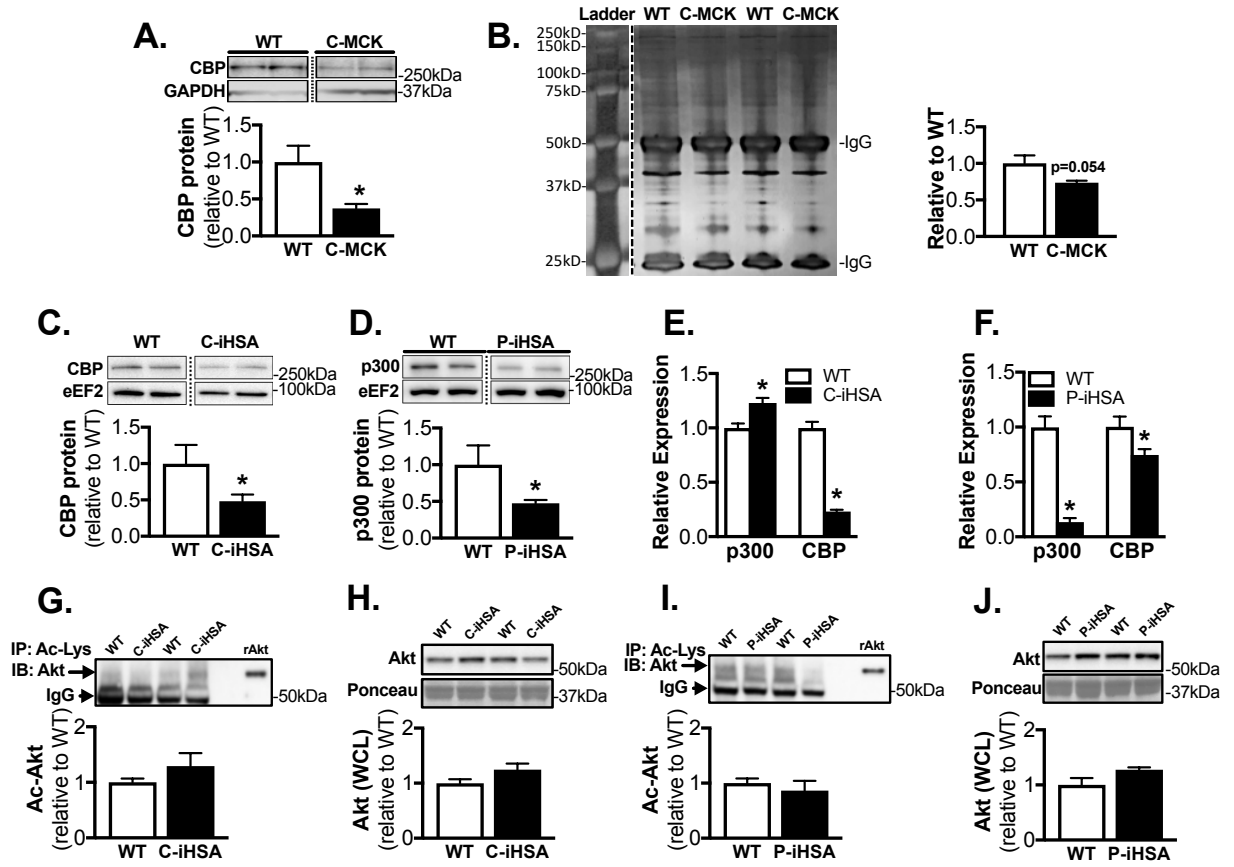

Figure 3.1: C-MCK and C-iHSA mice display reduced CBP protein abundance, while P-iHSA mice display reduced p300 protein abundance in skeletal muscle. A) Quantitation and representative images of CBP protein abundance in plantaris muscle of male C-MCK mice (n = 5/group). B) Silver stain of acetyl-lysine immunoprecipitates from C-MCK and WT tibialis anterior muscle (n = 4/group). Quantitation and representative images of C) CBP protein abundance in soleus muscle of male C-iHSA mice (n = 5-6/group) and D) p300 protein abundance in soleus muscle of male P-iHSA mice (n = 5-6/group). mRNA expression of p300 and CBP in gastrocnemius muscles of E) C-iHSA and F) P-iHSA mice (n = 5-6/group). The primers for p300 and CBP mRNA were designed to anneal onto exon 9 (exon that is floxed in P-iHSA and C-iHSA mouse) and exon 10. Representative images and quantification of acetylated-Akt (Ac-Akt), and total Akt from the whole cell lysate (WCL) of the same samples, in G-H) C-iHSA and I-J) P-iHSA tibialis anterior muscle (n = 4/group), which was determined by immunoprecipitation (IP) with an acetyl-lysine antibody and subsequent immunoblotting (IB) with an Akt antibody. Non-specific binding to IgG from IP antibody is indicated. There is a single empty lane between IPs and recombinant Akt (rAkt). Western blot intensity values were normalized to the protein loading control GAPDH, eEF2, or Ponceau stain while qPCR mRNA expression was normalized to mRNA expression of *tbp*; all values are presented relative to WT. *, $p<0.05$ unpaired Student's *t*-test, transgenic versus WT. Data reported as mean ± SEM.

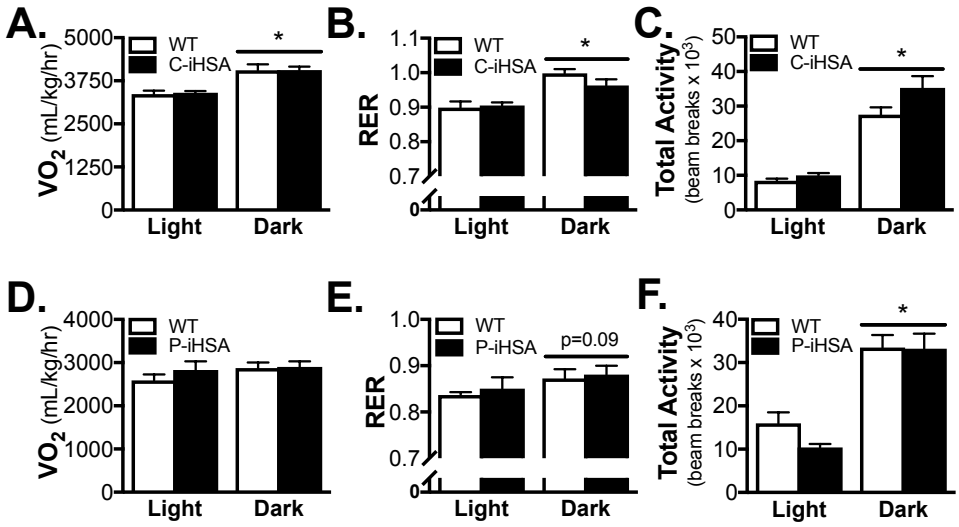

Figure 3.2: Energy expenditure and activity are comparable between C-iHSA or P-iHSA and WT mice. Energy expenditure and spontaneous activity measurements were made on male A-C) C-iHSA and D-F) P-iHSA mice using the CLAMS system over 3 consecutive days and averages for the light and dark cycles on days 2 and 3 are presented. A, D) Whole body oxygen consumption (VO_2) and B, E) Respiratory exchange ratio (RER) were measured by indirect calorimetry. C, F) Total activity (i.e., total z + x axis beam breaks). n = 5/group. *, $p<0.05$ 2-way ANOVA main effect of light cycle. Data reported as mean ± SEM.

Figure 3.3: Germline deletion of p300 in skeletal muscle does not alter glucose tolerance, or skeletal muscle insulin sensitivity. A) Blood glucose concentrations and B) area under the curve (AUC) of male P-MCK mice on control (CON) or HFD during an oral glucose tolerance test (OGTT; 2 g/kg); P-MCK CON (n=8), WT CON (n=8), P-MCK HFD (n=9), WT HFD (n=7). C) Blood glucose concentrations and D) area under the curve (AUC) of a separate cohort of male P-MCK mice on AL or CR diet during an oral glucose tolerance test (OGTT; 2 g/kg); P-MCK AL (n=8), WT AL (n=7), P-MCK CR (n=9), WT CR (n=7). *, $p<0.05$ 2-way ANOVA, main effect of diet (within a time point for OGTT). E-H) Basal 2-deoxy-glucose uptake (2DOGU), Insulin (0.36 nmol/L) 2DOGU, and insulin-stimulated 2DOGU (Insulin Stim.; calculated as insulin 2DOGU – basal 2DOGU) in isolated E-F) extensor digitorum longus (EDL) and G-H) soleus muscles from male P-MCK mice on AL or CR diet; P-MCK AL (n=6), WT AL (n=5), P-MCK CR (n=8), WT CR (n=5). #, $p<0.05$ 2-way ANOVA within ad libitum and within diet, main effect of insulin; *, $p<0.05$ 2-way ANOVA within basal and within insulin samples, main effect of diet. I) Phospho-Akt^{S473} (pAkt^{S473}), phospho-Akt^{T308} (pAkt^{T308}), total Akt, phospho-GSK3β^{S9} (pGSK3β^{S9}), and total GSK3β in basal and insulin-stimulated (- and +, respectively) soleus muscles from AL fed mice. J) Quantification of pAkt^{S473}, pAkt^{T308}, and pGSK3β^{S9} compared to total protein abundance of Akt or GSK3β in the soleus muscle; P-MCK (n=6), WT (n=6), values are presented relative to WT basal. *, $p<0.05$ 2-way ANOVA, main effect of insulin. Data reported as mean ± SEM.

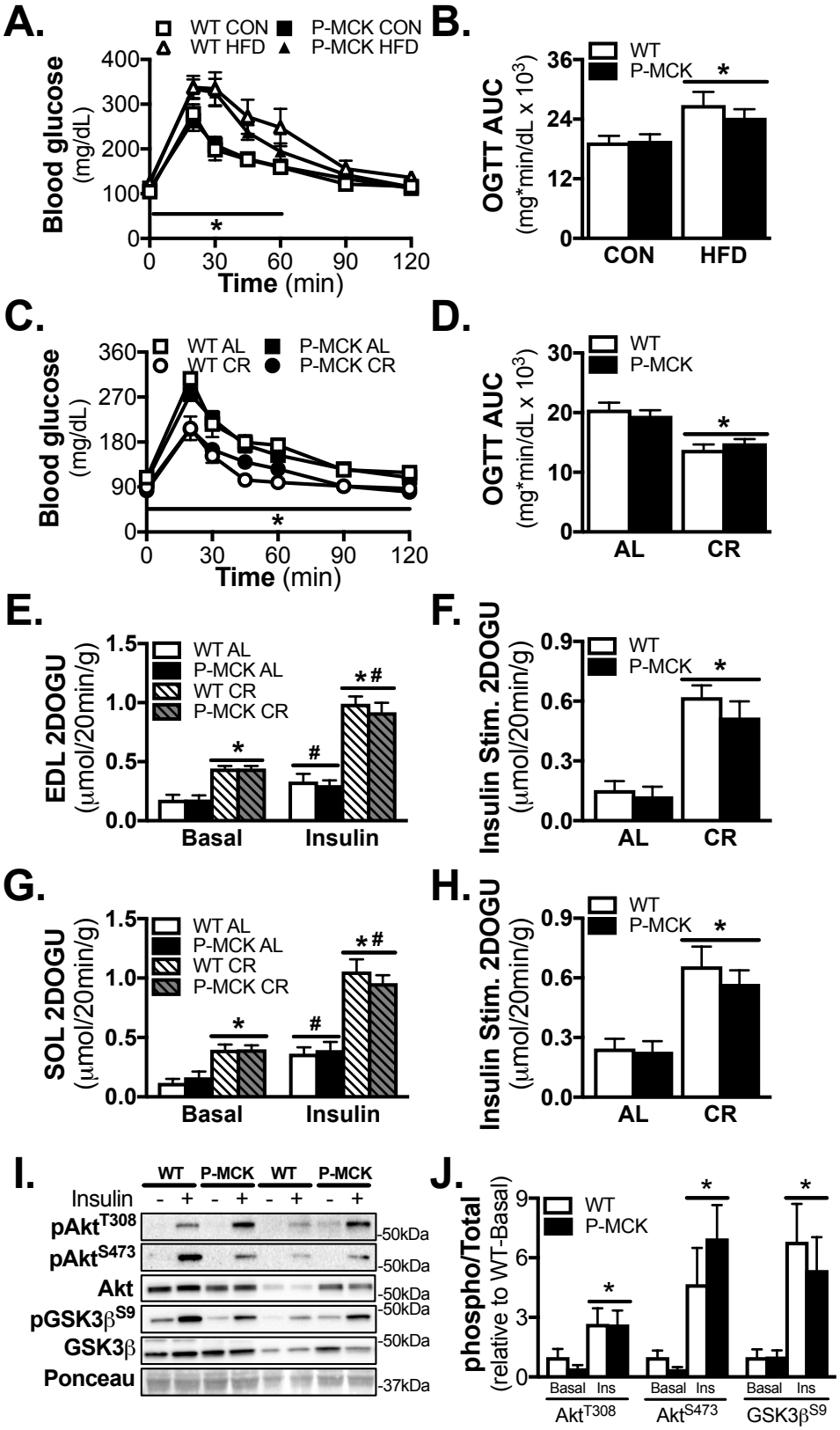
A.
WT CON
WT HFD
P-MCK CON
P-MCK HFD
Blood glucose (mg/dL)
Time (min)
B.
WT
P-MCK
OGTT AUC (mg*min/dL x 10^3)
CON
HFD
C.
WT AL
WT CR
P-MCK AL
P-MCK CR
Blood glucose (mg/dL)
Time (min)
D.
WT
P-MCK
OGTT AUC (mg*min/dL x 10^3)
AL
CR
E.
WT AL
P-MCK AL
WT CR
P-MCK CR
EDL 2DOGU (µmol/20min/g)
Basal
Insulin
F.
WT
P-MCK
Insulin Stim. 2DOGU (µmol/20min/g)
AL
CR
G.
WT AL
P-MCK AL
WT CR
P-MCK CR
SOL 2DOGU (µmol/20min/g)
Basal
Insulin
H.
WT
P-MCK
Insulin Stim. 2DOGU (µmol/20min/g)
AL
CR
I.
WT
P-MCK
WT
P-MCK
Insulin
pAkt^T308
pAkt^S473
Akt
pGSK3βS9
GSK3β
Ponceau
50kDa
37kDa
J.
WT
P-MCK
phospho/Total (relative to WT-Basal)
Basal
Ins
Akt^T308
Akt^S473
GSK3βS9

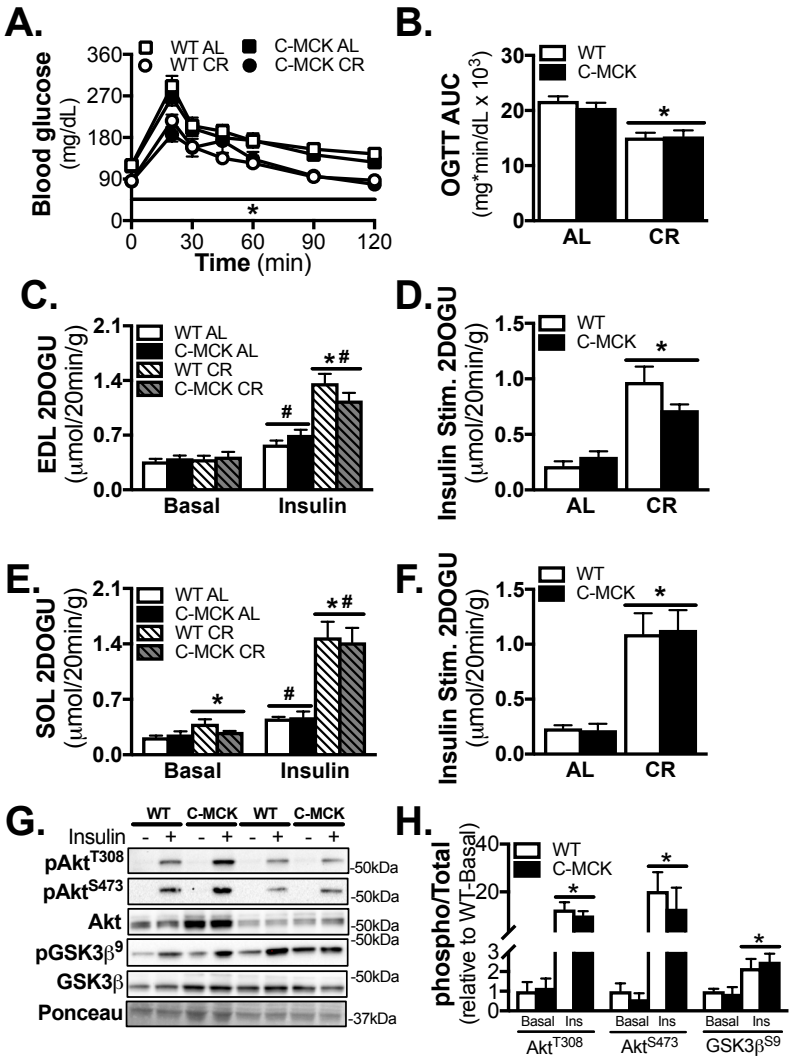

Figure 3.4: Germline deletion of CBP in skeletal muscle does not alter glucose tolerance or skeletal muscle insulin sensitivity. A) Blood glucose concentrations and B) area under the curve (AUC) of male C-MCK mice on AL or CR diet during an oral glucose tolerance test (OGTT; 2 g/kg); C-MCK AL (n=5), WT AL (n=5), C-MCK CR (n=7), WT CR (n=5). *, $p<0.05$ 2-way ANOVA, main effect of diet (within a time point for OGTT). C-F) Basal 2-deoxy-glucose uptake (2DOGU), Insulin (0.36 nmol/L) 2DOGU, and insulin-stimulated 2DOGU (Insulin Stim.; calculated as insulin 2DOGU – basal 2DOGU) in isolated C-D) extensor digitorum longus (EDL) and E-F) soleus muscles from male C-MCK mice on AL or CR diet; C-MCK AL (n=5), WT AL (n=7), C-MCK CR (n=5), WT CR (n=6). #, $p<0.05$ 2-way ANOVA within ad libitum and within diet, main effect of insulin; *, $p<0.05$ 2-way ANOVA within basal and within insulin samples, main effect of diet. G) Phospho-Akt^{S473} (pAkt^{S473}), phospho-Akt^{T308} (pAkt^{T308}), total Akt, phospho-GSK3β^{S9} (pGSK3β^{S9}), and total GSK3β in basal and insulin-stimulated (- and +, respectively) soleus muscles from AL fed mice. H) Quantification of pAkt^{S473}, pAkt^{T308}, and pGSK3β^{S9} compared to total protein abundance of Akt or GSK3β in the soleus muscle; C-MCK (n=4), WT (n=6), values are presented relative to WT basal. *, $p<0.05$ 2-way ANOVA, main effect of insulin. Data reported as mean ± SEM.

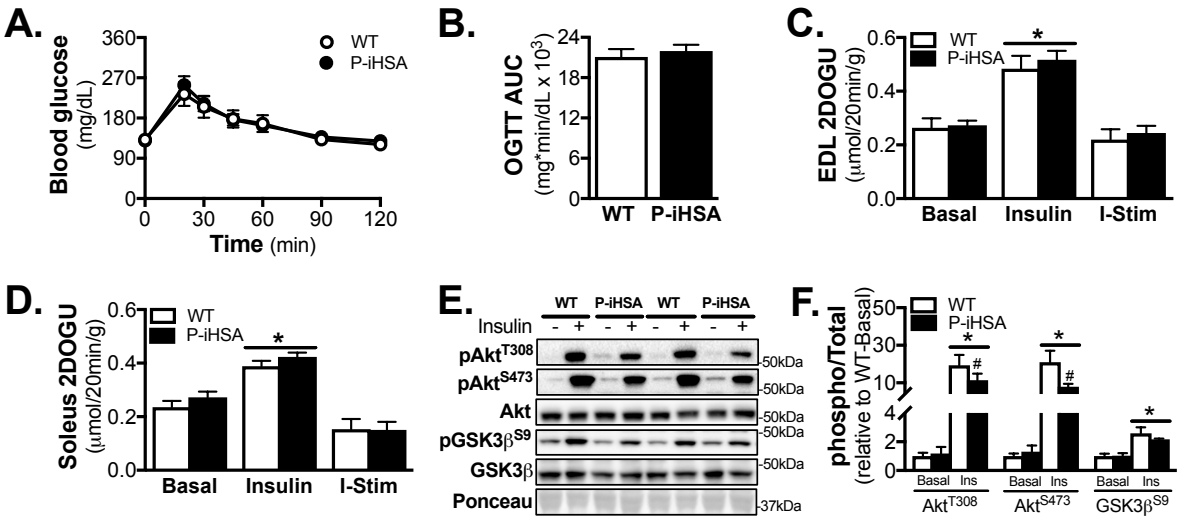

Figure 3.5: Inducible deletion of p300 in adult skeletal muscle does not alter glucose tolerance or skeletal muscle insulin sensitivity. A) Blood glucose concentrations and B) area under the curve (AUC) of male P-iHSA mice during an oral glucose tolerance test (OGTT; 2 g/kg); P-iHSA (n=9), WT (n=6). C-D) Basal 2-deoxy-glucose uptake (2DOGU), Insulin (0.36 nmol/L) 2DOGU, and insulin-stimulated 2DOGU (I-Stim.; calculated as insulin 2DOGU – basal 2DOGU) in isolated C) extensor digitorum longus (EDL) and D) soleus muscles from male P-iHSA mice; P-iHSA (n=8), WT (n=8). E) Phospho-Akt^{S473} (pAkt^{S473}), phospho-Akt^{T308} (pAkt^{T308}), total Akt, phospho-GSK3β^{S9} (GSK3β$^{S/9}$), and total GSK3β in basal and insulin-stimulated (- and +, respectively) soleus muscles. F) Quantification of pAkt^{S473}, pAkt^{T308}, and pGSK3β^{S9} compared to total protein abundance of Akt or GSK3β in the soleus muscle; P-iHSA (n=6), WT (n=5), values are presented relative to WT basal. *, $p<0.05$ 2-way ANOVA, main effect of insulin. #, $p<0.05$ Sidak's multiple comparison test, insulin P-iHSA vs insulin WT. Data reported as mean ± SEM.

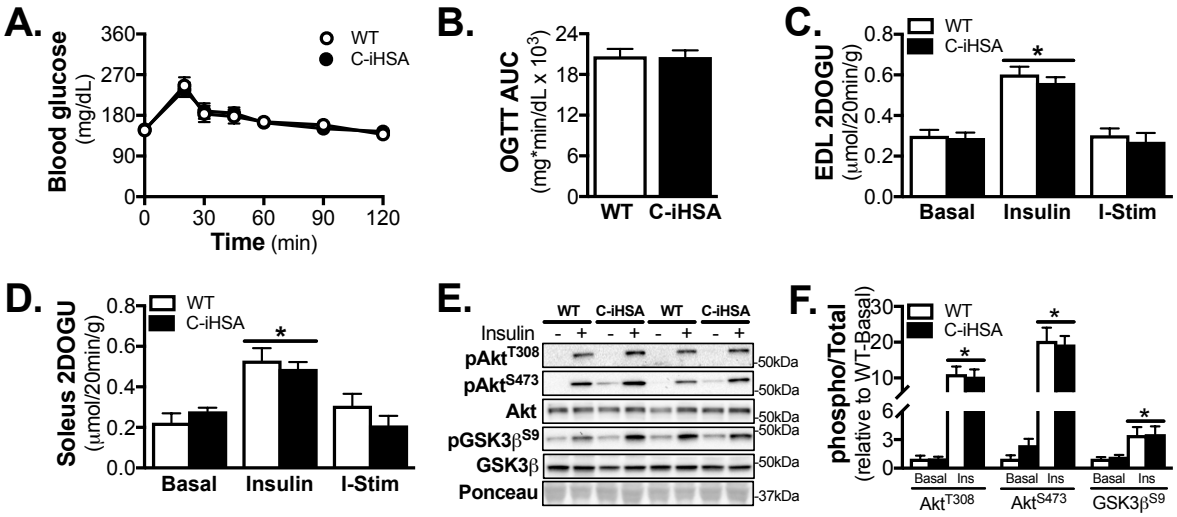

Figure 3.6: Inducible deletion of CBP in adult skeletal muscle does not alter glucose tolerance, skeletal muscle insulin sensitivity, or Akt phosphorylation. A) Blood glucose concentrations and B) area under the curve (AUC) of male C-iHSA mice during an oral glucose tolerance test (OGTT; 2 g/kg); C-iHSA (n=6), WT (n=8). C-D) Basal 2-deoxy-glucose uptake (2DOGU), Insulin (0.36 nmol/L) 2DOGU, and insulin-stimulated 2DOGU (I-Stim; calculated as insulin 2DOGU – basal 2DOGU) in isolated C) extensor digitorum longus (EDL) and D) soleus muscles from male C-iHSA mice; C-iHSA (n=6), WT (n=7). E) Phospho-Akt^{S473} (pAkt^{S473}), phospho-Akt^{T308} (pAkt^{T308}), total Akt, phospho-GSK3β^{S9} (pGSK3β^{S9}), and total GSK3β in basal and insulin-stimulated (- and +, respectively) soleus muscles. F) Quantification of pAkt^{S473}, pAkt^{T308}, and pGSK3β^{S9} compared to total protein abundance of Akt or GSK3β in the soleus muscle; C-MCK (n=6), WT (n=5), values are presented relative to WT basal. *, $p<0.05$ 2-way ANOVA, main effect of insulin. Data reported as mean ± SEM.

CHAPTER 4

p300 and CBP are necessary for skeletal muscle insulin-stimulated glucose uptake Abstract

Abstract

Introduction: The acetyltransferases, E1A binding protein p300 (p300) and cAMP response element-binding protein binding protein (CBP) transcriptionally regulate numerous biological processes within skeletal muscle, including glucose metabolism, however their importance to skeletal muscle insulin action is unclear. In Study 2, we demonstrate that p300 or CBP are, individually, dispensable for normal glucose tolerance and skeletal muscle insulin signaling and sensitivity. Our objective in this study was to determine the joint importance of p300 and CBP to skeletal muscle insulin sensitivity.

Methods: We used Cre-LoxP methodology to generate mice with a tamoxifen-inducible, conditional knock out of p300 and/or CBP in skeletal muscle; this was done in mice that were 13-15 weeks of age, with Cre recombinase being activated via oral gavage of tamoxifen. In the immediate days (i.e. between 1 to 5 days) after tamoxifen dosing, oral glucose tolerance and *ex vivo* skeletal muscle insulin sensitivity were measured. Moreover, microarray (day 5) and proteomics (Days 3 and 5) analysis was conducted on skeletal muscle.

Results: Within just 3 days of initiating knockout of p300 and CBP, whole-body glucose tolerance and skeletal muscle insulin sensitivity were severely impaired, and just 5 days after initiating the knockout, there was a complete loss of skeletal muscle insulin-stimulated glucose uptake. These impairments occurred despite no differences in activation of canonical insulin

signaling. Remarkably, this glucose intolerance and inability of skeletal muscle to respond to insulin did not occur in mice with just a single allele of either p300 or CBP. In the p300/CBP double-knockout mice, skeletal muscle insulin resistance was accompanied by significant changes in both mRNA and protein networks critical for insulin signaling, GLUT4 trafficking, and glucose metabolism.

Conclusions: p300 and CBP in skeletal muscle are jointly required for maintaining whole-body glucose tolerance and insulin sensitivity, at least in part, via transcriptional control of the insulin signaling pathway.

.

Introduction

Protein lysine acetylation is a major posttranslational modification that is able to alter the physical properties and function of thousands of proteins and numerous biological processes via regulation of histone function and gene transcription (1–7). Reversible acetylation requires the enzymatic addition or removal of acetyl groups to lysine residues of proteins via acetyltransferases (KATs) or deacetylases (DACs), respectively (8). While the deacetylases have been studied extensively for their transcriptional control of various biological processes in skeletal muscle such as differentiation, regeneration, and metabolism (9–13), the contribution of the acetyltransferases have been understudied in comparison.

The acetyltransferases E1A binding protein p300 (p300) and cAMP response element binding protein (CREB) binding protein (CBP) are functional homologs (8,14,15) that have been described to play a central role in transcriptional homeostasis of skeletal muscle (16–20). Indeed human primary myoblasts (16) and C2C12 myoblasts (17) fail to form myotubes when either p300 or CBP is knocked down. However, we have demonstrated, *in vivo*, that mice with a muscle-specific deletion of p300 have no deficits in skeletal muscle development (21), which we attributed to the well documented ability of p300/CBP to compensate for each other (14,22–24). Accordingly, we have recently generated a mouse model with inducible, muscle-specific double knockout of p300 and CBP (PCKO), and find that loss of both p300/CBP in adult muscle dramatically alters gene expression patterns fundamental to skeletal muscle function, development, and glucose metabolism (20). Interestingly, however, while p300/CBP has been studied in skeletal muscle in relation to muscle function and development (16–20), no studies have investigated their joint role in the regulation of muscle glucose metabolism.

The primary goal of this study was to investigate the combined contribution of p300 and CBP to insulin-mediated glucose uptake in skeletal muscle. In Study 2 we demonstrated that single loss of either p300 or CBP in skeletal muscle, be it during embryogenesis or in adulthood, does not impair glucose tolerance or skeletal muscle insulin sensitivity, which we attributed to compensation by the analogous acetyltransferase. Thus, here in Study 3, we utilized mice with inducible and skeletal muscle-specific double-knockout of p300 and CBP (PCKO). In addition, we studied mice with just one single allele of either p300 (PZ) or CBP (CZ), to better dissect the contribution of p300 or CBP to skeletal muscle insulin sensitivity. As p300 and CBP are global transcriptional regulators (16–18,25), including of glucose metabolism in skeletal muscle (20), we hypothesized that a double-knockout of p300/CBP in skeletal muscle would impair skeletal muscle insulin sensitivity via a down regulation of insulin signaling and GLUT4 trafficking genes. Furthermore, considering the well-established functional compensation between p300 and CBP (14,22–24), we hypothesized that a single allele of p300 or CBP would be sufficient to partially rescue the phenotype.

Methods

Mouse Models. Studies were conducted in both male and female mice on a C57BL/6J background and housed in a conventional facility with 12-h light/12-h dark cycle. Inducible, muscle-specific, p300 and CBP double knockout mice (PCKO), as well as mice with only one allele of either p300 (PZ) or CBP (CZ) in skeletal muscle, have been described previously (20). Respective floxed, but Cre negative, littermates were used as experimental controls for the mouse models; these mice are referred to as wild type (WT). At 13-15 weeks of age, all mice were orally gavaged with tamoxifen (TMX; 2 mg) for 5 consecutive days to activate Cre and induce the knockout.

Experimental design. For studies in PCKO, PZ, CZ, and WT mice, tissue collection, oral glucose tolerance tests (OGTT), and *ex vivo* 2-deoxyglucose (2DOG) uptake assays were performed at 1-, 3-, 5-, 21- or 28-days after initiating tamoxifen dosing, as indicated.

OGTT. Fasted (4h) mice were orally gavaged with dextrose (2 g/kg) and blood glucose concentration was measured via the tail vein at 0 (before gavage), 20, 30, 45, 60, 90, and 120 min after gavage using a handheld glucose meter (Ascensia Contour, Bayer HealthCare, Mishawaka, IL, USA). Area under the curve (AUC) was calculated using Prism 8 (GraphPad Software Incorporated, La Jolla, CA, USA) with 0 mg/dL used as the baseline.

Skeletal muscle 2DOG uptake. Basal and insulin-stimulated 2DOG uptake was measured in isolated and paired soleus and extensor digitorum longus (EDL) muscles, as described in Study 2 and previous studies (26–28). A physiological insulin concentration of 0.36 nM was used for muscles treated with insulin.

Tissue collection. Tissues were excised from fasted (4 h), anesthetized mice, and frozen in liquid nitrogen. Tissues were stored at -80°C for subsequent analysis. This study was carried out with the approval of, and in accordance with, the Animal Care Program and Institutional Animal Care and Use Committee at the University of California, San Diego.

Immunoblotting. Immunoblotting was performed, as described in Study 1. All antibodies were used at a dilution of 1:1000, unless stated otherwise. Akt (CS 9272B), phosphorylated (p)Akt^{T308} (CS 9275), pAkt^{S473} (CS 4058), and eukaryotic elongation factor 2 (eEF2; CS 2332), were from Cell Signaling. Densitometric analysis of immunoblots was performed using Image Lab (Bio-Rad, Hercules, CA, USA). Phosphorylated protein abundance was normalized to respective total protein abundance.

qPCR. Total RNA was isolated, cDNA was synthesized, and qPCR was performed as described in Study 2. Relative expression levels were calculated by the $\Delta\Delta C_t$ method, using TATA-box binding protein (*tbp*) as the normalization control. The *ep300* (p300) and *crebbp* (CBP) primers were designed so that one of the primers would anneal onto exon 9 (i.e. the exon that is floxed in the p300 and CBP floxed mouse) and the other to exon 10, as used in Study 2.

Microarray. Total RNA was isolated, and purified, and microarray analysis was performed as described in appendix A1 (20). The sorted list of genes was analyzed for over-represented biological processes defined by the Gene Ontology Consortium, using conditional gene ontology analysis (29,30).

Insulin signaling/GLUT4 trafficking network map. The network map was based on published transcriptional networks (31,32). Monochrome circles represent expression of individual genes, color coded by fold change (KO/WT) with red shades indicating upregulation and blue shades indicating downregulation. Gene labels are entrez gene symbols. Multicolored

circles within a grayed box indicate complexes (detailed in Figure 4.7) with the expression of each component gene indicated by ordered stripes. White squares with rounded edges indicate modules or functions and gray triangles indicate non-protein molecules. Connectivity between proteins encoded by specified genes is indicated by the following symbols: plus in white circle (positive), minus in red circle (negative), straight arrow (A proceeds to B), curved arrow (translocation of A). Proteins encoded by specified genes are drawn in their approximate anatomical location relative to cellular structures (yellow).

Tandem mass tag mass spectrometry. Samples were lysed, digested, run, and analyzed as described in appendix A2 (20). The sorted list of proteins was analyzed for enriched pathways using the Reactome database (33).

Statistics. For data other than microarray and proteomics analysis (see appendix A1, A2 (20)), an unpaired Student's t-test, 1-way or 2-way ANOVA (using repeated measurement where appropriate), followed by Sidak's or Tukey's post-hoc test, was used. Significance was set at $p<0.05$. When there were no significant differences amongst the respective WT mice (e.g. D1 vs D3 vs D5 or PZ vs CZ vs PCKO) data was pooled together, as noted. Statistical analyses were performed using Prism 8 (GraphPad Software Incorporated, La Jolla, CA, USA). All data are expressed as mean ± SEM.

Results

Severe insulin resistance develops rapidly in PCKO mice. As PCKO mice die spontaneously after 6-7 days of initiating tamoxifen treatment (20), all experiments were conducted in PCKO and WT mice at one (D1), three (D3), or five (D5) days after initiating tamoxifen treatment; these studies were only conducted in male mice. While PCKO mice had comparable blood glucose concentrations to WT mice during an OGTT at D1 (Figure 4.1A), PCKO mice become progressively glucose intolerant from D3 through D5 (Figure 4.1B-C). Accompanying this, the AUC during the OGTT was significantly higher in PCKO mice by D3 (Figure 4.1B, insert) and was further worsened by D5 (Figure 4.1C, insert; 24,658±1,266 vs 31,258±1,942, *t*-test $p<0.05$). Complementing the OGTT data, basal 2DOG uptake, 2DOG uptake in the presence of insulin, and "insulin-stimulated" 2DOG uptake (i.e. Insulin 2DOG uptake minus Basal 2DOG uptake) were comparable in soleus muscles from male PCKO and WT mice at D1 (Figure 4.1D, G). However, by D3 PCKO mice had significantly reduced insulin-stimulated 2DOG uptake (Figure 4.1E, H), and by D5 2DOG uptake in the presence of insulin insulin was not significantly different from basal (Figure 4.1F, I). The EDL muscle, in contrast, was more rapidly affected with statistically no insulin-stimulated glucose uptake by D3 (Figure 4.1H) that persisted to D5 (Figure 4.1I). Lastly, while PCKO mice are glucose intolerant and insulin resistant as early as D3, insulin significantly increased phosphorylation of Akt^{S473} and Akt^{T308} in the EDL of PCKO and WT mice equally, with no genotype or temporal differences (Figure 4.1J-L).

Validation of PZ and CZ mouse models. In order to determine dosage effects of p300 and CBP and/or to possibly rescue the insulin resistant phenotype of the PCKO mice, we generated mice with only a single allele of either p300 (PZ) or CBP (CZ) in skeletal muscle. As PCKO mice

can only be studied 6-7 days of initiating tamoxifen treatment (20), we studied a separate cohort of PCKO mice, along with CZ and PZ mice, at five days after initiating tamoxifen treatment. In PCKO mice, skeletal muscle p300 and CBP mRNA expression was reduced by ~80% and ~65% (Figure 4.2A), respectively. p300 mRNA expression in CZ muscle and CBP mRNA expression in PZ muscle were reduced to levels comparable to PCKO mice (~80% for both proteins), while CBP abundance in CZ and p300 abundance in PZ muscle demonstrate a heterozygous effect with reductions of ~30% and 35%, respectively (Figure 4.2A).

A single allele of p300 or CBP rescues the insulin resistant phenotype of PCKO mice. In a separate cohort, again PCKO mice demonstrated severe glucose intolerance during an OGTT compared to WT mice (Figure 4.2B, C). However, despite CZ and PZ mice having only one functional allele of CBP or p300, respectively, blood glucose concentrations during an OGTT were identical to WT mice (Figure 4.2B, C). Furthermore, while PCKO mice had statistically no insulin-stimulated 2DOG uptake in either soleus or EDL muscles (Figure 4.2D-F), basal 2DOG uptake, 2DOG uptake in the presence of insulin, and insulin-stimulated 2DOG uptake were not different amongst CZ, PZ, and WT mice in either soleus or EDL muscles (Figure 4.2D-F). Complementing the 2DOG uptake data, insulin significantly increased phosphorylation of Akt^{S473} and Akt^{T308} in the EDL of CZ, PZ, PCKO, and WT littermates. Notably, insulin-mediated phosphorylation of Akt^{T308}, but not Akt^{S473}, was significantly higher in CZ mice compared to WT littermates (Figure 4.2G-H). Importantly, there were no sex differences in our p300/CBP knockout models; female PCKO mice are also severely glucose intolerant and insulin resistant, which was reversed in female PZ and CZ mice (Figure 4.3).

Insulin action is normal in PZ and CZ mice long term. It is possible that development of the severe insulin resistant phenotype seen in PCKO mice is delayed in PZ and CZ mice. To

test this, we assessed glucose tolerance and insulin sensitivity at three and four weeks after initiating tamoxifen treatment, respectively. Blood glucose concentrations and AUC during an OGTT were comparable between CZ, PZ, and WT mice (Figure 4.4A-B). Furthermore, basal 2DOG uptake, 2DOG uptake in the presence of insulin, and insulin-stimulated 2DOG uptake were comparable in the soleus and EDL of CZ and PZ mice, as compared to WT mice (Figure 4.4C-F).

PCKO mice have significant changes in expression of mRNA involved in insulin signaling and GLUT4 trafficking. For insight into why PCKO mice develop severe glucose intolerance and skeletal muscle insulin resistance, we performed a gene microarray in the EDL of PCKO and WT mice at D5. Principal component analysis (PCA) demonstrated that PCKO mice had markedly altered mRNA expression of genes compared to WT mice, with the first principal component explaining 64.7% of the variance (Figure 4.5A). Furthermore, biological replicates were similar since they clustered closely together (Figure 4.5A). The mRNA expression of p300 and CBP (*Kat3a* and *Kat3b*, respectively) were the only acetyltransferases with significantly reduced mRNA expression in PCKO mice (~65% and ~40%; Figure 4.6A). In line with our findings of severe glucose intolerance and skeletal muscle insulin resistance in PCKO mice, gene ontology (GO) enrichment analysis for down regulated genes were enriched for biological processes important to insulin stimulation, glucose import and glucose metabolism (Figure 4.5B). An mRNA expression heatmap of the GO biological processes “glucose metabolic process”, “glucose homeostasis”, “response to insulin”, and “regulation of glucose import” (Same as in Figure 4.5B), reveals that the expression of the majority of these genes (>60%) are downregulated in PCKO mice. In fact, amongst these downregulated genes, expression is reduced by an average of ~70% in PCKO mice (Figure 4.5C). A subset of this data was superimposed in a graphical interpretation of the insulin signaling and GLUT4 trafficking pathway (Figure 4.5D, Figure 4.7),

again demonstrating PCKO mice have a global reduction the expression of genes relevant to insulin sensitivity.

PCKO mice have significant changes in the abundance of protein involved in insulin signaling and GLUT4 trafficking at D5, but not at D3. Similar to the microarray analysis, the PCA of TMT mass spectrometry demonstrated PCKO mice at D5 have a clearly altered protein abundance profile compared to WT mice (Figure 4.5E). Interestingly, however, PCKO mice at D3 cluster closer to WT than to PCKO mice at D5. GO enrichment analysis for all differentially expressed proteins were enriched in the Reactome database (33) for metabolic processes similar to the microarray data, including "translocation of SLC2A4 (GLUT4) to the plasma membrane" (Figure 4.5F; Reactome ID: R-HAS-1445148). Within this Reactome group, most proteins had significantly reduced abundance at D5 (10-50% reduction), while at D3 only TBC1D4 (~40%) and GLUT4 (~20%) had significantly reduced abundance compared to WT mice (Figure 4.5G).

Discussion

Protein lysine acetylation is a posttranslational modification responsible for altering the function of thousands of proteins and numerous biological processes, including within skeletal muscle (1–6). The acetyltransferases p300 and CBP are functional homologs (8,14,15) that play a central role in transcriptional homeostasis of skeletal muscle (16–20). Indeed, we recently determined that loss of both p300 and CBP in skeletal muscle leads to drastic changes in the expression of genes important to skeletal muscle function, development, and glucose metabolism (20). However, while p300/CBP has been studied in skeletal muscle in relation to muscle function and development (16–20), no studies have investigated their joint role in the regulation of muscle glucose metabolism. In Study 2, we demonstrated that p300 and CBP are dispensable, individually, for normal glucose tolerance and skeletal muscle insulin signaling and sensitivity (34). We hypothesized that this was likely due to the large redundancy of function between p300 and CBP and their ability to compensate for each other (14,22–24). To address this, herein we studied the combined role of p300/CBP towards skeletal muscle insulin sensitivity by utilizing a skeletal muscle specific and inducible p300/CBP double-knockout mouse. Our results demonstrate that p300 and CBP are together required for maintaining normal glucose tolerance and skeletal muscle insulin sensitivity, and that this regulation occurs, at least in part, via transcriptional regulation of the insulin signaling and GLUT4 trafficking pathways.

Various studies have eluded to the role of p300 and CBP towards glucose handling and insulin sensitivity (35–41). For example, in the liver insulin stimulation leads to the phosphorylation of CBP^{S436}, which suppresses hepatic gluconeogenesis (39,41). Indeed, mice carrying a mutation of this CBP phosphorylation site are more glucose intolerant during an OGTT

(39) and insulin is unable to suppress hepatic glucose production during a hyperinsulinemic-euglycemic clamp (41). Conversely, in the liver p300 is required to maintain hepatic gluconeogenesis with mice lacking p300 in the liver having lower fasting glucose levels (35,36) and decreased insulin-stimulated hepatic glucose production compared to WT mice during a hyperinsulinemic-euglycemic clamp (42). In skeletal muscle, however, we demonstrated in Study 2 that mice with germline or inducible knockout of either p300 or CBP have comparable glucose tolerance and skeletal muscle insulin sensitivity to WT mice. We hypothesized that the reason for this was due to the well-documented redundancy of function between p300 and CBP and their ability to compensate for each other (14,22–24). To address this, herein we studied mice with skeletal muscle-specific and inducible knockout of both p300 and CBP. In the present study, we demonstrate that PCKO mice exhibit severe glucose intolerance and skeletal muscle insulin resistance. Interestingly, PCKO mice develop this phenotype rapidly, displaying both glucose intolerance and a complete loss of the ability to further take up glucose in the presence of insulin in the EDL by D3. Importantly, insulin-stimulated glucose uptake is abolished in both soleus and EDL muscles of PCKO mice by D5, demonstrating that p300/CBP are required for insulin action, independent of muscle fiber type. Overall, our results establish that together, p300 and CBP in skeletal muscle are required for maintaining normal glucose tolerance and skeletal muscle insulin sensitivity.

p300 and CBP are functionally homologous acetyltransferases (8,14,15) with well-described compensatory actions when one of them is not present (14,22–24). Indeed, while pancreatic knockout of either p300 or CBP leads to impaired insulin secretion and reduced islet area, p300/CBP pancreatic double-knockout mice lack α and β cells completely (22). Interestingly, the analogous PZ and CZ pancreatic knockout mice demonstrated gene dosage effects, by having

a phenotype in between the single- and double-knockouts (22). In mice with p300/CBP knockout in rod or cone cells of the eyes, a single knockout of p300 or CBP led to no apparent morphological changes, while p300/CBP double knockouts have severe disruption of rod and cone cells, as well as retinal morphology (24). The analogous PZ and CZ rod or cone knockout mice, in this case, demonstrated a complete reversal of these phenotypes (24). Similarly, we have demonstrated that while knockout of p300 in skeletal muscle leads to no changes in muscle contractile function (21), p300/CBP double-knockout mice have severely impaired contractile function, which is rescued by a single allele of p300 or CBP (20). In the present study and Study 2, we describe a similar phenomenon where PCKO mice are severely insulin resistant, which is completely rescued not only by giving back one of the proteins, but remarkably, also by only giving back a single allele of either p300 or CBP. Hence, our data demonstrate, together with the literature, not only the large redundancy of function between p300 and CBP in skeletal muscle and their ability to compensate for the other, but also the sufficiency of a single allele of p300 or CBP for normal skeletal muscle insulin action.

p300 and CBP are critical regulators of cellular homeostasis, including in skeletal muscle, via their regulation of histone acetylation and gene transcription (16–18,25). Indeed, this is exemplified by the numerous mouse models in which p300 and/or CBP knockout is lethal (22,43,44), including in skeletal muscle (20). Included within the large network of genes p300/CBP regulates, are genes critical for the regulation of metabolism (20,37–40,45). In the liver, for example, CBP is necessary for the CREB-CBP-TORC2 complex which increases the transcription of gluconeogenic genes (37,38). In skeletal muscle, p300/CBP regulate FOXO activity (45), which is an important transcriptional regulator of glucose metabolism (40,46). In this study, the insulin resistance phenotype seen in PCKO mice was complemented by a

downregulation of gene networks in muscle crucial to insulin signaling, GLUT4 translocation and glucose metabolism. Notably, the mRNA expression of genes known to cause insulin resistance in knockout models, in either skeletal muscle or adipose tissue, were significantly reduced in PCKO mice such as *Foxo1* (~80%) (46), *Tbc1d1* (~80%) (47,48), *Tbc1d4* (~85%) (49–52), *Slc2a4* (~85%) (53–55), *Rab10* (~60%) (56–58), *Rhoq* (~60%) (59–61), and *Hk2* (~90%) (62–64). Hence, we proceeded to analyzing PCKO mice, temporally, for changes in protein abundance using TMT-MS. Similar to the microarray data, within just 5 days of initiating tamoxifen, loss of p300 and CBP in skeletal muscle led to significant changes in the abundance of proteins crucial to carbohydrate and fatty acid metabolism, as well as the translocation of GLUT4 to the plasma membrane, including decreased abundance of TBC1D1 (~50%), GLUT4 (~55%), and Rab10 (~30%). While these changes in protein abundance may, at least partially, explain the insulin resistant phenotype in PCKO mice at D5, it is important to note that mice with heterozygous knockout of these proteins (analogous to the protein reduction seen in PCKO mice) are not as insulin resistant as PCKO mice. For example, while complete knockout of GLUT4 blocks skeletal muscle insulin-stimulated glucose uptake to a similar degree as PCKO mice (55), heterozygous GLUT4 knockout only reduces skeletal muscle insulin-stimulated glucose uptake by at most ~50% (53,55,65). Additionally, complete knockout of TBC1D1 in skeletal muscle (47) and 90% knockdown of Rab10 in adipocytes (56–58) are not sufficient to block insulin-stimulated glucose uptake completely, thus a ~50%, and ~30% reduction, respectively, would have less of an effect. Furthermore, the abundance of these proteins were more modestly reduced at D3. In fact, the TMT-MS data suggests that PCKO mice at D3 are more similar to WT mice than to PCKO D5 mice, despite D3 PCKO mice exhibiting severe glucose intolerance and skeletal muscle insulin resistance. The reason this is important is that it suggests that changes in protein abundance in

PCKO mice do not fully explain the rapid and significant impairment of skeletal muscle insulin sensitivity.

While p300/CBP are well known regulators of transcription, via acetylation of nuclear proteins (16–18,25), p300/CBP also have a robust cytosolic presence (66–68). Indeed p300/CBP acetylate numerous cytosolic proteins (5,14,69,70), including proteins that are fundamental to insulin signaling and GLUT4 trafficking (5,42,71,72). Most notably, p300/CBP can interact with Akt (72–79), a fundamental signaling node in the insulin signaling pathway in skeletal muscle (80,81). Specifically, p300 (73–77) and CBP (78,79) can be phosphorylated by Akt, increasing their acetyltransferase activity (74,75,78), while Akt can be acetylated by p300/CBP (72), which indicate that they can be reciprocally regulated. However, there are other potentially important p300/CBP targets within the insulin signaling pathway. For example, in Hepa1-6 cells, IRS1/2 can be acetylated by p300, which leads to reduced phosphorylation of Akt^{S473} (42). Furthermore, Rictor, as part of the mammalian target of rapamycin complex 2 (mTOC2), can be acetylated by p300 in HEK293T cells, which increases mTORC2 activity towards phosphorylation of Akt^{S473} (71). Considering these points together with the TMT-MS data in D3 PCKO mice, it is possible that the insulin resistant phenotype of PCKO mice is also, at least in part, due to non-nuclear actions of p300/CBP. In the present study, while PCKO mice had reduced insulin-stimulated 2DOGU, this was not associated with a reduction in insulin-mediated phosphorylation of Akt at S473 or T308. This would suggest, that if p300/CBP do have a non-nuclear (i.e. non-transcriptional) role, then it is likely to be downstream of IRS/mTORC2/Akt. Thus, in future studies, it would be interesting to assess and alter the acetylation status of proteins downstream in the insulin signaling pathway, to determine how their acetylation status may impact skeletal muscle insulin action.

In summary, we demonstrate that loss of both p300 and CBP in skeletal muscle leads to rapid and severe whole-body glucose intolerance and skeletal muscle insulin resistance. Remarkably, this phenotype is completely reversed by giving back a single allele of either p300 or CBP. Complementing the insulin resistant phenotype, we also demonstrate that PCKO mice at D5 have significant downregulation of genes and proteins critical for insulin action. However, interestingly, while PCKO mice at D3 are already glucose intolerant and insulin resistant, there are minimal changes to the protein abundance of these same networks, leaving the possibility that non-nuclear acylation could contribute to the described phenotype. Thus, in future studies, it will be interesting to manipulate p300/CBP activity acutely, as we have done for deacetylases in Study 1, to better understand if p300/CBP can act on skeletal muscle biology via a non-transcriptional mechanism. Overall, our results establish p300/CBP as novel regulators of skeletal muscle insulin action via transcriptional regulation of the insulin signaling pathway. It will be of high interest in future studies to investigate how the acylation of p300/CBP substrates in skeletal muscle regulate the expression of insulin signaling genes, in order to develop novel treatments for enhancing skeletal muscle insulin sensitivity.

Acknowledgments

This work was supported, in part, by U.S. National Institutes of Health grants R01 AG043120 and R21 AR072882 (to S.S.), T32 AR060712 and F30 DK115035 (to V.F.M.), a UC San Diego Frontiers of Innovation Scholars Program grant (to S.S.), Graduate Student Research Support from the UC San Diego Institute of Engineering in Medicine (to V.F.M), and post-doctoral fellowships from the Swiss National Science Foundation P2BSP3-165311 and the American Federation of Aging Research PD18120 (to K.S.).

SS and VFM were responsible for the conception and design of the study. SS, VFM, SL, and DB, were responsible for the analysis and interpretation of the data. VFM was responsible for the design and drafting of the manuscript and SS revised the manuscript critically. KS, TPC, BH, GAM, AP, LLD, RRH, JEA, ARS, and CEM contributed to analysis, interpretation of data, and critical revision of the manuscript. All authors gave final approval.

Chapter 4, in full, is being prepared for publication. V. F. Martins, S. A. LaBarge, Svensson, D. Banoian, T.P. Ciaraldi, B. Hetrick, G.A. Meyer, A. Philp, L.L. David, R.R. Henry, J.E. Aslan, A.R. Saltiel, C.E. McCurdy, S. Schenk. The dissertation author was the primary investigator and author of this paper.

.

References

1. **Allfrey VG**, **Faulkner R**, **Mirsky AE**. Acetylation and methylation of histones and their possible role in the regulation of RNA synthesis. *Proc Natl Acad Sci* 51: 786–794, 1964.

2. **Arias EB**, **Zheng X**, **Agrawal S**, **Cartee GD**. Whole body glucoregulation and tissue-specific glucose uptake in a novel Akt substrate of 160 kDa knockout rat model. *PLoS One* 14: 1–22, 2019.

3. **Ashburner M**, **Ball CA**, **Blake JA**, **Botstein D**, **Butler H**, **Cherry JM**, **Davis AP**, **Dolinski K**, **Dwight SS**, **Eppig JT**, **Harris MA**, **Hill DP**, **Issel-Tarver L**, **Kasarskis A**, **Lewis S**, **Matese JC**, **Richardson JE**, **Ringwald M**, **Rubin GM**, **Sherlock G**. Gene ontology: tool for the unification of biology. The Gene Ontology Consortium. *Nat Genet* 25: 25–9, 2000.

4. **Aslan JE**, **Rigg RA**, **Nowak MS**, **Loren CP**, **Baker-Groberg SM**, **Pang J**, **David LL**, **McCarty OJT**. Lysine acetyltransfer supports platelet function. *J Thromb Haemost* 13: 1908–17, 2015.

5. **Cao J**, **Peng J**, **An H**, **He Q**, **Boronina T**, **Guo S**, **White MF**, **Cole PA**, **He L**. Endotoxemia-mediated activation of acetyltransferase P300 impairs insulin signaling in obesity. *Nat Commun* 8, 2017.

6. **Chang L**, **Chiang SH**, **Saltiel AR**. TC10α is required for insulin-stimulated glucose uptake in adipocytes. *Endocrinology* 148: 27–33, 2007.

7. **Chang PY**, **Jensen J**, **Printz RL**, **Granner DK**, **Ivy JL**, **Moller DE**. Overexpression of hexokinase II in transgenic mice: Evidence that increased phosphorylation augments muscle glucose uptake. *J Biol Chem* 271: 14834–14839, 1996.

8. **Chiang SH**, **Baumann CA**, **Kanzaki M**, **Thurmond DC**, **Watson RT**, **Neudauer CL**, **Macara IG**, **Pessin JE**, **Saltiel AR**. Insulin-stimulated GLUT4 translocation requires the CAP-dependent activation of TC10. *Nature* 410: 944–948, 2001.

9. **Chiang SH**, **Hou JC**, **Hwang J**, **Pessin JE**, **Saltiel AR**. Cloning and functional characterization of related TC10 isoforms, a subfamily of Rho proteins involved in insulin-stimulated glucose transport. *J Biol Chem* 277: 13067–13073, 2002.

10. **Choudhary C**, **Kumar C**, **Gnad F**, **Nielsen ML**, **Rehman M**, **Walther TC**, **Olsen J V**, **Mann M**. Lysine acetylation targets protein complexes and co-regulates major cellular functions. *Science* 325: 834–40, 2009.

11. **Choudhary C**, **Weinert BT**, **Nishida Y**, **Verdin E**, **Mann M**. The growing landscape of lysine acetylation links metabolism and cell signalling. *Nat Rev Mol Cell Biol* 15: 536–50, 2014.

12. **Dancy BM**, **Cole PA**. Protein lysine acetylation by p300/CBP. *Chem Rev* 115: 2419–52, 2015.

13. **Dokas J**, **Chadt A**, **Nolden T**, **Himmelbauer H**, **Zierath JR**, **Joost HG**, **Al-Hasani H**. Conventional knockout of Tbc1d1 in mice impairs insulin- and AICAR-stimulated glucose uptake in skeletal muscle. *Endocrinology* 154: 3502–3514, 2013.

14. **Dou C**, **Liu Z**, **Tu K**, **Zhang H**, **Chen C**, **Yaqoob U**, **Wang Y**, **Wen J**, **van Deursen J**, **Sicard D**, **Tschumperlin D**, **Zou H**, **Huang WC**, **Urrutia R**, **Shah VH**, **Kang N**. P300 Acetyltransferase Mediates Stiffness-Induced Activation of Hepatic Stellate Cells Into Tumor-Promoting Myofibroblasts. *Gastroenterology* 154: 2209-2221.e14, 2018.

15. **Eckner R**, **Yao TP**, **Oldread E**, **Livingston DM**. Interaction and functional collaboration of p300/CBP and bHLH proteins in muscle and B-cell differentiation. *Genes Dev* 10: 2478–2490, 1996.

16. **Fabregat A**, **Jupe S**, **Matthews L**, **Sidiropoulos K**, **Gillespie M**, **Garapati P**, **Haw R**, **Jassal B**, **Korninger F**, **May B**, **Milacic M**, **Roca CD**, **Rothfels K**, **Sevilla C**, **Shamovsky V**, **Shorser S**, **Varusai T**, **Viteri G**, **Weiser J**, **Wu G**, **Stein L**, **Hermjakob H**, **D'Eustachio P**. The Reactome Pathway Knowledgebase. *Nucleic Acids Res* 46: D649–D655, 2018.

17. **Fauquier L**, **Azzag K**, **Parra MAM**, **Quillien A**, **Boulet M**, **Diouf S**, **Carnac G**, **Waltzer L**, **Gronemeyer H**, **Vandel L**. CBP and P300 regulate distinct gene networks required for human primary myoblast differentiation and muscle integrity. *Sci Rep* 8: 12629, 2018.

18. **Fermento ME**, **Gandini NA**, **Salomón DG**, **Ferronato MJ**, **Vitale CA**, **Arévalo J**, **López Romero A**, **Nuñez M**, **Jung M**, **Facchinetti MM**, **Curino AC**. Inhibition of p300 suppresses growth of breast cancer. Role of p300 subcellular localization. *Exp Mol Pathol* 97: 411–24, 2014.

19. **Fueger PT**, **Hess HS**, **Bracy DP**, **Pencek RR**, **Posey KA**, **Charron MJ**, **Wasserman DH**. Regulation of insulin-stimulated muscle glucose uptake in the conscious mouse: Role of glucose transport is dependent on glucose phosphorylation capacity. *Endocrinology* 145: 4912–4916, 2004.

20. **Fueger PT**, **Lee-Young RS**, **Shearer J**, **Bracy DP**, **Heikkinen S**, **Laakso M**, **Rottman JN**, **Wasserman DH**. Phosphorylation Barriers to Skeletal and Cardiac Muscle Glucose Uptakes in High-Fat–Fed Mice. *Diabetes* 56: 2476–2484, 2007.

21. **Furuyama T**, **Kitayama K**, **Yamashita H**, **Mori N**. Forkhead transcription factor F0X01 (FKHR)-dependent induction of PDK4 gene expression in skeletal muscle during energy deprivation. *Biochem J* 375: 365–371, 2003.

22. **Glidden EJ**, **Gray LG**, **Vemuru S**, **Li D**, **Harris TE**, **Mayo MW**. Multiple site acetylation of rictor stimulates mammalian target of rapamycin complex 2 (mTORC2)-dependent phosphorylation of Akt protein. *J Biol Chem* 287: 581–588, 2012.

23. **Guo S**, **Cichy SB**, **He X**, **Yang Q**, **Ragland M**, **Ghosh AK**, **Johnson PF**, **Unterman TG**. Insulin suppresses transactivation by CAAT/enhancer-binding proteins beta (C/EBPbeta). Signaling to p300/CREB-binding protein by protein kinase B disrupts interaction with the major activation domain of C/EBPbeta. *J Biol Chem* 276: 8516–23, 2001.

24. **Halseth AE**, **Bracy DP**, **Wasserman DH**. Overexpression of hexokinase II increases insulin- and exercise- stimulated muscle glucose uptake in vivo. *Am J Physiol - Endocrinol Metab* 276, 1999.

25. **He L**, **Cao J**, **Meng S**, **Ma A**, **Radovick S**, **Wondisford FE**. Activation of basal gluconeogenesis by coactivator p300 maintains hepatic glycogen storage. *Mol Endocrinol* 27: 1322–32, 2013.

26. **He L**, **Naik K**, **Meng S**, **Cao J**, **Sidhaye AR**, **Ma A**, **Radovick S**, **Wondisford FE**. Transcriptional Co-activator p300 maintains basal hepatic gluconeogenesis. *J Biol Chem* 287: 32069–32077, 2012.

27. **He L**, **Sabet A**, **Djedjos S**, **Miller R**, **Sun X**, **Hussain MA**, **Radovick S**, **Wondisford FE**. Metformin and Insulin Suppress Hepatic Gluconeogenesis through Phosphorylation of CREB Binding Protein. *Cell* 137: 635–646, 2009.

28. **Hennig AK**, **Peng GH**, **Chen S**. Transcription Coactivators p300 and CBP Are Necessary for Photoreceptor-Specific Chromatin Organization and Gene Expression. *PLoS One* 8, 2013.

29. **Huang W-C**, **Chen C-C**. Akt phosphorylation of p300 at Ser-1834 is essential for its histone acetyltransferase and transcriptional activity. *Mol Cell Biol* 25: 6592–602, 2005.

30. **Karunanithi S**, **Xiong T**, **Uhm M**, **Leto D**, **Sun J**, **Chen X-W**, **Saltiel AR**. A Rab10:RalA G protein cascade regulates insulin-stimulated glucose uptake in adipocytes. *Mol Biol Cell* 25: 3059–69, 2014.

31. **Kim SC**, **Sprung R**, **Chen Y**, **Xu Y**, **Ball H**, **Pei J**, **Cheng T**, **Kho Y**, **Xiao H**, **Xiao L**, **Grishin N V.**, **White M**, **Yang X-J**, **Zhao Y**. Substrate and functional diversity of lysine acetylation revealed by a proteomics survey. *Mol Cell* 23: 607–18, 2006.

32. **Koo SH**, **Flechner L**, **Qi L**, **Zhang X**, **Screaton RA**, **Jeffries S**, **Hedrick S**, **Xu W**, **Boussouar F**, **Brindle P**, **Takemori H**, **Montminy M**. The CREB coactivator TORC2 is a key regulator of fasting glucose metabolism. *Nature* 437: 1109–1114, 2005.

33. **Kuhlmann N**, **Wroblowski S**, **Knyphausen P**, **de Boor S**, **Brenig J**, **Zienert AY**, **Meyer-Teschendorf K**, **Praefcke GJK**, **Nolte H**, **Krüger M**, **Schacherl M**, **Baumann U**, **James LC**, **Chin JW**, **Lammers M**. Structural and Mechanistic Insights into the Regulation of the Fundamental Rho Regulator RhoGDIα by Lysine Acetylation. *J Biol Chem* 291: 5484–99, 2016.

34. **LaBarge SA**, **Migdal CW**, **Buckner EH**, **Okuno H**, **Gertsman I**, **Stocks B**, **Barshop BA**, **Nalbandian SR**, **Philp A**, **McCurdy CE**, **Schenk S**. p300 is not required for metabolic

adaptation to endurance exercise training. *FASEB J* 30: 1623–33, 2016.

35. **Lai Y-C**, **Liu Y**, **Jacobs R**, **Rider MH**. A novel PKB/Akt inhibitor, MK-2206, effectively inhibits insulin-stimulated glucose metabolism and protein synthesis in isolated rat skeletal muscle. *Biochem J* 447: 137–147, 2012.

36. **Lansey MN**, **Walker NN**, **Hargett SR**, **Stevens JR**, **Keller SR**. Deletion of Rab GAP AS160 modifies glucose uptake and GLUT4 translocation in primary skeletal muscles and adipocytes and impairs glucose homeostasis. *Am J Physiol - Endocrinol Metab* 303: 1273–1286, 2012.

37. **Leto D**, **Saltiel AR**. Regulation of glucose transport by insulin: traffic control of GLUT4. *Nat Rev Mol Cell Biol* 13: 383–96, 2012.

38. **Liu Y**, **Denlinger CE**, **Rundall BK**, **Smith PW**, **Jones DR**. Suberoylanilide hydroxamic acid induces Akt-mediated phosphorylation of p300, which promotes acetylation and transcriptional activation of RelA/p65. *J Biol Chem* 281: 31359–31368, 2006.

39. **Liu Y**, **Xing Z**, **Zhang J**, **Fang Y**. Akt kinase targets the association of CBP with histone H3 to regulate the acetylation of lysine K18. *FEBS Lett* 587: 847–853, 2013.

40. **Lundell LS**, **Massart J**, **Altıntaş A**, **Krook A**, **Zierath JR**. Regulation of glucose uptake and inflammation markers by FOXO1 and FOXO3 in skeletal muscle. *Mol Metab* 20: 79–88, 2019.

41. **Martins VF**, **Dent JR**, **Svensson K**, **Tahvilian S**, **Begur M**, **Lakkaraju S**, **Buckner EH**, **LaBarge SA**, **Hetrick B**, **McCurdy CE**, **Schenk S**. Germline or inducible knockout of p300 or CBP in skeletal muscle does not alter insulin sensitivity. *Am J Physiol Metab* 316: E1024–E1035, 2019.

42. **Martins VF**, **Tahvilian S**, **Kang JH**, **Svensson K**, **Hetrick B**, **Chick WS**, **Schenk S**, **McCurdy CE**. Calorie Restriction-Induced Increase in Skeletal Muscle Insulin Sensitivity Is Not Prevented by Overexpression of the p55α Subunit of Phosphoinositide 3-Kinase. *Front Physiol* 9: 789, 2018.

43. **McCurdy CE**, **Cartee GD**. Akt2 is essential for the full effect of calorie restriction on insulin-stimulated glucose uptake in skeletal muscle. *Diabetes* 54: 1349–56, 2005.

44. **McKinsey TA**, **Zhang CL**, **Lu J**, **Olson EN**. Signal-dependent nuclear export of a histone deacetylase regulates muscle differentiation. *Nature* 408: 106–111, 2000.

45. **Moreno CL**, **Yang L**, **Dacks PA**, **Isoda F**, **Van Deursen JMA**, **Mobbs C V.** Role of hypothalamic Creb-binding protein in obesity and molecular reprogramming of metabolic substrates. *PLoS One* 11: 1–15, 2016.

46. **Moresi V**, **Carrer M**, **Grueter CE**, **Rifki OF**, **Shelton JM**, **Richardson JA**, **Bassel-Duby R**, **Olson EN**. Histone deacetylases 1 and 2 regulate autophagy flux and skeletal muscle homeostasis in mice. *Proc Natl Acad Sci U S A* 109: 1649–1654, 2012.

47. **Puri PL**, **Avantaggiati ML**, **Balsano C**, **Sang N**, **Graessmann A**, **Giordano A**, **Levrero M**. p300 is required for MyoD-dependent cell cycle arrest and muscle-specic gene transcription. *EMBO J* 16: 369–383, 1997.

48. **Raichur S**, **Teh SH**, **Ohwaki K**, **Gaur V**, **Long YC**, **Hargreaves M**, **McGee SL**, **Kusunoki J**. Histone deacetylase 5 regulates glucose uptake and insulin action in muscle cells. *J Mol Endocrinol* 49: 203–211, 2012.

49. **Ravnskjaer K**, **Kester H**, **Liu Y**, **Zhang X**, **Lee D**, **Yates JR**, **Montminy M**. Cooperative interactions between CBP and TORC2 confer selectivity to CREB target gene expression. *EMBO J* 26: 2880–2889, 2007.

50. **Renzini A**, **Marroncelli N**, **Noviello C**, **Moresi V**, **Adamo S**. HDAC4 Regulates Skeletal Muscle Regeneration via Soluble Factors. *Front Physiol* 9: 1–11, 2018.

51. **Roth JF**, **Shikama N**, **Henzen C**, **Desbaillets I**, **Lutz W**, **Marino S**, **Wittwer J**, **Schorle H**, **Gassmann M**, **Eckner R**. Differential role of p300 and CBP acetyltransferase during myogenesis: p300 acts upstream of MyoD and Myf5. *EMBO J* 22: 5186–5196, 2003.

52. **Ruiz L**, **Gurlo T**, **Ravier MA**, **Wojtusciszyn A**, **Mathieu J**, **Brown MR**, **Broca C**, **Bertrand G**, **Butler PC**, **Matveyenko A V**, **Dalle S**, **Costes S**. Proteasomal degradation of the histone acetyl transferase p300 contributes to beta-cell injury in a diabetes environment. *Cell Death Dis* 9: 600, 2018.

53. **Sanchez M**, **Sauvé K**, **Picard N**, **Tremblay A**. The hormonal response of estrogen receptor beta is decreased by the phosphatidylinositol 3-kinase/Akt pathway via a phosphorylation-dependent release of CREB-binding protein. *J Biol Chem* 282: 4830–40, 2007.

54. **Sano H**, **Eguez L**, **Teruel MN**, **Fukuda M**, **Chuang TD**, **Chavez JA**, **Lienhard GE**, **McGraw TE**. Rab10, a Target of the AS160 Rab GAP, Is Required for Insulin-Stimulated Translocation of GLUT4 to the Adipocyte Plasma Membrane. *Cell Metab* 5: 293–303, 2007.

55. **Schenk S**, **McCurdy CE**, **Philp A**, **Chen MZ**, **Holliday MJ**, **Bandyopadhyay GK**, **Osborn O**, **Baar K**, **Olefsky JM**. Sirt1 enhances skeletal muscle insulin sensitivity in mice during caloric restriction. *J Clin Invest* 121: 4281–8, 2011.

56. **Sen N**, **Hara MR**, **Kornberg MD**, **Cascio MB**, **Bae B-I**, **Shahani N**, **Thomas B**, **Dawson TM**, **Dawson VL**, **Snyder SH**, **Sawa A**. Nitric oxide-induced nuclear GAPDH activates p300/CBP and mediates apoptosis. *Nat Cell Biol* 10: 866–73, 2008.

57. **Senf SM**, **Sandesara PB**, **Reed SA**, **Judge AR**. p300 Acetyltransferase activity differentially regulates the localization and activity of the FOXO homologues in skeletal muscle. *Am J Physiol Cell Physiol* 300: C1490-501, 2011.

58. **Shikama N**, **Lutz W**, **Kretzschmar R**, **Sauter N**, **Roth J-F**, **Marino S**, **Wittwer J**, **Scheidweiler A**, **Eckner R**. Essential function of p300 acetyltransferase activity in heart, lung and small intestine formation. *EMBO J* 22: 5175–85, 2003.

59. **Smith LR**, **Meyer G**, **Lieber RL**. Systems analysis of biological networks in skeletal muscle function. *Wiley Interdiscip Rev Syst Biol Med* 5: 55–71, 2014.

60. **Stenbit AE**, **Burcelin R**, **Katz EB**, **Tsao TS**, **Gautier N**, **Charron MJ**, **Le Marchand-Brustel Y**. Diverse effects of Glut 4 ablation on glucose uptake and glycogen synthesis in red and white skeletal muscle. *J Clin Invest* 98: 629–634, 1996.

61. **Stenbit AE**, **Tsao TS**, **Li J**, **Burcelin R**, **Geenen DL**, **Factor SM**, **Houseknecht K**, **Katz EB**, **Charron MJ**. GLUT4 heterozygous knockout mice develop muscle insulin resistance and diabetes. *Nat Med* 3: 1096–101, 1997.

62. **Sundaresan NR**, **Pillai VB**, **Wolfgeher D**, **Samant S**, **Vasudevan P**, **Parekh V**, **Raghuraman H**, **Cunningham JM**, **Gupta M**, **Gupta MP**. The deacetylase SIRT1 promotes membrane localization and activation of Akt and PDK1 during tumorigenesis and cardiac hypertrophy. *Sci Signal* 4: ra46, 2011.

63. **Svensson K**, **LaBarge SA**, **Martins VF**, **Schenk S**. Temporal overexpression of SIRT1 in skeletal muscle of adult mice does not improve insulin sensitivity or markers of mitochondrial biogenesis. *Acta Physiol* 221: 193–203, 2017.

64. **Svensson K**, **LaBarge SA**, **Sathe A**, **Martins VF**, **Tahvilian S**, **Cunliffe JM**, **Sasik A**, **Mahata SK**, **Meyer GA**, **Philp A**, **David LL**, **Ward SR**, **McCurdy CE**, **Aslan JE**, **Schenk S**. p300 and CBP are essential for skeletal muscle homeostasis, contractile function and survival. *J Cachexia Sarcopenia Muscle* In Press, 2019.

65. **Szekeres F**, **Chadt A**, **Tom RZ**, **Deshmukh AS**, **Chibalin A V.**, **Björnholm M**, **Al-Hasani H**, **Zierath JR**. The Rab-GTPase-activating protein TBC1D1 regulates skeletal muscle glucose metabolism. *Am J Physiol - Endocrinol Metab* 303: 524–533, 2012.

66. **The Gene Ontology Consortium**. The Gene Ontology Resource: 20 years and still GOing strong. *Nucleic Acids Res* 47: D330–D338, 2019.

67. **Thébault S**, **Verdin E**, **Lu J**, **McKinsey TA**, **Zhang CL**, **Olson NE**. Regulation of skeletal myogenesis by association of the MEF2 transcription factor with class II histone deacetylases. *Chemtracts* 14: 720–726, 2001.

68. **Turner BM**. Histone acetylation and control of gene expression. *J Cell Sci* 99 (Pt 1): 13–20, 1991.

69. **Turner BM**, **Thangue NB La**. Histone acetylation and control of gene expression. *J Cell Sci* 99 (Pt 1): 13–20, 1991.

70. **Vazirani RP**, **Verma A**, **Sadacca LA**, **Buckman MS**, **Picatoste B**, **Beg M**, **Torsitano C**, **Bruno JH**, **Patel RT**, **Simonyte K**, **Camporez JP**, **Moreira G**, **Falcone DJ**, **Accili D**, **Elemento O**, **Shulman GI**, **Kahn BB**, **McGraw TE**. Disruption of adipose Rab10-dependent insulin signaling causes hepatic insulin resistance. *Diabetes* 65: 1577–1589, 2016.

71. **Verdin E**, **Ott M**. 50 years of protein acetylation: from gene regulation to epigenetics, metabolism and beyond. *Nat Rev Mol Cell Biol* 16: 258–64, 2015.

72. **Vo N**, **Goodman RH**. CREB-binding protein and p300 in transcriptional regulation. *J Biol Chem* 276: 13505–8, 2001.

73. **Wang HY**, **Ducommun S**, **Quan C**, **Xie B**, **Li M**, **Wasserman DH**, **Sakamoto K**, **Mackintosh C**, **Chen S**. AS160 deficiency causes whole-body insulin resistance via composite effects in multiple tissues. *Biochem J* 449: 479–489, 2013.

74. **Wang QE**, **Han C**, **Zhao R**, **Wani G**, **Zhu Q**, **Gong L**, **Battu A**, **Racoma I**, **Sharma N**, **Wani AA**. P38 MAPK- and Akt-mediated p300 phosphorylation regulates its degradation to facilitate nucleotide excision repair. *Nucleic Acids Res* 41: 1722–1733, 2013.

75. **Weinert BT**, **Narita T**, **Satpathy S**, **Srinivasan B**, **Hansen BK**, **Schölz C**, **Hamilton WB**, **Zucconi BE**, **Wang WW**, **Liu WR**, **Brickman JM**, **Kesicki EA**, **Lai A**, **Bromberg KD**, **Cole PA**, **Choudhary C**. Time-Resolved Analysis Reveals Rapid Dynamics and Broad Scope of the CBP/p300 Acetylome. *Cell* 174: 231-244.e12, 2018.

76. **Wong CK**, **Wade-Vallance AK**, **Luciani DS**, **Brindle PK**, **Lynn FC**, **Gibson WT**. The p300 and CBP Transcriptional Coactivators are Required for Beta Cell and Alpha Cell Proliferation. *Diabetes* : db170237, 2017.

77. **Xie B**, **Chen Q**, **Chen L**, **Sheng Y**, **Wang HY**, **Chen S**. The Inactivation of RabGAP Function of AS160 Promotes Lysosomal Degradation of GLUT4 and Causes Postprandial Hyperglycemia and Hyperinsulinemia. *Diabetes* 65: 3327–3340, 2016.

78. **Yao TP**, **Oh SP**, **Fuchs M**, **Zhou ND**, **Ch'ng LE**, **Newsome D**, **Bronson RT**, **Li E**, **Livingston DM**, **Eckner R**. Gene dosage-dependent embryonic development and proliferation defects in mice lacking the transcriptional integrator p300. *Cell* 93: 361–372, 1998.

79. **Zhao S**, **Xu W**, **Jiang W**, **Yu W**, **Lin Y**, **Zhang T**, **Yao J**, **Zhou L**, **Zeng Y**, **Li H**, **Li Y**, **Shi J**, **An W**, **Hancock SM**, **He F**, **Qin L**, **Chin J**, **Yang P**, **Chen X**, **Lei Q**, **Xiong Y**, **Guan K-L**. Regulation of cellular metabolism by protein lysine acetylation. *Science* 327: 1000–4, 2010.

80. **Zhou XY**, **Shibusawa N**, **Naik K**, **Porras D**, **Temple K**, **Ou H**, **Kaihara K**, **Roe MW**, **Brady MJ**, **Wondisford FE**. Insulin regulation of hepatic gluconeogenesis through phosphorylation of CREB-binding protein. *Nat Med* 10: 633–637, 2004.

81. **Zisman A**, **Peroni OD**, **Abel ED**, **Michael MD**, **Mauvais-Jarvis F**, **Lowell BB**, **Wojtaszewski JF**, **Hirshman MF**, **Virkamaki A**, **Goodyear LJ**, **Kahn CR**, **Kahn BB**. Targeted disruption of the glucose transporter 4 selectively in muscle causes insulin resistance and glucose intolerance. *Nat Med* 6: 924–8, 2000.

Figure 4.1: p300 and CBP are required for skeletal muscle insulin stimulated glucose uptake. Male PCKO mice were assessed at one (D1), three (D3), or five (D5) days after initiating tamoxifen. A-C) Blood glucose concentrations and area under the curve (AUC; inset) for male PCKO mice at D1, D3, and D5 during an oral glucose tolerance test (OGTT; 2 g/kg); D1: WT/PCKO = 5/9, D3: WT/PCKO = 6/10, D5: WT/PCKO = 6/11. *, $p<0.05$ 2-way ANOVA, PCKO vs WT within a time point for OGTT, and *, $p<0.05$ *t*-test for AUC. D-F) Basal 2-deoxy-glucose uptake (2DOGU), Insulin (0.36 nmol/L) 2DOGU, and G-I) insulin-stimulated 2DOGU (I-Stim.; calculated as insulin 2DOGU – basal 2DOGU) in isolated extensor digitorum longus (EDL) and soleus muscles from male WT and PCKO mice at D1, D3, and D5; D1: WT/PCKO = 11/10, D3: WT/PCKO = 6/7, D5: WT/PCKO = 7/10. *, $p<0.05$ 2-way ANOVA with Sidak's multiple comparison vs basal within genotype for basal and insulin 2DOGU. *, $p<0.05$ *t*-test for I-Stim. ^, $p>0.05$ one sample *t*-test vs "0". J) Phospho-Akt^{S473} (pAkt^{S473}), phospho-Akt^{T308} (pAkt^{T308}), and total Akt in basal and insulin-stimulated (- and +, respectively) EDL muscles from WT and PCKO mice at D1, D3, and D5. Quantification of K) pAkt^{T308} and L) pAkt^{S473} compared to total protein abundance of Akt in the EDL muscle; WT/D1/D3/D5 n = 15/5/6/11. Values are presented relative to WT basal. *, $p<0.05$ 2-way ANOVA, main effect of insulin. Data reported as mean ± SEM. For western blots, there were no significant differences between WT mice at the different time points (D1, D3, and D5) therefore WT data was collapsed.

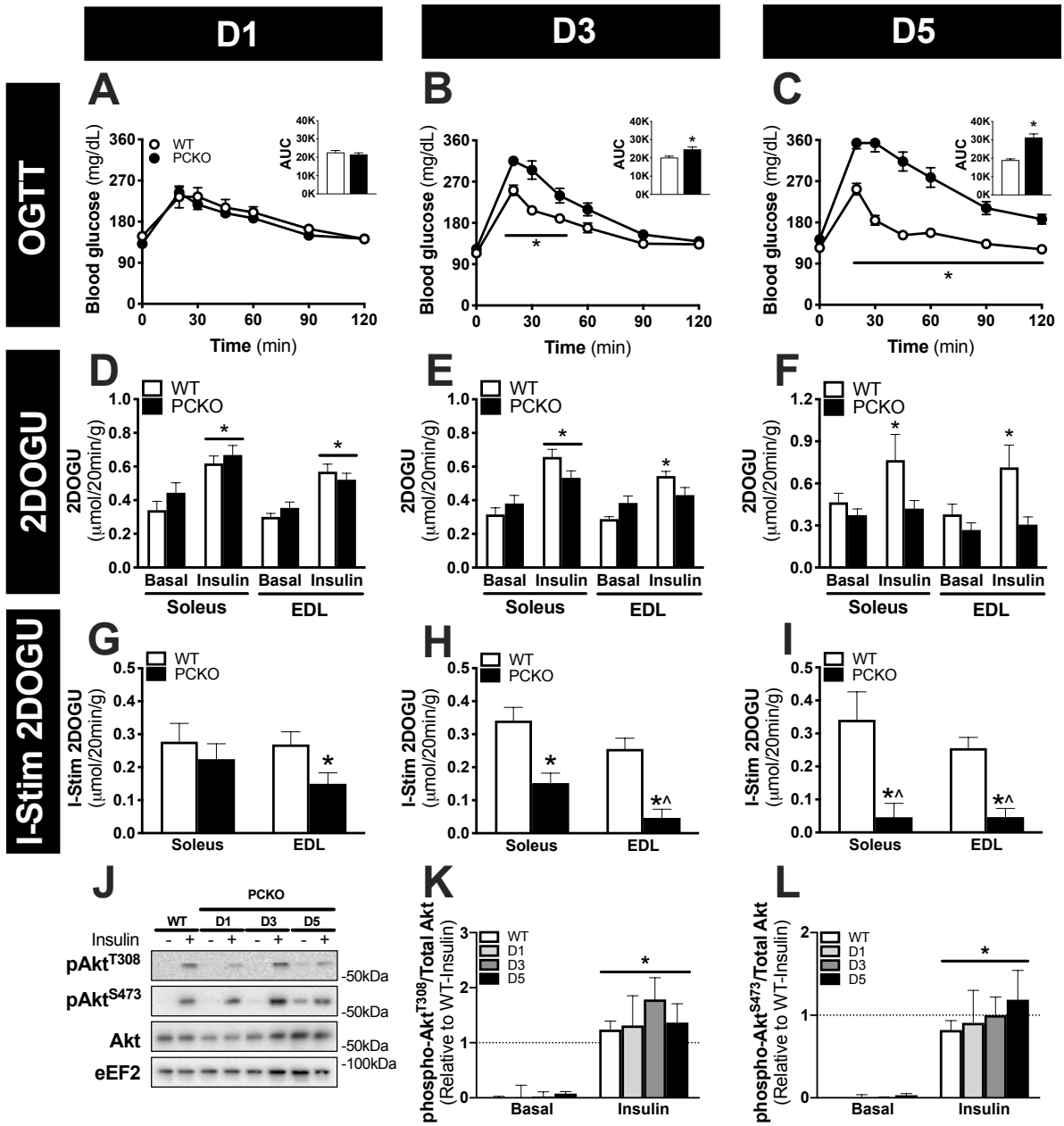
D1
D3
D5
OGTT
2DOGU
I-Stim 2DOGU
A
B
C
D
E
F
G
H
I
J
K
L
Blood glucose (mg/dL)
Time (min)
WT
PCKO
AUC
2DOGU (μmol/20min/g)
I-Stim 2DOGU (μmol/20min/g)
Basal
Insulin
Soleus
EDL
Insulin
pAktT308
pAktS473
Akt
eEF2
-50kDa
-100kDa
phospho-AktT308/Total Akt (Relative to WT-Insulin)
phospho-AktS473/Total Akt (Relative to WT-Insulin)

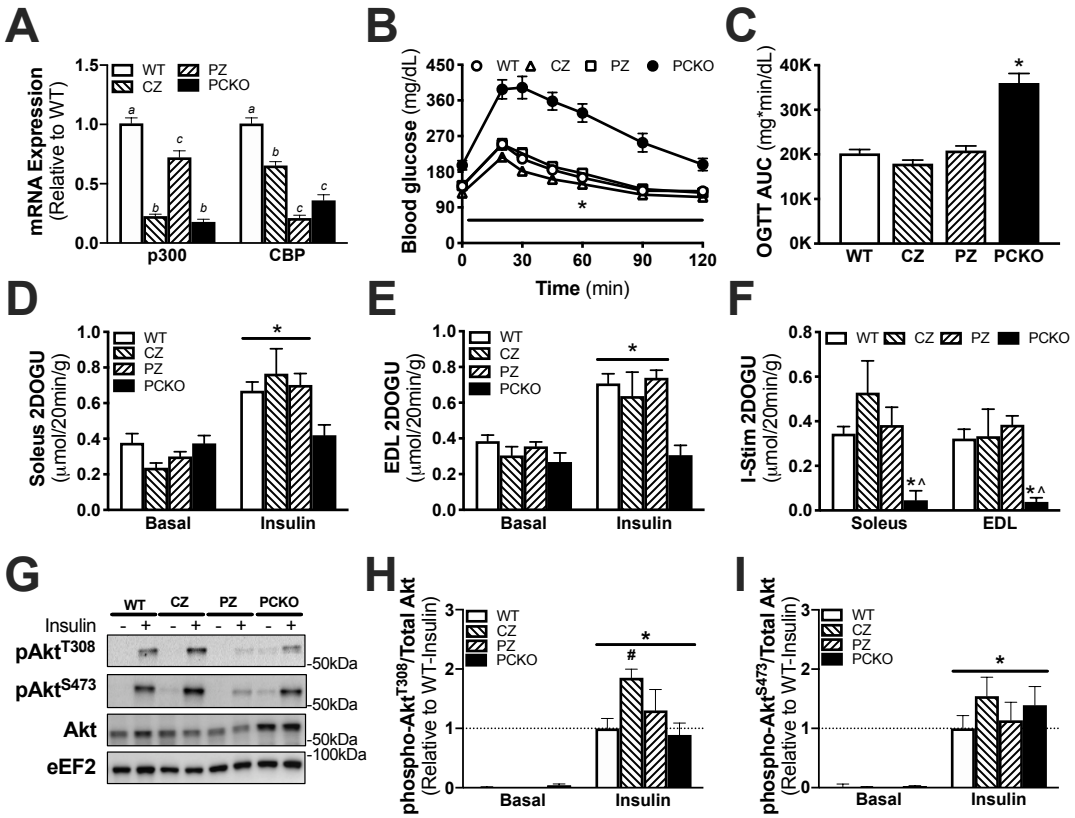

Figure 4.2: Mice with a single allele of either p300 or CBP have normal glucose tolerance and skeletal muscle insulin action. Male WT, CZ, PZ, and PCKO mice were assessed at five days after initiating tamoxifen. A) mRNA expression of p300 and CBP in quadriceps muscles of WT, CZ, PZ, and PCKO mice; WT/CZ/PZ/PCKO n=15/5/5/5. Different letters signify $p<0.05$ 1-way ANOVA, Tukey's multiple comparison test. The primers for p300 and CBP mRNA were designed to anneal onto exon 9 (exon that is floxed) and exon 10. B) Blood glucose concentrations and C) area under the curve (AUC) for male WT, CZ, PZ, and PCKO mice during an oral glucose tolerance test (OGTT; 2 g/kg); for WT/CZ/PZ/PCKO n = 18/16/9/7. *, $p<0.05$ 2-way ANOVA, PCKO vs WT within a time point for OGTT, and *, $p<0.05$ 1-way ANOVA, vs WT for AUC. D-E) Basal 2-deoxy-glucose uptake (2DOGU), Insulin (0.36 nmol/L) 2DOGU, and F) insulin-stimulated 2DOGU (I-Stim.; calculated as insulin 2DOGU – basal 2DOGU) in isolated extensor digitorum longus (EDL) and soleus muscles from male WT, CZ, PZ, and PCKO mice; WT/CZ/PZ/PCKO n = 20/8/7/10. *, $p<0.05$ 2-way ANOVA with Sidak's multiple comparison vs basal within genotype for basal and insulin 2DOGU. *, $p<0.05$ 1-way ANOVA with Tukey's multiple comparison vs WT for I-Stim. ^, $p>0.05$ one sample *t*-test vs "0". G) Phospho-Akt^{S473} (pAkt^{S473}), phospho-Akt^{T308} (pAkt^{T308}), and total Akt in basal and insulin-stimulated (- and +, respectively) EDL muscles from WT, CZ, PZ, and PCKO mice. Quantification of H) pAkt^{T308} and I) pAkt^{S473} compared to total protein abundance of Akt in the EDL muscle; WT/CZ/PZ/PCKO n = 10/5/5/6. Values are presented relative to WT basal. *, $p<0.05$ 2-way ANOVA, main effect of insulin. #, $p<0.05$ 2-way ANOVA, multiple comparison vs WT-insulin. Data reported as mean ± SEM. For all data, there were no significant differences between WT mice for the respective lines (CZ, PZ, and PCKO) therefore WT data was collapsed.

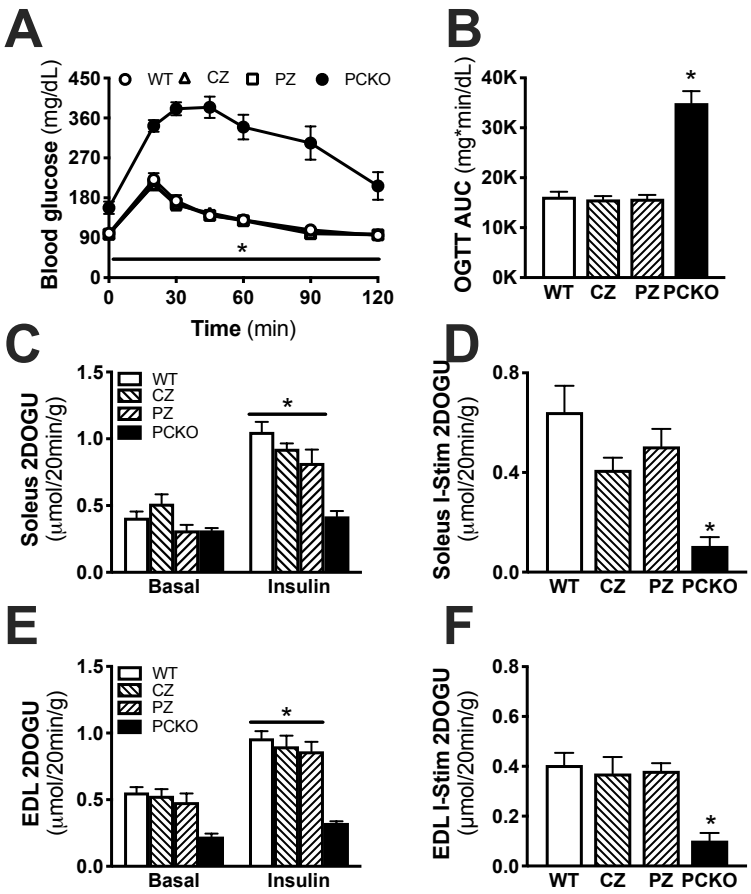

Figure 4.3: PCKO female mice are glucose intolerant and insulin resistant. Female WT, CZ, PZ, and PCKO mice were assessed at five days after initiating tamoxifen. A) Blood glucose concentrations and B) area under the curve (AUC) for female WT, CZ, PZ, and PCKO mice during an oral glucose tolerance test (OGTT; 2 g/kg); for WT/CZ/PZ/PCKO n = 12/10/13/8. *, $p<0.05$ 2-way ANOVA, PCKO vs WT within a time point for OGTT, and *, $p<0.05$ 1-way ANOVA, vs WT for AUC. C-F) Basal 2-deoxy-glucose uptake (2DOGU), Insulin (0.36 nmol/L) 2DOGU, and insulin-stimulated 2DOGU (I-Stim.; calculated as insulin 2DOGU – basal 2DOGU) in isolated C-D) soleus and E-F) extensor digitorum longus (EDL) muscles from female WT, CZ, PZ, and PCKO mice; WT/CZ/PZ/PCKO n = 14/7/5/8. *, $p<0.05$ 2-way ANOVA with Sidak's multiple comparison vs basal within genotype for basal and insulin 2DOGU. *, $p<0.05$ 1-way ANOVA with Tukey's multiple comparison vs WT for I-Stim. Values are presented relative to WT basal. For all data, there were no significant differences between WT mice for the respective lines (CZ, PZ, and PCKO) therefore WT data was collapsed.

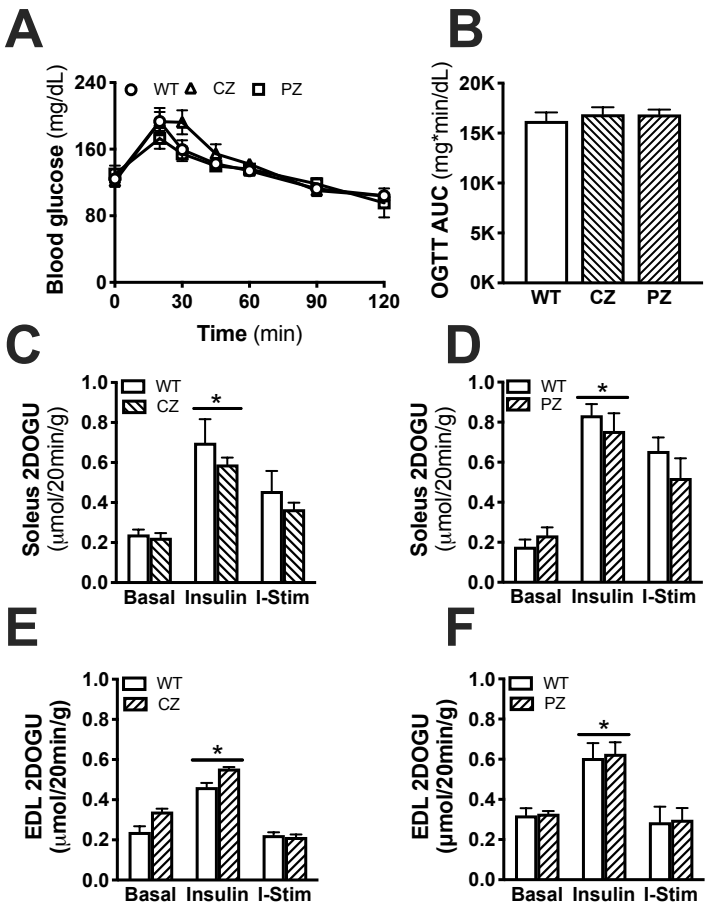

Figure 4.4: CZ and PZ female mice continue to be phenotypically normal one month after initiating tamoxifen. Female WT, CZ and PZ mice were assessed at 21 days after initiating tamoxifen for the oral glucose tolerance test (OGTT) and 28 days after initiating tamoxifen for insulin sensitivity. A) Blood glucose concentrations and B) area under the curve (AUC) for female WT, CZ, and PZ mice during an oral glucose tolerance test (OGTT; 2 g/kg); WT/CZ/PZ n = 12/6/5. C-F) Basal 2-deoxy-glucose uptake (2DOGU), Insulin (0.36 nmol/L) 2DOGU, and insulin-stimulated 2DOGU (I-Stim.; calculated as insulin 2DOGU – basal 2DOGU) in isolated C-D) soleus and E-F) extensor digitorum longus (EDL) muscles from female WT, CZ, and PZ mice; CZ: WT/KO: 5/6, PZ: WT/KO: 7/7. *, $p<0.05$ 2-way ANOVA with Sidak's multiple comparison vs basal within genotype.

Figure 4.5: Loss of p300/CBP in skeletal muscle leads to the downregulation of insulin signaling and GLUT4 trafficking genes and proteins. A) Principal component analysis (PCA) plot for gene expression during microarray in WT and PCKO extensor digitorum longus (EDL) muscles; WT/PCKO n = 4/4. B) Gene ontology (GO) biological processes terms relating to metabolism (FDR <0.1) for significantly down regulated genes in PCKO vs WT muscles. C) Expression profile (down [blue] and up [red]) for genes within biological processes GO categories from B. D) Graphical representation of differentially expressed genes within the insulin signaling, GLUT4 trafficking, and metabolism pathways. E) PCA plot for protein abundance during TMT mass spectrometry in WT, D3 PCKO, and D5 PCKO tibialis anterior muscle; WT/D3/D5 n = 3/3/3. F) Gene ontology (GO) Reactome terms relating to metabolism (FDR <0.1) for all differentially expressed proteins in PCKO D5 vs WT muscles. G) Protein abundance for proteins within Reactome ID: R-HAS-1445148 "Translocation of GLUT4 to the plasma membrane" for WT, and PCKO D3 and D5 muscle. *, FDR <0.1 vs WT. Data reported as mean ± SEM.

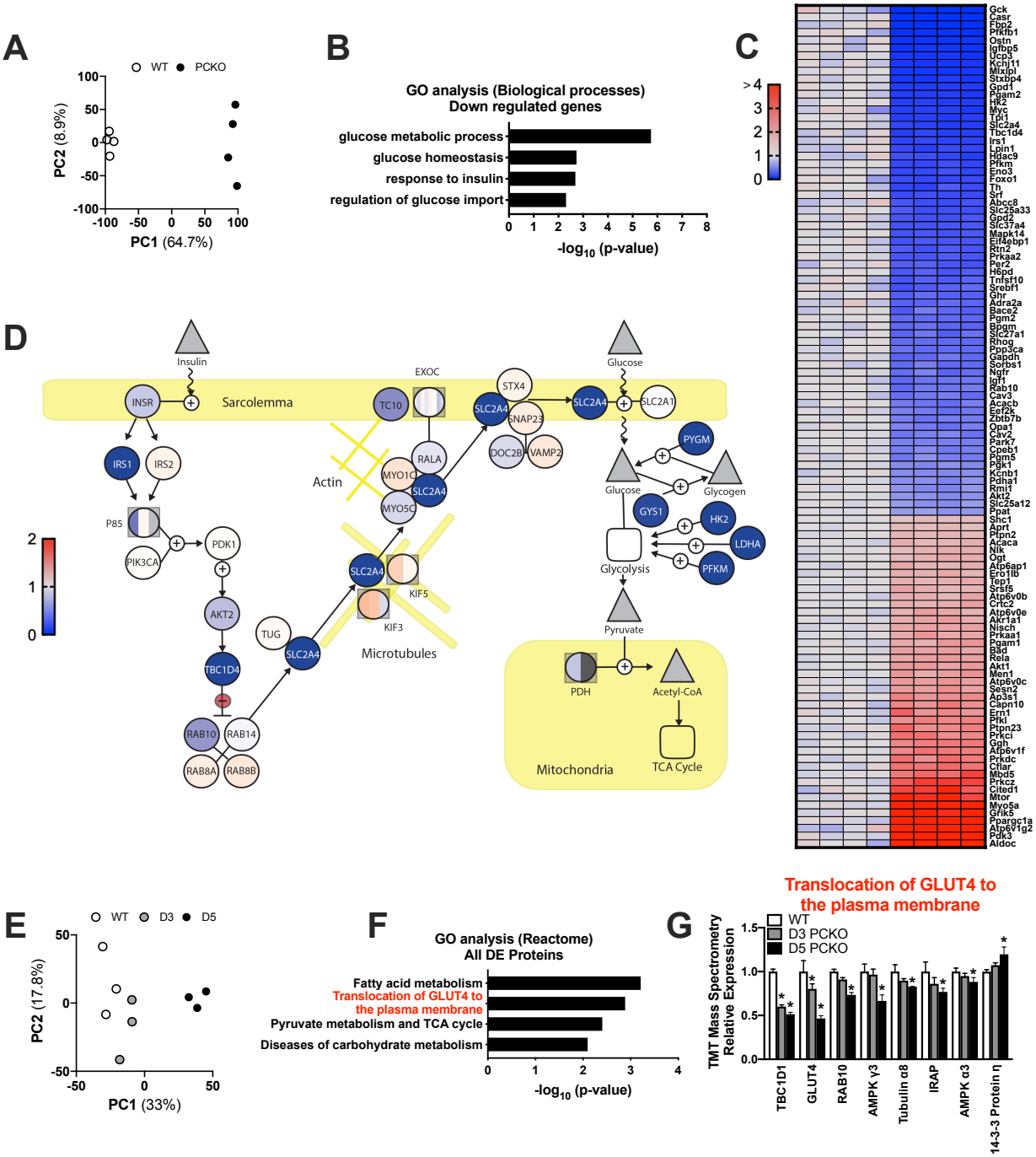
A
WT
PCKO
PC2 (8.9%)
PC1 (64.7%)
B
GO analysis (Biological processes)
Down regulated genes
glucose metabolic process
glucose homeostasis
response to insulin
regulation of glucose import
-log10 (p-value)
C
D
Insulin
Sarcolemma
INSR
IRS1
IRS2
P85
PIK3CA
PDK1
AKT2
TBC1D4
RAB10
RAB14
RAB8A
RAB8B
TUG
SLC2A4
EXOC
TC10
STX4
SNAP23
VAMP2
RALA
MYO1C
MYO5C
Actin
KIF5
KIF3
Microtubules
Glucose
SLC2A1
PYGM
Glycogen
GYS1
HK2
LDHA
PFKM
Glycolysis
Pyruvate
PDH
Acetyl-CoA
TCA Cycle
Mitochondria
E
WT
D3
D5
PC2 (17.8%)
PC1 (33%)
F
GO analysis (Reactome)
All DE Proteins
Fatty acid metabolism
Translocation of GLUT4 to the plasma membrane
Pyruvate metabolism and TCA cycle
Diseases of carbohydrate metabolism
-log10 (p-value)
G
Translocation of GLUT4 to the plasma membrane
TMT Mass Spectrometry Relative Expression
WT
D3 PCKO
D5 PCKO
TBC1D1
GLUT4
RAB10
AMPK γ3
Tubulin α8
IRAP
AMPK α3
14-3-3 Protein η

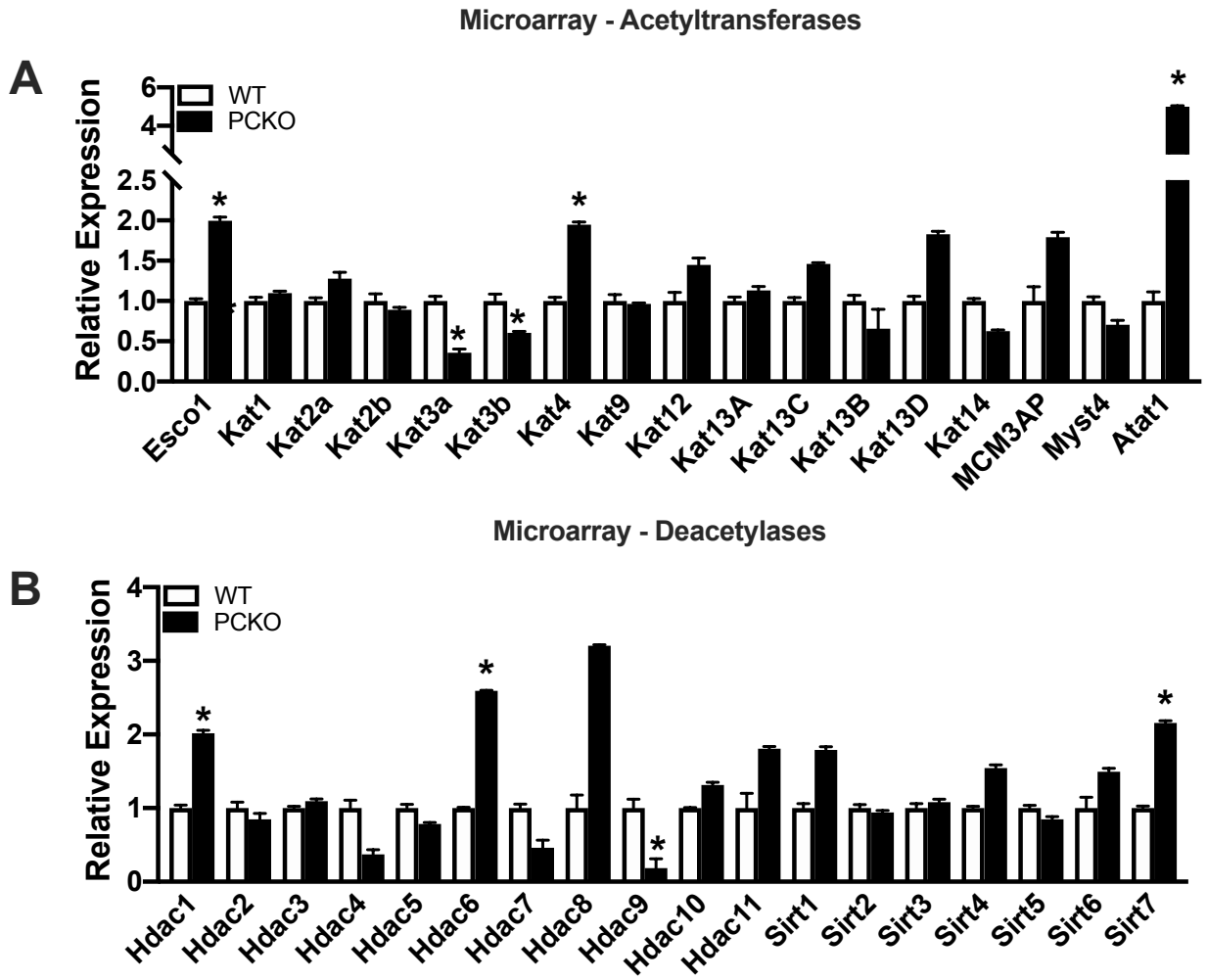

Figure 4.6: Acetyltransferase and deacetylase mRNA expression in PCKO mice. mRNA expression of all A) acetyltransferases and B) deacetylases detected on microarray analysis in PCKO and WT extensor digitorum longus (EDL) muscles; WT/PCKO n = 4/4. *, FDR <0.1 vs WT. Values are presented relative to WT basal and are expressed as mean ± SEM.

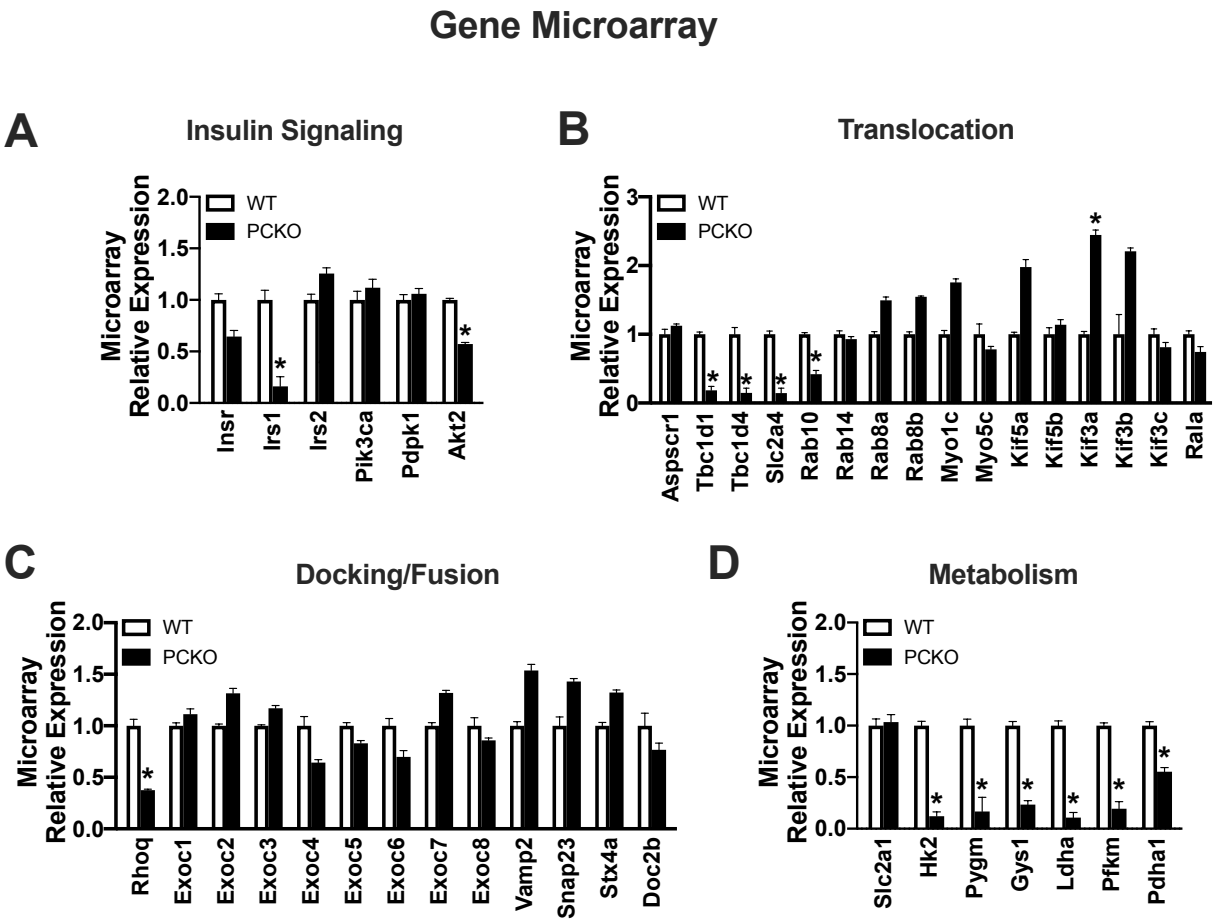

Figure 4.7: Insulin signaling, GLUT4 trafficking, and metabolism mRNA expression in PCKO mice. mRNA expression of genes related to A) insulin signaling, B) translocation of GLUT4, C) docking/fusion of GLUT4 to the plasma membrane, and D) metabolism in PCKO and WT extensor digitorum longus (EDL) muscles; WT/PCKO n = 4/4. *, FDR <0.1 vs WT. Values are presented relative to WT basal and are expressed as mean ± SEM. Genes are the same ones depicted in Figure 4.5D.

Chapter 5: Conclusion of Dissertation

For over 50 years, protein lysine acetylation has been known to be a major posttranslational modification responsible for the alteration of physical properties and function of thousands of proteins and biological processes (1, 6, 20, 45, 48, 54). Reversible acetylation requires the enzymatic addition or removal of acetyl groups, provided by acetyl-CoA, to lysine residues of proteins via acetyltransferases or deacetylases, respectively (7). Initially defined as histone acetyltransferases (HATs)/deacetylases (HDACs) for their well-established role in modifying lysine residues of histones (43), the concept that acetylation may affect the function of non-histone and non-nuclear proteins is a more recent discovery (23, 33). Indeed, recent proteomic studies have identified more than 2,000 acetylated non-histone proteins, many localized to the cytoplasm, and many part of metabolic pathways, including in skeletal muscle (6, 20, 48, 54). The deacetylases, in particular, have been investigated thoroughly for their potential role in regulating skeletal muscle insulin sensitivity (2, 11, 50, 51, 22, 28, 31, 36, 38, 41, 42, 47), however, whether their mechanism of action is via changes in transcription of insulin signaling proteins, acetylation of cytosolic insulin signaling proteins, or a combination of the two was a fundamental gap in knowledge. Conversely, to our knowledge, there were no studies published investigating the role of acetyltransferases towards regulating skeletal muscle insulin sensitivity.

The contribution of both the HDAC (28, 31, 38, 42, 47) and sirtuin (2, 11, 22, 36, 41) class of deacetylases towards skeletal muscle insulin action has been heavily studied. HDACs 4, 5, and 9, for example, work to repress the transcription of the GLUT4 (28, 31, 47), while SIRT1 is required for the enhancement of skeletal muscle insulin sensitivity via deacetylation and inactivation of the transcription factor Stat3, which results in decreased gene and protein

expression of the p55α/p50α regulatory subunits of PI3K (36). Notably, however, these studies do not discern whether deacetylases regulate insulin action via a purely transcriptional or a combination of transcriptional and non-transcriptional mechanisms. We directly tested this notion, in Study 1, by utilizing small molecule inhibitors of different classes of deacetylases acutely (i.e. 1 hour), in order to remove transcription as a confounding variable. We found that 1 hour treatment with deacetylase inhibitors was sufficient to increase both global acetylation and acetylation of deacetylase targets in both L6 myotubes and mouse skeletal muscle. However, this did not translate into changes in insulin-stimulated glucose uptake or signaling in L6 myotubes or mouse skeletal muscle. Considering that the same inhibitors increase insulin action in skeletal muscle when treated for over 24 hours (13, 31, 38, 42), our results suggest that deacetylases modulate skeletal muscle insulin action purely via transcriptional mechanisms.

Considering the primary method of regulation of deacetylases towards skeletal muscle insulin sensitivity is through a transcriptional mechanism, we turned towards the acetyltransferases. In Study 2, specifically, we investigated the individual contributions of p300 and CBP, *in vivo*, to whole-body glucose tolerance and skeletal muscle insulin action. The motivation behind studying p300 and CBP is because they can be phosphorylated by both insulin stimulation (15, 46, 55) and Akt (17, 24, 25, 34), and they have a robust cytosolic presence (3, 10, 32) which allows them to acetylate insulin signaling and GLUT4 trafficking proteins downstream of Akt (48). Taken together, it provides the premise for a putative Akt-p300/CBP axis in the regulation of insulin signaling to glucose uptake. We hypothesized, therefore, that knockout of either p300 or CBP in skeletal muscle would be sufficient to perturb the putative Akt-p300/CBP axis in muscle, leading to an impairment of insulin action. To directly test this hypothesis, we generated 4 novel mouse models: germline-mediated or adulthood-mediated, muscle-specific

knockout of p300 or CBP. We found, however, that p300 and CBP, individually, were dispensable for normal glucose tolerance, and insulin stimulated glucose uptake. Furthermore, while studies demonstrate that p300/CBP can acetylate and alter the function of Akt (39), IRS1/2 (5), and mTORC2 (14) leading to altered phosphorylation of Akt, we determined that Akt acetylation, and insulin-stimulated Akt phosphorylation were not different in p300 or CBP knockout muscle, indicating that Akt, PDK1, and mTORC2 function were likely not altered. Given that certain strains of genetically-modified mice to not demonstrate a phenotype until they have been metabolically stressed (30, 36), we decided to study the p300 and CBP knockout mice utilizing both a calorie restriction and high fat diet, which are known to improve (27, 36) and hinder (40, 49, 51) insulin sensitivity, respectively. However, while high-fat diet worsened glucose tolerance and calorie restriction enhanced glucose tolerance and skeletal muscle insulin sensitivity in WT mice, these dietary effects were not affected by the loss of p300 or CBP. Hence, while p300 and CBP are connected to both Akt and insulin signaling in other cell and tissue types, they are dispensable, individually, for skeletal muscle insulin action.

We attributed the lack of a phenotype in the p300 and CBP single knockout mice to the well documented redundancy of function between p300 and CBP, and their ability to compensate for one another (8, 16, 29, 52). Hence, in Study 3, we generated mice with skeletal muscle-specific and inducible, double knockout of p300/CBP. Interestingly, mice lacking both p300 and CBP in skeletal muscle become severely glucose intolerant and skeletal muscle insulin resistant within just days of inducing the knockout. To better understand the dosage effects of p300 and CBP, we also generated mice that had only a single allele of either p300 (PZ) or CBP (CZ). Remarkably, giving back a single allele of either p300 or CBP completely rescued the insulin resistant phenotype of p300/CBP double knockout mice. Not only do our results demonstrate the functional

redundancy of p300 and CBP, but it establishes p300/CBP as jointly required for skeletal muscle insulin action. For insight into what could be causing this dramatic phenotype, we utilized both microarray and TMT mass spectrometry to assess the transcriptome and proteome of double knockout mice muscle. p300/CBP double knockout muscles had markedly downregulated mRNA expression of genes and protein abundance of critical proteins in the insulin signaling pathway, such as TBC1D1 (~50%), GLUT4 (~55%), and Rab10 (~30%), only 5 days after initiating tamoxifen treatment. While these changes in protein abundance may, at least partially, explain the insulin resistant phenotype, it is important to note that mice with heterozygous knockout of these proteins (analogous to the protein reduction seen in PCKO mice at D5) are not as insulin resistant as PCKO mice (9, 12, 19, 35, 37, 44, 56). Furthermore, while double knockout mice at D3 are severely insulin resistant, based on the proteomics analysis PCKO mice at D3 are more similar to WT mice than PCKO mice at D5. Hence, while knocking out p300/CBP leads to the downregulation of the expression of insulin signaling and GLUT4 trafficking gene and protein networks, this does not fully explain the phenotype seen in p300/CBP double knockout mice, suggesting that non-nuclear acetylation could contribute to the described phenotype.

In conclusion, the findings from the three Studies of this Dissertation provide important insights into the role of p300/CBP and acetylation towards the regulation of skeletal muscle insulin sensitivity. Study 1 of this Dissertation revealed that deacetylases do not modulate skeletal muscle insulin action via non-nuclear acetylation, but rather likely do so via purely transcriptional mechanisms. In Study 2, we demonstrate that individual knockouts of p300 or CBP are insufficient to alter skeletal muscle insulin action, likely due to compensation. Accordingly, in Study 3, we establish p300/CBP, jointly, as novel critical regulators of skeletal muscle insulin sensitivity, via transcriptional, and potentially non-transcriptional, mechanisms of action. Thus, the Studies from

this Dissertation have contributed to significant gaps in the literature and broaden our current understanding of deacetylases/acetyltransferases towards skeletal muscle insulin action. Taken together, while it is clear that acetylation is a prevalent post-translational modification in skeletal muscle (21, 26), which can act to modify the function of insulin signaling proteins (4, 5, 14, 18, 39, 53), further studies are needed to clarify the role of p300/CBP towards skeletal muscle insulin signaling and action. In future studies, it will be interesting to manipulate p300/CBP activity acutely, as we have done for deacetylases in Study 1, to better understand if the phenotype of the p300/CBP double knockout mice are due to changes in transcription of insulin signaling proteins, acetylation of cytosolic insulin signaling proteins, or a combination of the two. Furthermore, given that transcriptional changes do not fully explain the insulin resistance of PCKO mice, it will be of high interest in future studies to probe p300/CBP substrates in order to determine how their acetylation status can alter skeletal muscle insulin sensitivity and overall muscle physiology. The potential future applications of this work would allow us to better understand the insulin signaling and GLUT4 trafficking pathway, under the lens of acetylation as a novel regulatory mechanism. This new understanding of the pathway and targets could yield entirely novel strategies to optimize insulin signaling that 'work' downstream and/or independently of PI3K-Akt, increasing specificity to insulin-stimulated glucose uptake and decreasing the risk of off-target effects, which would have great potential to improve human health and quality of life.

References

1. **Allfrey VG**, **Faulkner R**, **Mirsky AE**. Acetylation and methylation of histones and their possible role in the regulation of RNA synthesis. *Proc Natl Acad Sci* 51: 786–794, 1964.

2. **Arora A**, **Dey CS**. SIRT2 negatively regulates insulin resistance in C2C12 skeletal muscle cells. *Biochim Biophys Acta - Mol Basis Dis* 1842: 1372–1378, 2014.

3. **Aslan JE**, **Rigg RA**, **Nowak MS**, **Loren CP**, **Baker-Groberg SM**, **Pang J**, **David LL**, **McCarty OJT**. Lysine acetyltransfer supports platelet function. *J Thromb Haemost* 13: 1908–17, 2015.

4. **Belman JP**, **Bian RR**, **Habtemichael EN**, **Li DT**, **Jurczak MJ**, **Alcázar-Román A**, **McNally LJ**, **Shulman GI**, **Bogan JS**. Acetylation of TUG protein promotes the accumulation of GLUT4 glucose transporters in an insulin-responsive intracellular compartment. *J Biol Chem* 290: 4447–63, 2015.

5. **Cao J**, **Peng J**, **An H**, **He Q**, **Boronina T**, **Guo S**, **White MF**, **Cole PA**, **He L**. Endotoxemia-mediated activation of acetyltransferase P300 impairs insulin signaling in obesity. *Nat Commun* 8, 2017.

6. **Choudhary C**, **Kumar C**, **Gnad F**, **Nielsen ML**, **Rehman M**, **Walther TC**, **Olsen J V**, **Mann M**. Lysine acetylation targets protein complexes and co-regulates major cellular functions. *Science* 325: 834–40, 2009.

7. **Choudhary C**, **Weinert BT**, **Nishida Y**, **Verdin E**, **Mann M**. The growing landscape of lysine acetylation links metabolism and cell signalling. *Nat Rev Mol Cell Biol* 15: 536–50, 2014.

8. **Dancy BM**, **Cole PA**. Protein lysine acetylation by p300/CBP. *Chem Rev* 115: 2419–52, 2015.

9. **Dokas J**, **Chadt A**, **Nolden T**, **Himmelbauer H**, **Zierath JR**, **Joost HG**, **Al-Hasani H**. Conventional knockout of Tbc1d1 in mice impairs insulin- and AICAR-stimulated glucose uptake in skeletal muscle. *Endocrinology* 154: 3502–3514, 2013.

10. **Fermento ME**, **Gandini NA**, **Salomón DG**, **Ferronato MJ**, **Vitale CA**, **Arévalo J**, **López Romero A**, **Nuñez M**, **Jung M**, **Facchinetti MM**, **Curino AC**. Inhibition of p300 suppresses growth of breast cancer. Role of p300 subcellular localization. *Exp Mol Pathol* 97: 411–24, 2014.

11. **Fröjdö S**, **Durand C**, **Molin L**, **Carey AL**, **El-Osta A**, **Kingwell BA**, **Febbraio MA**, **Solari F**, **Vidal H**, **Pirola L**. Phosphoinositide 3-kinase as a novel functional target for the regulation of the insulin signaling pathway by SIRT1. *Mol Cell Endocrinol* 335: 166–176, 2011.

12. **Fueger PT**, **Hess HS**, **Bracy DP**, **Pencek RR**, **Posey KA**, **Charron MJ**, **Wasserman DH**. Regulation of insulin-stimulated muscle glucose uptake in the conscious mouse: Role of

glucose transport is dependent on glucose phosphorylation capacity. *Endocrinology* 145: 4912–4916, 2004.

13. **Gaur V**, **Connor T**, **Venardos K**, **Henstridge DC**, **Martin SD**, **Swinton C**, **Morrison S**, **Aston-Mourney K**, **Gehrig SM**, **van Ewijk R**, **Lynch GS**, **Febbraio MA**, **Steinberg GR**, **Hargreaves M**, **Walder KR**, **McGee SL**. Scriptaid enhances skeletal muscle insulin action and cardiac function in obese mice. *Diabetes, Obes Metab* 19: 936–943, 2017.

14. **Glidden EJ**, **Gray LG**, **Vemuru S**, **Li D**, **Harris TE**, **Mayo MW**. Multiple site acetylation of rictor stimulates mammalian target of rapamycin complex 2 (mTORC2)-dependent phosphorylation of Akt protein. *J Biol Chem* 287: 581–588, 2012.

15. **He L**, **Sabet A**, **Djedjos S**, **Miller R**, **Sun X**, **Hussain MA**, **Radovick S**, **Wondisford FE**. Metformin and Insulin Suppress Hepatic Gluconeogenesis through Phosphorylation of CREB Binding Protein. *Cell* 137: 635–646, 2009.

16. **Hennig AK**, **Peng GH**, **Chen S**. Transcription Coactivators p300 and CBP Are Necessary for Photoreceptor-Specific Chromatin Organization and Gene Expression. *PLoS One* 8, 2013.

17. **Huang W-C**, **Chen C-C**. Akt phosphorylation of p300 at Ser-1834 is essential for its histone acetyltransferase and transcriptional activity. *Mol Cell Biol* 25: 6592–602, 2005.

18. **Kaiser C**, **James SR**. Acetylation of insulin receptor substrate-1 is permissive for tyrosine phosphorylation. *BMC Biol* 2: 23, 2004.

19. **Karunanithi S**, **Xiong T**, **Uhm M**, **Leto D**, **Sun J**, **Chen X-W**, **Saltiel AR**. A Rab10:RalA G protein cascade regulates insulin-stimulated glucose uptake in adipocytes. *Mol Biol Cell* 25: 3059–69, 2014.

20. **Kim SC**, **Sprung R**, **Chen Y**, **Xu Y**, **Ball H**, **Pei J**, **Cheng T**, **Kho Y**, **Xiao H**, **Xiao L**, **Grishin N V.**, **White M**, **Yang X-J**, **Zhao Y**. Substrate and functional diversity of lysine acetylation revealed by a proteomics survey. *Mol Cell* 23: 607–18, 2006.

21. **Koltai E**, **Szabo Z**, **Atalay M**, **Boldogh I**, **Naito H**, **Goto S**, **Nyakas C**, **Radak Z**. Exercise alters SIRT1, SIRT6, NAD and NAMPT levels in skeletal muscle of aged rats. *Mech Ageing Dev* 131: 21–8, 2010.

22. **Lantier L**, **Williams AS**, **Williams IM**, **Yang KK**, **Bracy DP**, **Goelzer M**, **James FD**, **Gius D**, **Wasserman DH**. SIRT3 Is Crucial for Maintaining Skeletal Muscle Insulin Action and Protects Against Severe Insulin Resistance in High-Fat–Fed Mice. *Diabetes* 64: 3081–3092, 2015.

23. **Lee KK**, **Workman JL**. Histone acetyltransferase complexes: One size doesn't fit all. *Nat Rev Mol Cell Biol* 8: 284–295, 2007.

24. **Liu Y**, **Denlinger CE**, **Rundall BK**, **Smith PW**, **Jones DR**. Suberoylanilide hydroxamic acid induces Akt-mediated phosphorylation of p300, which promotes acetylation and

transcriptional activation of RelA/p65. *J Biol Chem* 281: 31359–31368, 2006.

25. **Liu Y**, **Xing Z**, **Zhang J**, **Fang Y**. Akt kinase targets the association of CBP with histone H3 to regulate the acetylation of lysine K18. *FEBS Lett* 587: 847–853, 2013.

26. **Lundby A**, **Lage K**, **Weinert BT**, **Bekker-Jensen DB**, **Secher A**, **Skovgaard T**, **Kelstrup CD**, **Dmytriyev A**, **Choudhary C**, **Lundby C**, **Olsen J V**. Proteomic analysis of lysine acetylation sites in rat tissues reveals organ specificity and subcellular patterns. *Cell Rep* 2: 419–31, 2012.

27. **Martins VF**, **Tahvilian S**, **Kang JH**, **Svensson K**, **Hetrick B**, **Chick WS**, **Schenk S**, **McCurdy CE**. Calorie Restriction-Induced Increase in Skeletal Muscle Insulin Sensitivity Is Not Prevented by Overexpression of the p55α Subunit of Phosphoinositide 3-Kinase. *Front Physiol* 9: 789, 2018.

28. **McGee SL**, **Van Denderen BJW**, **Howlett KF**, **Mollica J**, **Schertzer JD**, **Kemp BE**, **Hargreaves M**. AMP-activated protein kinase regulates GLUT4 transcription by phosphorylating histone deacetylase 5. *Diabetes* 57: 860–867, 2008.

29. **Moreno CL**, **Yang L**, **Dacks PA**, **Isoda F**, **Van Deursen JMA**, **Mobbs C V.** Role of hypothalamic Creb-binding protein in obesity and molecular reprogramming of metabolic substrates. *PLoS One* 11: 1–15, 2016.

30. **Pfluger PT**, **Herranz D**, **Velasco-Miguel S**, **Serrano M**, **Tschop MH**. Sirt1 protects against high-fat diet-induced metabolic damage. *Proc Natl Acad Sci* 105: 9793–9798, 2008.

31. **Raichur S**, **Teh SH**, **Ohwaki K**, **Gaur V**, **Long YC**, **Hargreaves M**, **McGee SL**, **Kusunoki J**. Histone deacetylase 5 regulates glucose uptake and insulin action in muscle cells. *J Mol Endocrinol* 49: 203–211, 2012.

32. **Ruiz L**, **Gurlo T**, **Ravier MA**, **Wojtusciszyn A**, **Mathieu J**, **Brown MR**, **Broca C**, **Bertrand G**, **Butler PC**, **Matveyenko A V**, **Dalle S**, **Costes S**. Proteasomal degradation of the histone acetyl transferase p300 contributes to beta-cell injury in a diabetes environment. *Cell Death Dis* 9: 600, 2018.

33. **Sadoul K**, **Wang J**, **Diagouraga B**, **Khochbin S**. The tale of protein lysine acetylation in the cytoplasm. *J Biomed Biotechnol* 2011: 970382, 2011.

34. **Sanchez M**, **Sauvé K**, **Picard N**, **Tremblay A**. The hormonal response of estrogen receptor beta is decreased by the phosphatidylinositol 3-kinase/Akt pathway via a phosphorylation-dependent release of CREB-binding protein. *J Biol Chem* 282: 4830–40, 2007.

35. **Sano H**, **Eguez L**, **Teruel MN**, **Fukuda M**, **Chuang TD**, **Chavez JA**, **Lienhard GE**, **McGraw TE**. Rab10, a Target of the AS160 Rab GAP, Is Required for Insulin-Stimulated Translocation of GLUT4 to the Adipocyte Plasma Membrane. *Cell Metab* 5: 293–303, 2007.

36. **Schenk S**, **McCurdy CE**, **Philp A**, **Chen MZ**, **Holliday MJ**, **Bandyopadhyay GK**,

Osborn O, **Baar K**, **Olefsky JM**. Sirt1 enhances skeletal muscle insulin sensitivity in mice during caloric restriction. *J Clin Invest* 121: 4281–8, 2011.

37. **Stenbit AE**, **Tsao TS**, **Li J**, **Burcelin R**, **Geenen DL**, **Factor SM**, **Houseknecht K**, **Katz EB**, **Charron MJ**. GLUT4 heterozygous knockout mice develop muscle insulin resistance and diabetes. *Nat Med* 3: 1096–101, 1997.

38. **Sun C**, **Zhou J**. Trichostatin A improves insulin stimulated glucose utilization and insulin signaling transduction through the repression of HDAC2. *Biochem Pharmacol* 76: 120–127, 2008.

39. **Sundaresan NR**, **Pillai VB**, **Wolfgeher D**, **Samant S**, **Vasudevan P**, **Parekh V**, **Raghuraman H**, **Cunningham JM**, **Gupta M**, **Gupta MP**. The deacetylase SIRT1 promotes membrane localization and activation of Akt and PDK1 during tumorigenesis and cardiac hypertrophy. *Sci Signal* 4: ra46, 2011.

40. **Svensson K**, **Dent JR**, **Tahvilian S**, **Martins VF**, **Sathe A**, **Ochala J**, **Patel MS**, **Schenk S**. Defining the contribution of skeletal muscle pyruvate dehydrogenase α1 to exercise performance and insulin action. *Am J Physiol Metab* 315: E1034–E1045, 2018.

41. **Svensson K**, **LaBarge SA**, **Martins VF**, **Schenk S**. Temporal overexpression of SIRT1 in skeletal muscle of adult mice does not improve insulin sensitivity or markers of mitochondrial biogenesis. *Acta Physiol* 221: 193–203, 2017.

42. **Takigawa-Imamura H**, **Sekine T**, **Murata M**, **Takayama K**, **Nakazawa K**, **Nakagawa J**. Stimulation of Glucose Uptake in Muscle Cells by Prolonged Treatment with Scriptide, a Histone Deacetylase Inhibitor. *Biosci Biotechnol Biochem* 67: 1499–1506, 2003.

43. **Turner BM**. Histone acetylation and control of gene expression. *J Cell Sci* 99 (Pt 1): 13–20, 1991.

44. **Vazirani RP**, **Verma A**, **Sadacca LA**, **Buckman MS**, **Picatoste B**, **Beg M**, **Torsitano C**, **Bruno JH**, **Patel RT**, **Simonyte K**, **Camporez JP**, **Moreira G**, **Falcone DJ**, **Accili D**, **Elemento O**, **Shulman GI**, **Kahn BB**, **McGraw TE**. Disruption of adipose Rab10-dependent insulin signaling causes hepatic insulin resistance. *Diabetes* 65: 1577–1589, 2016.

45. **Verdin E**, **Ott M**. 50 years of protein acetylation: from gene regulation to epigenetics, metabolism and beyond. *Nat Rev Mol Cell Biol* 16: 258–64, 2015.

46. **Wan W**, **You Z**, **Xu Y**, **Zhou L**, **Guan Z**, **Peng C**, **Wong CCL**, **Su H**, **Zhou T**, **Xia H**, **Liu W**. mTORC1 Phosphorylates Acetyltransferase p300 to Regulate Autophagy and Lipogenesis. *Mol Cell* 68: 323-335.e6, 2017.

47. **Weems J**, **Olson AL**. Class II histone deacetylases limit GLUT4 gene expression during adipocyte differentiation. *J Biol Chem* 286: 460–468, 2011.

48. **Weinert BT**, **Narita T**, **Satpathy S**, **Srinivasan B**, **Hansen BK**, **Schölz C**, **Hamilton WB**,

Zucconi BE, **Wang WW**, **Liu WR**, **Brickman JM**, **Kesicki EA**, **Lai A**, **Bromberg KD**, **Cole PA**, **Choudhary C**. Time-Resolved Analysis Reveals Rapid Dynamics and Broad Scope of the CBP/p300 Acetylome. *Cell* 174: 231-244.e12, 2018.

49. **White AT**, **LaBarge SA**, **McCurdy CE**, **Schenk S**. Knockout of STAT3 in skeletal muscle does not prevent high-fat diet-induced insulin resistance. *Mol Metab* 4: 569–75, 2015.

50. **White AT**, **McCurdy CE**, **Philp A**, **Hamilton DL**, **Johnson CD**, **Schenk S**. Skeletal muscle-specific overexpression of SIRT1 does not enhance whole-body energy expenditure or insulin sensitivity in young mice. *Diabetologia* 56: 1629–37, 2013.

51. **White AT**, **Philp A**, **Fridolfsson HN**, **Schilling JM**, **Murphy AN**, **Hamilton DL**, **McCurdy CE**, **Patel HH**, **Schenk S**. High-fat diet-induced impairment of skeletal muscle insulin sensitivity is not prevented by SIRT1 overexpression. *Am J Physiol Endocrinol Metab* 307: E764-72, 2014.

52. **Wong CK**, **Wade-Vallance AK**, **Luciani DS**, **Brindle PK**, **Lynn FC**, **Gibson WT**. The p300 and CBP Transcriptional Coactivators are Required for Beta Cell and Alpha Cell Proliferation. *Diabetes* : db170237, 2017.

53. **Zhang J**. The direct involvement of SirT1 in insulin-induced insulin receptor substrate-2 tyrosine phosphorylation. *J Biol Chem* 282: 34356–34364, 2007.

54. **Zhao S**, **Xu W**, **Jiang W**, **Yu W**, **Lin Y**, **Zhang T**, **Yao J**, **Zhou L**, **Zeng Y**, **Li H**, **Li Y**, **Shi J**, **An W**, **Hancock SM**, **He F**, **Qin L**, **Chin J**, **Yang P**, **Chen X**, **Lei Q**, **Xiong Y**, **Guan K-L**. Regulation of cellular metabolism by protein lysine acetylation. *Science* 327: 1000–4, 2010.

55. **Zhou XY**, **Shibusawa N**, **Naik K**, **Porras D**, **Temple K**, **Ou H**, **Kaihara K**, **Roe MW**, **Brady MJ**, **Wondisford FE**. Insulin regulation of hepatic gluconeogenesis through phosphorylation of CREB-binding protein. *Nat Med* 10: 633–637, 2004.

56. **Zisman A**, **Peroni OD**, **Abel ED**, **Michael MD**, **Mauvais-Jarvis F**, **Lowell BB**, **Wojtaszewski JF**, **Hirshman MF**, **Virkamaki A**, **Goodyear LJ**, **Kahn CR**, **Kahn BB**. Targeted disruption of the glucose transporter 4 selectively in muscle causes insulin resistance and glucose intolerance. *Nat Med* 6: 924–8, 2000.

APPENDIX

Microarray methods. RNA was extracted from EDL muscle by Tri reagent (Sigma Aldrich, Kent, UK) and purified on Reliaprep spin columns (Promega, Wisconsin, USA) using the manufacturer's instructions. RNA concentrations were determined using the LVis function of the FLUOstar Omega microplate reader (BMG Labtech, Buckinghamshire, UK) and RNA integrity number (RIN) assessed using an Agilent 2100 Bioanalyzer System (Agilent Technologies LDA, Cheshire, UK). A RIN value >9 per sample was deemed appropriate for Microarray analysis. Microarray analysis was performed at the Functional Genomics and Proteomics Facility, University of Birmingham, UK, using Agilent SurePrint G3 Mouse GE 8x60K Microarrays (Agilent Technologies LDA, Cheshire, UK) according to the manufacturers instructions. Differential expression was assessed with an R package limma (5) applied to log2-transformed signal intensities. Statistical significance of each test was expressed in terms of local false discovery rate (lfdr) (1) using the limma function eBayes. Probes were sorted by lfdr and gene-level summaries were made by annotating probes with Entrez gene ID's and assigning the lowest observed lfdr to a gene (usually, several probes map onto the same gene ID because of multiplicity of transcripts and redundancy of the microarray design). In the end, we report 15,330 detected genes and lncRNA loci, of which 3,310 are significantly differentially expressed at the level of lfdr < 0.1, i.e., they each have better than 90% probability of being differentially expressed.

Tandem mass tag mass spectrometry methods. Sample lysis - The samples (~50 mg of muscle tissue) were resuspended in 200 uL of ice cold 50 mM ammonium bicarbonate (ABC) in a vial containing 2.4 mm stainless steel beads (Omni International, Kennesaw GA). The samples

were lysed on an Omni Bead Ruptor 24 homogenizer at speed 6 for 30 s followed by a one minute rest on ice. This was repeated 4 times for a total of 5 cycles. The beads were then rinsed with an additional 200 uL of 50 mM ABC, and tissue homogenate was placed on ice and lysed by probe sonication (3x for 15 s with a 30 s rest between cycles). An additional 200 uL aliquot of 50 mM ABC was added, and protein concentrations were determined using the Pierce™ BCA Protein Assay Kit (Thermo Scientific, Rockford, IL). Sample digestion - Samples were digested using the protease max protocol (Promega, Madison, WI). Briefly, a 1% protease max solution was added to 60 µg of each sample in 50 mM ABC for a final concentration of 0.2%. The samples were gently vortexed for 30 min at room temperature, and further diluted with 50 mM ABC to achieve a protease max concentration of 0.046%. The samples were reduced with dithiothreitol (final concentration of 6 mM) for 20 min at 50°C and alkylated with iodoacetamide (final concentration of 6 mM) for 15 min at room temperature in the dark. The protease max concentration was adjusted to 0.05% before 2.4 µg of trypsin (sequencing grade modified trypsin, Promega, Madison, WI) was added to each sample. The samples were incubated for 6 h at 37°C. After the incubation, TFA was added to a final concentration of 1% to quench the samples. The samples were incubated with mixing for 15 min at room temperature. Peptide sample cleanup - Peptides were purified by solid phase extraction using BioPureSPN MIDI cartridges (Nest Group, Inc., Southborough, MA). The cartridges were conditioned 3x with 100 µL of 80% ACN/0.1% TFA and equilibrated 3x with 100 µL of 0.1% TFA. The samples were loaded and passed through the cartridges three times. The samples were washed 3x with 75 µL of 0.1%TFA then eluted 4x with 50 µL 80% ACN/0.1% FA. Peptide concentrations were determined using the Pierce™ Quantitative Colorimetric Peptide Assay (Thermo Scientific, Rockford, IL). The peptide samples were dried by speed vacuum in preparation for TMT labeling. TMT labeling - The TMT 10-plex reagents (0.2 mg) were each

dissolved in 12 µL of anhydrous ACN. The peptides were reconstituted in 100 mM triethylammonium bicarbonate (TEAB) and 20 µg (25 µL) was added to 0.2 mg of its respective 10-plex TMT reagent. The samples were incubated for 1 hour at room temperature with gentle mixing. Two µL of each reaction mixture was then mixed, 2 µL of 5% hydroxylamine added, and the combined sample incubated for a further 15 min with gentle mixing. The mixture was then dried down, dissolved in 5% formic acid, and 2 µg of peptide analyzed by a single 2 h LC-MS/MS method using an Orbitrap Fusion as described below. This run was performed to normalize the total reporter ion intensity of each multiplexed sample and check TMT labeling efficiency. The remaining samples were quenched by addition of 2 µL of 5% hydroxylamine as above, then combined in a 1:1:1:1:1:1:1:1:1:1 ratio based on total reporter ion intensities determined during the normalization run, and dried down in preparation for 2D-LC-MS/MS analysis. LC-MS/MS analysis - Multiplexed TMT-labeled samples were reconstituted in 10 mM ammonium formate pH 9 and separated by two-dimensional reverse-phase liquid chromatography using a Dionex NCS-3500RS UltiMate RSLCnano UPLC system. A 40 µl sample (60 µg) was injected onto a NanoEase 5 µm XBridge BEH130 C18 300 µm x 50 mm column (Waters) at 3 µL/min in a mobile phase containing 10 mm ammonium formate (pH 9). Peptides were eluted by sequential injection of 20 µL volumes of 14, 17, 20, 21, 22, 23, 24, 25, 26, 27, 28, 29, 30, 35, 40, 45, 50 and 90% ACN in 10 mm ammonium formate (pH 9) at 3 µL/min flow rate. Eluted peptides were diluted with mobile phase containing 0.1% formic acid at 24 µL/min flow rate and delivered to an Acclaim PepMap 100 µm x 2 cm NanoViper C18, 5 µm trap on a switching valve. After 10 min of loading, the trap column was switched on-line to a PepMap RSLC C18, 2 µm, 75 µm x 25 cm EasySpray column (Thermo Scientific). Peptides were then separated at low pH in the second dimension using a 7.5–30% ACN gradient over 90 min in mobile phase containing 0.1% formic acid at 300 nl/min flow

rate. Each second-dimension LC run required 2 h for separation and re-equilibration, so each 2D LC-MS/MS method required 36 h for completion. Tandem mass spectrometry data was collected using an Orbitrap Fusion Tribrid instrument configured with an EasySpray NanoSource (Thermo Scientific). Survey scans were performed in the Orbitrap mass analyzer (resolution = 120,000), and data-dependent MS2 scans performed in the linear ion trap using collision-induced dissociation (normalized collision energy = 35) following isolation with the instrument's quadrupole. Reporter ion detection was performed in the Orbitrap mass analyzer (resolution = 60,000) using MS3 scans following synchronous precursor isolation of the top 10 ions in the quadrupole, and higher-energy collisional dissociation in the ion-routing multipole (normalized collision energy = 65). TMT Data Analysis - RAW instrument files were processed using Proteome Discoverer (PD) version 1.4.1.14 (Thermo Scientific). For each of the TMT experiments, raw files from the 18 fractions were merged and searched with the SEQUEST HT search engine with a *Mus musculus* canonical uniprot protein database downloaded January 2018 (22,276 entries) along with 179 common contaminant sequences. Searches were configured with static modifications for the TMT reagents (+229.163 Da) on lysines and N termini, carbamidomethyl (+57.021 Da) on cysteines, dynamic modifications for oxidation of methionine residues (+15.9949 Da), parent ion tolerance of 1.25 Da, fragment mass tolerance of 1.0005 Da, monoisotopic masses, and trypsin cleavage (max 2 missed cleavages). The large parent ion tolerance was used to increase the number of peptides being scored to improve discrimination of true *versus* false identifications (2). Searches used a reversed sequence decoy strategy to control peptide false discovery and identifications were validated by Percolator software (3). Only peptides with q scores ≤ 0.05 were accepted, and at least one unique peptide was required for matching a protein entry for its identification. Search results and TMT reporter ion intensities were exported as text files and processed with in-house

scripts. A median reporter ion intensity peak height cutoff of 750 was used, along with an additional cutoff of 20 ppm parent ion tolerance and all reporter ion intensities for unique peptides matched to each respective protein were summed to create total protein intensities. Zero values were substituted with an intensity of 150, which is approximately half of the minimum observed reporter ion intensity in any given channel. Proteins where quantitation was based on a single spectra, or where the average reporter ion intensity was below 4,000, were flagged as poor quality data and were excluded from further analysis. Differential protein abundance between groups was then determined by comparing the total reporter ion intensities using the Bioconductor package edgeR (4), which uses quasi negative binomial and the quantile-adjusted conditional maximum likelihood (qCML) method for experiments with single factor. Additional data normalizations, multiple testing corrections, and calculation of false discovery rates were performed within edgeR.

References

1. **Wu D, Smyth GK, Ritchie ME, Law CW, Phipson B, Hu Y, Shi W**. limma powers differential expression analyses for RNA-sequencing and microarray studies. *Nucleic Acids Res.* 43(7): e47, 2015.

2. **Efron B**. Rejoinder: Microarrays, Empirical Bayes and the Two-Groups Model. *Stat Sci.* 23(1): 45–7, 2008.

3. **Hsieh EJ, Hoopmann MR, MacLean B, MacCoss MJ**. Comparison of database search strategies for high precursor mass accuracy MS/MS data. *J Proteome Res.* 9(2): 1138–43, 2010.

4. **Käll L, Canterbury JD, Weston J, Noble WS, MacCoss MJ**. Semi-supervised learning for peptide identification from shotgun proteomics datasets. *Nat Methods* 4(11): 923–5, 2007.

5. **Robinson MD, McCarthy DJ, Smyth GK**. edgeR: A Bioconductor package for differential expression analysis of digital gene expression data. *Bioinformatics* 26(1): 139–40, 2009.